THE DRIVING FORCES OF CRANIAL EXTRA-AXIAL SPACE MORPHOLOGY: AGE, SEX, AND DRUGS

A Dissertation

Presented to

the Faculty of the Graduate School

at the University of Missouri – Columbia

In Partial Fulfillment

of the Requirements of the Degree

Doctor of Philosophy

by

SEAN Y. GREER

Dr. Kristina Aldridge, Dissertation Supervisor

May 2022

The undersigned, appointed by the dean of the Graduate School, have examined the dissertation entitled

THE DRIVING FORCES OF CRANIAL EXTRA-AXIAL SPACE MORPHOLOGY: AGE, SEX, AND DRUGS

presented by Sean Y. Greer

a candidate for the degree of Doctor of Philosophy,

and hereby certify that, in their opinion, it is worthy of acceptance.

_____

Professor Kristina J. Aldridge

_____

Professor Kevin M. Middleton

_____

Professor Richard J. Sherwood

_____

Professor David Q. Beversdorf

This dissertation is dedicated to my parents, Cathy J. Greer and Yates C. Greer. Thank you for literally everything. If only you had taken me home after that first day in Minnesota, none of this would have happened. It is all basically your fault. I love you both so much!

Acknowledgements

First, I would like to thank all the participants in the Human Connectome Projects whose dedication to science and whose literal anatomy made this project possible. Second, my deepest gratitude to my academic mentor, Dr. Kristina J. Aldridge whose support and guidance over the last few years has been invaluable to me as not only a scientist, but as a model of a good and kind human being. Thank you to Dr. Kevin M. Middleton for getting me closer to understanding statistics than anyone has before, and always providing clean and simple solutions to my insurmountable problems. Thank you to Dr. Richard J. Sherwood for always making me question my own questions, and reminding me to focus on the underlying goal of graduate school to not get too lost in the weeds of a passing scientific endeavor. Finally, thank you to Dr. David Q. Beversdorf for shedding a direct clinical light on my research and helping me to see the vast realm of potential applications for my work, and for not making me look like a complete ass hat at my proposal defense when I didn't know anything about HbA1c. I have a substantial amount of respect for each of these professionals, and am eternally grateful for their scientific input and personal guidance on my little project.

I also want to thank Dr. Steven A. Symes, whose insistence that I get a *useful* Ph.D. led me down this particular path. I owe you more than words can express, and will forever cherish talking trauma over beers on the utility roof of the Hotel Stanza in D.F.

Contents

List of Tables

List of Figures

Abstract

Surrounding the brain but contained within the skull is a dynamic organ that functions to physically and chemically maintain the typical functioning of the brain. This organ is usually appreciated only as a series of layered supportive tissues, and a substantial collection of fluid suspended within them. In understanding it as such, the potential insights that its distinctive morphology has on our understanding of human anatomy have gone essentially unexamined. From here on out this organ or the collection of tissues that separate the brain from the skull will be referred to as the cranial extra-axial space (cEAS). In the research that follows, the normal morphology of the cEAS is examined with respect to variation with age, sex, body size, and marijuana use in an attempt to better characterize its normal morphology. Size, shape, and distribution of the cEAS were found to be highly variable in response to a number of individualistic characteristics. More absolute space was seen in taller, older, and male individuals than those that were shorter, younger, and/or female. Overall morphologic interactions of the cEAS are however complex, and cannot be explained by these characteristics alone.

Chapter 1

Introduction

1.0 Introduction

Surrounding the brain but contained within the skull is a dynamic organ that functions to physically and chemically maintain the typical functioning of the brain. This organ is usually appreciated only as a series of layered supportive tissues, and a substantial collection of fluid suspended within them. In understanding it as such, the potential insights that its distinctive morphology has on our understanding of human anatomy have gone essentially unexamined. From here on out this organ or the collection of tissues that separate the brain from the skull will be referred to as the cranial extra-axial space (cEAS). The term “extra-axial” is taken from the descriptor denoting lesions that occur outside of the central nervous system tissues and here, therefore, represents the tissues outside of the brain (Curnes, 1987). The term “cranial” is included to differentiate from the similar but distinctive area around the spinal cord. “Space,” an already too heavily used term in anatomy, describes how the cEAS is typically observed directly through dissection. As the cEAS’s largest constituent component is fluid, its loss results in a literal gap between two of the most studied distinctive ‘organs’ in the human body: the brain and skull.

1.1 Historic Record of the cEAS

The accumulation of fluid around the brains of humans has been observed by physicians and anatomists for more than a millennium. The earliest recorded reference to the fluid tissues surrounding the brain, and the earliest written reference to the actual brain come from what is itself the oldest known text on trauma, the Edwin Smith Papyrus from 16th-17th Dynasty Ancient Egypt (1600BCE) (James, 2005). In the anthology of case studies, one particular description includes that of a “membrane” that was “enveloping his brain” and “fluid” that actively “runs out” of the wound (Breasted, 1930). Unfortunately for the individual whose meninges and cerebrospinal fluid are immortalized forever as Case 6 in the papyrus, the recording physician recommends only supportive treatment and implies the case is essentially hopeless (Breasted, 1930).

This fluid’s presence appears again in writing some thousand years later, at which time its role in disease was supposed. This text, attributed largely to Hippocrates (460-375BCE), describes an accumulation of “phlegm” around the brain in individuals afflicted by “sacred” disease. The text in question describes what has been deemed a likely case of epilepsy and hydrocephalus (Hajdu, 2003). Frequently and yet equally incorrectly called “water” today, cerebrospinal fluid (CSF) is the largest component of cEAS by volume. Despite its varied mechanical and physiological functions, the CSF and the spaces it occupies have been given scant attention from a morphological perspective. This is perhaps unsurprising given CSF exists as a liquid at both room and body temperature, and it is therefore readily lost to any attempt at direct observation of

its shape or perhaps more properly its distribution around the brain within the cranium.

1.2 Components of the cEAS

As with all liquids, CSF's morphology depends entirely on the form of its container. In the case of CSF, this container is the cEAS. Specifically, CSF resides within the subarachnoid space (SAS). The deepest layer of the subarachnoid space is the pia, or 'pious,' mater. Pia mater is a delicate one-to-two cells thick membrane firmly attached to the surface of the central nervous system. This membrane precisely matches the various gyri and sulci of the cerebral cortex in form, and is indistinguishable in gross anatomy from the outermost layer of the brain in general.

The CSF container's surface opposite the pia mater is most directly and properly the arachnoid mater. Arachnoid mater receives its named for the spider's web-like trabeculae that span the SAS and connect the arachnoid mater to the pia. Together the pia and arachnoid are referred to as the lepto- or 'thin' meninges. The leptomeninges together with the CSF contained between them constitute the majority of the cEAS's volume, and a substantial fraction of its overall morphology.

The arachnoid mater is itself firmly attached to the outermost meningeal layer, the dura mater. Meaning hard or tough, and sometimes called pachymeninx (thick membrane) in contrast to the leptomeninges (thin membrane), the dura is considerably thicker and tougher than the pia or

arachnoid. The dura is composed of two distinct layers, that are typically well adherent to one another. The outermost periosteal dura layer lines and is firmly attached to the skeletal surfaces of the endocranial cavity. At four largely interrelated locations, the periosteal layer of dura is separated from the deeper meningeal layer resulting in a gap between the two dural layers resulting in a series of angular canals within the dura. These spaces within act much like a network of veins, draining venous blood from the brain and CSF from internal circulation. The most prominent of these dural venous sinuses include the cavernous, superior sagittal, transverse, and sigmoid sinuses as depicted in figure 1.1. These dural sinuses contain no circulating CSF, but are important to reabsorption of CSF into the systemic bloodstream (Sakka et al., 2011). Attached to these dural sinuses are the dural folds that separate the CSF containing portions of cEAS into partially discreet components, and dictate some of the flow of CSF around them. From the pia mater to periosteal dura mater, the morphology of CSF *in vivo* is at the largest scale dependent on and indistinguishable from the shape of the brain and the shape of the skull.

2.0 Anatomic History of the cEAS

2.1 Evolution of the cEAS

A primitive form of the CSF and meninges is present in all vertebrates. In amphioxus, this consists of a single layer of fibrous and relatively avascular tissue homologous to the dura (Brocklenhurst, 1979). In other aquatic animals (Lamprey, Goldfish, Lungfish, and Dogfish), an additional fibrous but highly

vascular layer of tissue surrounds the central nervous system and is called pia, though the homology of this to mammalian pia is uncertain. The CSF of fish is enclosed fully within the CNS, but in some groups, a separate extradural fluid also exists outside the brain (Jones, 1979). In amphibians, there is a clearly defined arachnoid mater with distinctive CSF-filled subarachnoid space evident (Brocklehurst 1979). The appearance of a CSF-filled space coinciding with an increased propensity to live on land is considered to be adaptive to transitioning from aquatic to terrestrial habitat. Living on land comes with added constant shocks of terrestrial locomotion, and CSF contained in the cEAS provides a highly effective shock absorber for the delicate neural tissues (Kardong, 2008). Preventing the brain from damaging contact with its protective skull is only one of the cEAS's many functions. The cEAS develops in humans primarily from mesoderm, as its physical components, the meninges, are derived from the primary meninx (Adeeb et al., 2013, 2012).

2.3 Functions of cEAS

In routine operation, the various components of the cEAS provide a variety of disparate yet interconnected support functions for the brain. As a fluid-filled container surrounding the brain, the cEAS functions both as a chemical buffer and a structural entity. The SAS typically contains approximately 125mL of CSF in humans. This subarachnoid CSF is predominantly produced by the choroid plexus within in the ventricles of the brain, with additional volume coming from the ependymal lining of those ventricles (Sakka et al., 2011). Homeostasis in the

chemical environment of the brain is tightly maintained through constant production and circulation of CSF throughout the cEAS's extent. The CSF has been described as a "nourishing liquor" for the fact that it supplies the brain with ions and macronutrients. In the case of some molecules, such as vitamin C and folate, a normal human diet provides an inadequate supply to the brain via vascular pathways alone when the choroid plexus is nonfunctional (Spector et al., 2015). Waste products from brain metabolism increase in CSF with age, as the CSF turnover rate decreases allowing for this waste buildup (Sakka et al., 2011). Altered CSF composition and toxicity has also been shown to play a role in the pathophysiology of amyotrophic lateral sclerosis (Ng Kee Kwong et al., 2021).

Structurally and anatomically, the cEAS provides buoyancy to the brain by essentially suspending it within the CSF. This function of the cEAS is best appreciated anatomically when it fails. In cases of aliquorrhea, or intracranial hypotension from a spontaneous CSF leak, patients frequently present with postural headache as a direct result of the brain sinking within the skull and pulling on the pain-sensitive dura (Schievink 2006). Visualized on MRI, this downward displacement or sagging of the brain is highly specific to intracranial hypotension resulting from CSF leakage (Schievink 2003). In severe or prolonged cases, loss of CSF can progress to brain ischemia or herniation through the foramen magnum (Iencean et al., 2008; Schievink, 2003) When the cEAS is properly filled with the appropriate amount of CSF, this fluid-filled organ

functions as a mechanical and pressure shock absorber for the sensitive neural tissues of the brain.

The skull is a rigid structure and endocranial volume is therefore stable over relatively long periods of time. In the 18th century, anatomist Alexander Monro made a series of interrelated judgments based on this assumption. He reasoned that as the brain is relatively incompressible within this non-expandable endocranium, the volume of blood within the endocranium must also be constant. It also stood to reason that the arterial inflow and venous outflow to the endocranium must also, therefore, be equal (Monro, 1783). This hypothesis was later supported by observations on drowned animals by George Kellie, and with exsanguination experiments done by John Abercrombie (Mokri, 2001). Animals that were exsanguinated showed a distinct lack of blood in all organs less for the brain, except in cases where the endocranium's integrity had been interrupted. This series of observations now known as the "Monro-Kellie Doctrine" can be reduced to a simple equation: (1) brain volume + (2) endocranial blood volume = (3) total endocranial capacity. None of these early observers recognized the importance of the fourth and most dynamic component, the CSF. Despite its presence in literature dating to before the 5th century, CSF was essentially unappreciated, ignored, or unidentified by anatomists until the 1700s. This has been attributed to dissection techniques of the time, which frequently included removal of the head and the resulting loss of intracranial blood and CSF (Hajdu, 2003).

With the addition of CSF to the Monro-Kellie doctrine, the picture of how cEAS regulate the brain's pressure stability on a pulse-to-pulse basis is clearer. Instead of a constant flow of blood in and out of the endocranium, increased blood volume from each ventricular systole displaces CSF from the endocranium into the spinal canal. For each beat of the heart sending fresh blood to the brain, an equal amount of CSF must be displaced from the endocranium to maintain a constant pressure on the delicately enclosed brain (Kedarasetti et al., 2020). The mechanical and barotrauma-absorbing ability of the cEAS through CSF displacement is applicable over different time scales and volumes. With pulsatile changes, a very small volume of CSF is displaced from the cEAS but rapidly returns as arterial pressure again reduces (Frydrychowski et al., 2011). However, space-occupying lesions such as hematomas also invariably take up endocranial volume and require an equal displacement of a remaining intracranial component: blood, brain, or CSF.

3.0 Current Knowledge of the cEAS

3.1 The cEAS in Children

The cEAS has been examined most thoroughly in infants. Congenital anomalies in the flow, distribution, and volume of the CSF are common and easy to detect in newborns (Kahle et al. 2016). Hydrocephalus, from Latin for "water" + "head", is the most common diagnosed pathology of infancy classified as a brain disorder. An excess of CSF either in the ventricles due to a physical blockage and/or accumulation within the cEAS, hydrocephalus affects more than 400,000

births globally every year (Dewan et al., 2019). Early in development and into the first years after birth, the cranial sutures do not yet interlock and the endocranium does not conform to the rigid model of the Monroe-Kellie doctrine. As CSF is continually produced with no route to leave the skull it pushes against and deforms the vault, resulting in extreme morphologic consequences such as macrocephaly when left untreated. The commonality and dangers of hydrocephalies combined with the ease of ultrasound to measure the subarachnoid space in infants has led to it being a well assessed area for normal morphologic variability. Ultrasonography studies show the developing brain and skull to be separated by anywhere from < 0.5mm up to > 6mm (Armstrong, 2002; Lam et al., 2001; Malinger et al., 2000). Put another way, the structure imminently proximal to the developing brain varies in its typical thickness by a factor of twelve in neurologically normal infant individuals. I challenge the reader to identify another supportive tissue structure that varies to such an extreme magnitude and is not considered pathological.

Even more extreme examples of ‘benign’ anatomical variation are quite common with respect to the cEAS. The overall production rate of CSF and relatedly the amount contained within the ventricles and subarachnoid space varies leading up to and immediately after birth (Lam et al. 2001). The amount of CSF external to the brain does not vary consistently in thickness with during development, some areas increase in size, others decrease, and some appear to reach a peak width before subsiding again (Watanabe et al., 2005). This is in part due to the passive occlusion and clearing of the ventricular system and spinal

cord lumen or central canal, causing CSF production internal to the central nervous system to exert pressure on the more proximal structures of the ventricular system (Scelsi et al., 2020). A similar process may be responsible for benign enlargement of the subarachnoid spaces in infancy also called benign external hydrocephalus (Armstrong, 2002; Ment et al., 1981).

Hydrocephalus is not the only disease that can alter the relationship between the brain and skull during development. Craniosynostosis occurs when individual or multiple cranial sutures interdigitate and fuse prematurely in infants. Broadly speaking this condition is thought to restrict growth in the perpendicular direction of the fused suture (Reardon, 2000). In these cases of what one might call a restricted example of Monro-Kellie, the continued growth of the developing crania and brain can lead to variable dysmorphology in both. The cEAS is by its definition affected in these cases, and although total endocranial growth is restricted, the cEAS is locally enlarged in many cases (Chadduck et al., 1992). Examination of the brain and skull together in individuals affected by various subtypes of craniosynostosis has revealed global changes to the brain's morphology even in cases of isolated synostosis (Aldridge et al., 2002, 2005b, 2005c). As a layered entity between the brain and the endocranium, the cEAS acts as a morphological buffer and therefore may contain additional shape variation useful for the understanding, diagnosis, and treatment of disease.

Measuring the cEAS for indications of a neuropathology that less directly impacts the cranial anatomy has recently shown potential predictive. In a couple of small longitudinal samples individuals that would later go on to be diagnosed

with ASD were found to have typically sized brains surrounded by an increased volume of extra-axial CSF (Shen et al., 2018, 2017). Later attempts to validate and expand on that research however have not found the same patterns, and indicate the association may disappear quickly with increasing age (Peterson et al., 2021)

3.2 The cEAS in Adults

The thickness of the cEAS in adults has been examined peripherally in studies more broadly aimed at examining brain morphology. One such study examined SAS thickness with CT at one location in the frontal region, for comparisons between alcoholics with *delirium tremens* and healthy controls. In the research's healthy sample (n=10), the mean maximum frontal subarachnoid space was 3mm, with a 95% confidence interval of ± 1.4mm (Maes et al., 2000). Even with an extraordinarily small sample of normal "healthy volunteers", the range of variation in cEAS in this study was within a quarter millimeter to nearly six full millimeters of cEAS tissues. This study sample included both male and female normal healthy controls (male:female ratio of 6:4), and spanned several decades in patient ages (43 ± 24 years). The authors do not speculate as to the origins or meaning of this range of variation. Considering the multitude of functions ascribed to the cEAS, an approximately 19-fold difference of thickness across a handful of individuals warrants further investigation.

One additional assessment performed a more detailed investigation of the cEAS explicitly, specifically measuring frontal and occipital SAS thicknesses

bilaterally at the MRI level superior to the lateral ventricles (Frydrychowski et al., 2012). SAS thickness was found to vary from 0.50 to 2.10mm between locations, with significantly less SAS in the occipital region compared to the frontal, specifically when patients were supine (n = 15). Males (n = 6) were found to have significantly thicker SAS than females (n = 9) with subarachnoid space averaging 3mm in the frontal in males, while SAS in females averaged than 1mm. In a test of gravity's influence on the SAS, Frydrychowski et al. measured SAS thickness in the frontal region interindividual and compared prone vs supine positioning of patients in the MRI scanner (2012). With a small sample of nine individuals (male = 1, female = 8) the authors were limited in statistical analyses, but observed changes of greater than 1mm and up to a 56% decrease in frontal SAS thickness when measurements were obtained in supine versus prone positioning. In contrast, one individual experienced only a 9% decrease in frontal SAS thickness. These results indicate that within an individual, the morphology of cEAS space varies in response to changes in head position.

The most detailed study of variation in normal cEAS morphology (n = 523) examined the presence and appearance on MRI of the *cisterna magna* (Whitney et al., 2013). The *cisterna magna* is an expansion of subarachnoid space between the inferior cerebellum and medulla oblongata with variable extensions posteriorly. With their large sample, the authors were able to group individuals into five distinct morphotypes of *cisterna magna* depending on the cerebellum's relative location to occipital bone at several locations. This suggests the CSF

spaces continues to be highly variable into adulthood, and that this variation is distinctly related to potentially clinically relevant processes.

Another avenue of insight into anatomical variability of cEAS comes from the necessities of craniotomies and other transcranial surgical interventions. With the intent of locating underlying endocranial structures using overlying ectocranial landmarks, researchers have repeatedly found compelling diversity in relative ectocranial-endocranial structure locations. Ucerler and Govsa (2006) assessed placement of the transverse-sigmoid sinus relative to ectocranial landmark asterion. Drilling 2mm burr holes into 100 dry crania at asterion and noting the location of resulting endocranial holes relative to the grooves left by the dural sinuses, the authors note that in most individuals (87%) asterion is immediately superficial to the junction of sinuses. However, in 11% of cases, the burr hole entered the cranium superior to the sinus grooves, and in 2% it entered inferiorly (Ucerler and Govsa, 2006). The relationship between ectocranial asterion and the transverse/sigmoid sinus has since been explored independently in several populations using similar methods. Results have found the two structures to be directly overlapping in as low as 60% of individuals or as high as 91% (Mwachaka et al., 2009; Wirakiat et al., 2021).

In addition to structures of the cEAS like the dural sinuses, the positioning of the brain itself is variably placed within its overlying skull. Although the brain is grossly buckled into the skull by the dural folds, any differences in the relative size or shape of one brain region may result in a displacement of local brain structure relative to the neighboring skull anatomy. The central sulcus for

instance shows consideration variability in its raw distance from the coronal suture, displaced between two and six centimeters posteriorly (Ribas et al., 2006; Sarmento et al., 2008).

Unfortunately, while convenient and still illustrative of anatomic variation, preservation and post-mortem processes are likely to influence brain-skull congruence to an unknown extent. Using living participants of lateral angiographs aimed at discerning the relationship between the precentral gyrus and the coronal suture three decades prior concluded that “A more exact localization of the precentral gyrus…can be obtained with CT and intraoperative cortical stimulation of the motor strip” (Ebeling et al. 1987). The implication being such extreme variation exists in relative brain-suture positioning that it is more accurate to look at the brain directly than to divine its location from the overlying sutures.

The consequences of variable anatomy are exemplified by Ersoy and colleagues’ (2003) description of the potential dangers in misinterpreting sutural intersections at the ectocranial landmark pterion. Unaccustomed to atypical presentation, a surgeon may inadvertently place a burr hole that penetrates the endocranial cavity rather than the orbit or vice versa While accomplishing the task of noting variation, many of these studies stop short of addressing the shape and magnitude of variation due to small sample sizes.

Traumatic brain injuries have a high incidence of morbidity and mortality, and are inherently difficult to study *in vivo*. As a result, computer modeling and finite element analyses (FEA) are becoming standard methods for understanding

how stress and strain propagate through the head (Zhu et al., 2003). In addition to the external force being applied and the properties of the anatomical elements (i.e. brain and skull), a critical factor in accurately modeling trauma to the head is the condition of the interface between the brain and skull.

4.0 Discussion

The layers of meninges and cerebrospinal fluid contained within them that collectively make up the cEAS have been known for centuries. Interest in these structures has, however, been greatly outweighed by interest in the brain and skull independently. The brain and skull are undeniably tied to one another especially in development when rapid and dramatic changes take place in the cEAS. However, this brain-skull relationship (cEAS morphology) becomes gradually underappreciated in normal adults as the morphologies begin to settles. What little investigations to the cEAS have been undertaken have found exceptional levels of variation in its presentation, but had little consideration for identifying the driving forces of that variation. In the work that follows, we will attempt to model the cEAS as a distinct anatomic entity, and address potential major driving influences of its size and distribution.

In Chapter 2, the baseline normal anatomy of the cEAS in “young” adults will be assessed in the framework of body size, asymmetry, and sex differences. We anticipate that the cEAS as a distinct anatomic entity is not influenced by the same factors in its superior or vault component as in its inferior or basal areas. In Chapter 3, aging’s effect, a feature known to be extreme on the brain, will be assessed with respect to the cEAS. Wes suspect that as the cEAS ages, it does

so non-homogeneously across its extent with some areas more drastically altered with age than other. Lastly, in Chapter 4, we attempt to use the cEAS to identify differences associated with cannabis use and abuse. Cannabis' effect on the brain is still hotly debated, and we believe that as a highly variable and readily adaptable structure, the cEAS may provide a structure easier to assess than the brain itself, even though the effects are more likely to be taking place on within the brain proper. We suspect these morphologic associations will be correlated to characteristics of an individual's cannabis use history, with more frequent, longer, and dependent users showing greater departures from normal cEAS morphology.

In each of these studies, cEAS will be assessed at several scales. Overall volume of the cEAS, hemispheric volume, and superior/inferior component volumes were assessed, as was the local thickness of the cEAS at preidentified locations of interest. Finally, landmark data that describe features of the cEAS are also assessed for differences of shape. Interconnected, each of these lines of evidence describes a slightly different aspect of the overall cEAS morphology. Agreement on positive results between multiple lines of evidence may indicate stronger support for an patterns that are identified over any one of the models of cEAS alone.

Chapter 2

Cranial Extra-Axial Space: Normal Variation

Abstract

Leveraging the high-quality structural MRI data collected through the Human Connectome Project, this study examined the variation in volume and distribution of cranial extra-axial space (cEAS) as a morphological entity. Structural data were collected and assessed from 68 individuals to determine whether patterns in variation associated with overall body-size, asymmetry, and biological sex exist in the cEAS. Regional volume, linear thickness, and shape-based analyses all reveal a greater influence of demographic characteristics of young individuals on cEAS morphology in the cranial base than that observed in the cranial vault.

1.0 Introduction

Assessment of cranial extra-axial space (cEAS) morphology has only been truly accessible with the advent of non-invasive medical imaging such as magnetic resonance imaging (MRI). Any direct observation and measurement of the cEAS results in the loss and redistribution of the CSF within the cEAS's subarachnoid space across the entirety of the cranial cavity. This fact limits any ability to quantify the shape (distribution) of CSF or cEAS that contains it beyond that of an amorphous overall volume measurement. Understanding how this volume of cEAS is distributed across the brain, however, has great potential use

for differentiating the prominent influences of normal anatomic variation that may be observed in research as well as clinically, and for diagnosis and assessment of neural diseases and their progression. In this chapter, volume, asymmetry, and distribution of cEAS will be assessed in normal healthy adults as it relates to broad demographic and individual characteristics that are suspected to influence its morphology. Rudimentary total volume measurements of cEAS have identified variation associated with both sex and age (Allen et al., 2002; Frydrychowski et al., 2012; Good et al., 2001a; Lemaître et al., 2005; Raz et al., 2001; Ruigrok et al., 2014; Sowell et al., 2007) . Effects of age on the cEAS are more substantial in magnitude than other demographic characteristics and will be discussed in detail in chapter 3.

Occasionally called ‘pericerebral space’ in earlier publications, the shape of cEAS or the CSF it contains has been problematic to quantify exhaustively. These early assessments used water displacement to measure volumes of the brain and polyurethane foam models of endocrania after stripping of the dura at autopsy to calculate cEAS volumes. Using this methodology, the first published accounts of cEAS found it occupies between 1% and 8.3% of intracranial volume in healthy young-adult individuals (Davis and Wright, 1977; Harper and Kril, 1985). This methodology, though practical, was limited in precision by postmortem edema, shrinkage, and other artifacts of physically modeling the endocast. In the decades since then, these findings have been reassessed using MRI methods on living individuals.

Variation in the distribution of this volume of cEAS in adults has been examined somewhat in the context of CSF volumes, and the location or size of the dural venous sinuses. There is typically more CSF contained within the cEAS on the right side than on the left (Frydrychowski et al., 2012; Good et al., 2001a; Leonard et al., 2008). Clinically, hemispheric volume ratios of CSF have been recently suggested as reliable and early biomarkers of brain edema severity (Dhar et al., 2021).

One of the earliest attempts to directly measure the CSF reported a cEAS CSF volume of 97.6± 36.6mL in a sample of ten healthy individuals averaging 37 years old at assessment (Condon et al., 1986). A later study with similar MRI methods reports a similar value of 96±25mL of subarachnoid CSF, accounting for 6% of total intracranial volume in their youngest age group (n = 12, mean = 35 years) (Matsumae et al., 1996a, 1996b). Even with these relatively small sample sizes, significant variations in cEAS volume were readily apparent in these assessments. Larger (n > 50) and higher resolution imaging studies have since reported a consistently higher average-value for subarachnoid CSF of between 150mL and 400mL (Good et al., 2001b; Leonard et al., 2008; Mortamet et al., 2005; Sowell et al., 2007). In each of these cases however cEAS or CSF morphology was only being assessed with respect to its overall size. With the advent of increased imaging precision also came the ability to more easily subdivide the cEAS's volume into discrete regions, and to assess its morphology through differences in its distribution not just volume.

The remaining cEAS space that is not occupied by CSF is largely the realm of dural venous sinuses. These sinuses can be found consistently in predictable locations, and are visibly asymmetrical in most individuals. In adulthood, there is notable variation in the precise subset of these dural sinuses that carries the majority of venous fluid and therefore remains significantly larger than the others (Meila et la. 2012). These larger sinuses leave visible imprints in the endocranium, and are directly a part of the cEAS's superficial morphology. Despite their predictable locations, these sinuses are not directly isolatable using only overlying ectocranial structures, and their placement varies with sex (Mwachaka et al. 2010; Tubbs et al. 2000).

The brain and endocranium, though not technically components of the cEAS, also provide some direct insight into the sources of its variation as they are the two surfaces that define the space. Sex differences in the metric description of the endocranium has taken place most thoroughly in light of forensic anthropology and the context of identification of skeletal remains. Though less pronounced than ectocranial sex traits, the basal cranium and of the petrous portion of the temporal bone have been found to be larger in males than in females (Bruner et al., 2003; Isaza et al., 2014; Kalmey and Rathbun, 1996). Total volume of the endocast, synonymous with the endocranial volume or intracranial volume is also significantly larger in males than in females (Rametti et al., 2011; van der Linden et al., 2017). The brains that occupy the majority of this endocranial volume have also shown consistently to be dimorphic. Males' brains typically are larger than females' brains (Rametti et al., 2011; Ruigrok et

al., 2014; Sowell et al., 2007). Brain size does correlate with body-size, and as males and females tend to differ in body size, some of this effect is reflected in the brain volume. Even after controlling for height, however, males are frequently found to have larger total brain volumes than females (Allen et al., 2002; Burgaleta et al., 2012; van der Linden et al., 2017).

Despite the great deal of attention paid to the shape and size of the various contents of the head, there has been surprisingly little examination of the driving forces that directly influence the relative position of the brain within the skull, i.e., the morphology of the cEAS as a whole. The aim of the present study is to identify the driving forces of normal variation in different regions of the cEAS. We hypothesize that: (1) the factors influencing cEAS morphology differ between its vault and basal components, and (2) that the basal cEAS is driven by size factors, while (3) vault cEAS is influenced more by general characteristics such as sex and cerebral asymmetry.

2.0 Methods

All magnetic resonance imaging (MRI) data used in this study were originally collected as part of the Human Connectome Project (HCP) and were drawn from the Connectome Coordinating Facility (CCF) database (Van Essen et al., 2013). The HCP is a now significantly expanded National Institutes of Health (NIH) initiative aimed at mapping the white-matter connectivity of the brain by collecting multiple MRI modalities, including structural, functional, and diffusion tensor imaging from a varied and extensively documented sample. Data-sets

collected using HCP protocols and now housed collectively as part of the greater HCP include normal healthy individuals from development to senescence, and patients with numerous neurologic disease states. The result has been an extensive collection of comprehensive MRI data from a broad sample of the general United States population (Van Essen et al. 2013). Two particular projects housed by the CCF were used in this study, the original HCP 'young-adults' data (HCP-YA) and the aging sample (HCP-A), collected later and described in detail in part 3.

Participants in HCP-YA were scanned with a 32-channel head coil on a custom built high-resolution 3T 100mT/m gradient "ConnectomeScanner" adapted from a Siemens Skyra (Siemens AG, Erlanger, Germany) at Washington University in St. Louis, Missouri (van Essen et al. 2013). Detailed explanations of the scanning protocols from a mathematical and quality control perspectives are available (Marcus et al. 2013, Uğurbil et al. 2013). Structural T1w/T2w, functional resting-state, functional task, and diffusion-based imaging modalities were collected for each individual in the HCP-YA. Only the T1 and T2-weighted (the structural modalities) were used in the current study. All structural MRIs (sMRI) were collected with the same scanning parameters, as follows: rep time 2400ms, echo time 2.14ms, inversion time 1000ms, flip angle 8deg, field of view 224mm, matrix 320x320, and voxel size 0.7x0.7x07mm (Van Essen et al., 2013). This is higher resolution than the typical resolution in clinical scans of 1mm isotropic voxels. Structural scans were all assessed by a trained scorer for overall quality from poor to excellent, and only structural scans rated as good or excellent were

put forth into the HCP pipelines used here (Marcus et al., 2013). Additional genetic, behavioral, blood-draw, and urine drug-screen results were also collected by the HCP-YA team, and are associated with the participants' scans in the sample database.

2.1 Participants

The HCP-YA sample contains MRI scans, health, demographic, and behavioral data from 1200 normal healthy individuals between the ages of 22 and 35. "Healthy" was defined broadly by the original data collection team to include tobacco smokers, individuals categorized as obese, and individuals with a history of drug/alcohol use. This was definition was used to avoid creating what Van Essen et al. termed a "supernormal" case series that does not well represent the general population (2013). Criteria for exclusion from the HCP-YA sample included having a severe neuropsychiatric disorder (e.g., schizophrenia, severe depression), diabetes, high blood-pressure, or having a sibling with severe neurodevelopmental disorders (e.g., autism) (Van Essen et al. 2013). A complete list of the original data collection group's inclusion/exclusion criteria can be found in the supplemental materials to Van Essen et al. (2013).

Additional exclusionary criteria were applied to the HCP-YA sample for the assessments performed here. Individuals with pre-hypertension (> 120/80), high HbA1c levels, predominant left-handedness, twin pairs, any self-reported history of drug use (except alcohol, tobacco, or THC), and individuals with a positive urine drug screening for any substances were excluded. Self-reported race,

ethnicity, income, and education were left uncontrolled for when selecting individuals. Due to the lengthy data collection procedure described below, a relatively small but still statistically powerful sample was desirable. Statistical power analysis revealed that a sample of approximately 35 individuals per pair-wise group would be sufficient to detect the level of differences expected here in cEAS morphology. From the more selective sampling of the HCP-YA, 70 individuals were randomly chosen for modeling, data collection, and analysis. Of these individuals, two were removed following 3D modeling for gross anatomic abnormalities affecting the cEAS. The final sample (see table 2.1) therefore was 68 individuals (average age: 29±3 years), consisting of 36 females and 32 males. Ten individuals self-identified race as Asian/Native Hawaiian or Other Pacific Islander, 15 as Black or African American, one “more than one” and 45 as White. Of those 45, nine self-identified as Hispanic/Latino ethnicity, no other race included reported Hispanic ethnicity.

2.2 Three-Dimensional Modeling Procedure

Three-dimensional computer models of the constituent components of cEAS first had to be derived to collect data describing its morphological characteristics. While it is possible to digitally model the cEAS as a singular structure using MRI segmentation methods similar to those described below, to easily assess and demonstrate both of its surfaces (brain and endocranium) simultaneously, they must be modeled individually. This process also allows for the simultaneous collection of volume data of both the brain and endocranium,

which otherwise would not be components of a digital model consisting of the cEAS alone. For each individual in the sample, three-dimensional (3D) *in-silico* (digital) models of brain, endocast, and lateral ventricles were produced in AVIZO 8.1 (Thermo Fisher Scientific 2014). Models were developed using a combination of automated and manual segmentation methods, and varied slightly between the anatomical structures being modeled.

Endocast and lateral ventricle models were derived de novo. Rough preliminary models of the endocast and ventricles were created by adjusting voxel selection thresholds of brightness values for CSF and dura mater on an individual-to-individual basis. Each individual's vault CSF was selected on T1-weighted images and the brightness selection thresholds adjusted until the most CSF with least extraneous anatomy was selected. To these CSF models, dura mater and associated sinuses were added using the same thresholding method but on the individual's T2-weighted images. The result of this process is a model of the superior elements of the endocast, with varying degrees of extraneous and missing data around the basicranium. These rough thresholded models were then manually refined and completed. Manual MRI segmentation refinement entails sequential analysis of each transverse image slice within an individual's scan, and delineating areas up to the dura's attachment on the endocranium. This process included both removal of extraneous tissues collected in the automated portion, as well as demarcation of the more complex basicranial anatomy. The endocast model was closed across the foramen magnum at the transverse slice level of the most inferior cerebellar tonsil so as to include the

entire brain model within its respective endocast model. Endocast models were then checked for completeness slice-by-slice in the orthogonal coronal and sagittal planes.

Lateral ventricle models were derived in much the same way as the endocast. The CSF contained in the right and left lateral ventricles was selected and brightness threshold adjusted to create a model of only ventricular CSF. Discontinuous areas of CSF contained within the occipital and temporal horns of the lateral ventricles were included in these models. Any fluid within the ventricular system more distal to the interventricular foramina was removed from these models. The ventricle models were then checked manually in the transverse section to ensure accuracy and consistency in the resulting voxel selections. The completion of this entire process results in three separate 3D models derived from the same individual's structural MRI data. As these models are derived from the same underlying coordinate space, positional data can be freely collected from any model and be directly compared with any other model. These digital reconstructions act as the foundation to collect volume data of the cEAS, its constituent components, and the lateral ventricles of the brain.

The 3D brain models used here were created using a modified version of the method described above. Previously generated brain models are available with each individual in the HCP's data files. These models are the result of an automated pipeline process running through FreeSurfer (Van Essen and Glasser 2016). While these total brain models are remarkably accurate, they frequently include extraneous material from the dural sinuses, cranial nerves, and arterial

supply to the brain. Studies comparing FreeSurfer derived volume estimates to manual segmentation methods have also found that FreeSurfer is capable of inducing size-biases, especially when estimating intracranial and brain volumes (Klasson et al., 2018; Shen et al., 2010). Each available brain model was therefore compared to their respective individual's corresponding MRI dataset to remove extraneous data, and check for discrepancies. Any islands of voxels not connected to the brain model were removed manually. Following that, additional undesired voxels were removed from the model by assessing the individual's anatomy at each transverse MRI slice, similar to a typical manual slice-by-slice segmentation used to refine the endocast and ventricle models.

2.3 Model and Landmark Data Collection

Total volume data were collected as a material property of the 3D digital brain, endocast, and lateral ventricle models in AVIZO 8.1 following the segmentation procedure. Each volume was collected as a voxel count, and converted to volume (mL) metric based on the $0.7mL^3$ voxel dimensions provided by the HCP.

Each 3D model was bisected into right and left sides by visually assessing the location of the most midsagittal slice, and dividing each model by that plane, see figure 2.1. Midsagittal here was defined as the sagittal plane in which the brain's septum pellucidum, cranial base's crista galli, and cranial vault's lambda are most closely aligned. Superior and inferior volume subdivisions were also collected by visually assessing the transverse plane that most closely intersected

the left anterior and posterior poles of the endocast, and dividing brain and endocast models by that plane. This process resulted in each brain and endocast model being composed of four quadrants: right superior, left superior, right inferior, and left inferior. Ventricular volumes were only subdivided by right and left as the ventricular volume inferior to this plane is small enough to be more substantially affected by any inconsistencies in measurement. Volume of the total cEAS was assessed by subtracting the total brain and lateral ventricle volumes from the total digital endocast volume. The same was done for each quadrant to determine subsection volumes of cEAS corresponding to the four model subsections listed above as well as intermediate subsections right/left, and superior/inferior.

Landmark data were collected in AVIZO 8.1 following 3D model creation. Three-dimensional coordinate data for a total of 102 landmarks were collected from each individual. These include midline and bilateral landmarks that describe anatomical positions on the brain, endocast, and ventricles. Landmarks were collected in the same order for each individual, and as five distinctive subsets. Landmark sets include midsagittal slice (20 landmarks), parasagittal slice landmarks (40), 3D brain model (26), and 3D endocast model (16). Names and definitions of landmarks are described in Table 2.2. Figures 2.2-2.4 depict these landmarks by the section with which they were collected. Not all landmarks were used for each analysis, and some landmarks were removed for imprecision (section 3.1 of this chapter)

2.4 Statistical and Mathematical Methods

The three-dimensional landmark coordinate data were used to calculate interlandmark distances (ILDs) that describe the thickness of the cEAS at distinctive locations. Thickness of the cEAS was measured at 19 locations (8 bilateral and 3 midline) using interlandmark distances (Figure 2.4). Mathematical descriptions of thickness calculated using 3-D coordinate data are provided for each location in Supplemental Table S2.1. Generally, ILDs were calculated using the differences in each corresponding landmark coordinate plane and applying multidimensional Pythagorean theorem as needed depending on the number of planes of interest.

Statistical analyses were performed using the software package R (R Core Team 2021). Volume data were assessed for assumptions of normality both visually with QQ-plots and quantitatively using Shapiro-Wilks tests. Group means were assessed using Students' t-tests (base R: t.test) for mean level differences in volume and thickness measurements. Pearson's product moment correlations and Spearman rank correlation were used to asses for correlations between body size and cEAS metrics as well as within cEAS metrics (base R: cor.test).

Landmark data were also assessed for differences in cEAS morphology between males and females using winEDMA (Cole, 2002). Euclidean distance matrix (EDM) analyses can be used to compare collections of landmarks for similarity in their distribution or form. To do so, a form matrix [F] containing all possible interlandmark distances (ILDs) between unique landmark pairs is calculated (Lele, 1993; Lele and Richtsmeier, 1991). The distribution of resulting

ILDs is compared between groups to assess relative similarity in the form of the landmark set. Unlike other shape analyses that rely on rotating, translating, and scaling the coordinate data in a form matrix, EDM analyses' form matrix is invariant concerning translation or rotation as ILDs values do not change with landmark orientation. Comparing two form matrices is done through a form-difference matrix [FD] which is made up of the ratios of one form matrix to another. The ratios of ILDs between groups can then be assessed for patterns in overall or regional size and for clusters of ILDs that indicate shape differences associated with one or multiple landmarks' movement relative to others in the set.

Confidence intervals for ratios contained in the [FD] were calculated using parametric (Monte-Carlo) resampling (x1000) with an $\alpha=0.01$. Any calculated confidence interval ranges containing 1 for a given [FD] ILD do not differ significantly at this alpha level between the compared matrices (Lele and Richtsmeier, 1991). Parametric (re)sampling generally makes assumptions regarding the normalcy of the data being input to provide accurate results. In the case of EDM analyses, the input data is landmark coordinate data which were here not specifically checked for normalcy using mathematical testing. The data from which the 3-D coordinates were derived however was assessed for and found to be normal. The landmark data are assumed to be accurate and representative of the sample. For these reasons, the slightly stricter than typical morphometric research alpha level was chosen for reporting of results. Two subsets of landmarks were analyzed using a form-difference matrix and marginal

confidence intervals produced through EDMA. Twelve landmarks representing the vault component of cEAS, and nine that describe the basal cEAS were selected for these analyses. These landmarks are listed in table 2.7

2.4 Error Assessment

There are three sources of potential error and noise accumulation in the data collected for these analyses. The first source is associated with MRI scanner and Human Connectome Project related processing of the available data. Error in the available structural MRI data is assumed to be low due to the strict quality control protocols under which the data were collected and processed for release (Harms et al., 2018; Van Essen et al., 2013). Second, the previously described creation of volumetric models for the brain, endocast, and lateral ventricles from these MRI scans may introduce additional unassessed error in the data collected and analyzed here. Lastly, error may enter the data through the placement of landmarks used in EDM analyses and for extracting linear distances.

To address the replicability of the three-dimensional modeling process, ten randomly selected individuals were modeled on two separate and distinct occasions using the semi-automated thresholding and manual segmentation methods described above. The two modeling sessions were separated by more than one month. Differences in the volumes of paired brain, endocast, and lateral ventricle models were then assessed with technical error of measurement (TEM), relative TEM (rTEM) and the TEM coefficient of reliability (R) (Lewis, 1999; Perini

and de Oliveira, 2005). TEM is mathematically the square root of the sum of squared differences between observations divided by two times the total number of observations (see equation 1). More easily understandable is rTEM, defined as the percentage of the total variable value variability that is accounted for by error (Perini and de Oliveira, 2005). Mathematically, rTEM is the raw TEM score divided by the variable average value times 100 (see equation 2). A raw TEM value can also be easily converted to an R value by dividing TEM by the standard deviation of all observations and subtracting this value from one (see equation 3). The R value represents the fraction of inter-individual variance free of measurement error, with values closer to 1 indicating variation in the variable due to factors other than measurement differences (Lewis 1999).

3.0 Results

3.1 Error Assessment

Table 2.2 contains the results of TEM analyses. Endocast models were the most consistent in volume between trials as reflected in a rTEM of 0.84, and R value of 0.95. Measurement of brain volume varied slightly more due to measurement error with an R = 0.94. Error in volume of lateral ventricle models was significantly greater with approximately 20% (R = 0.80) of variation in ventricle volume due to model building error. This is a significant fraction of measurement error, and while ventricle volume is still considered in some analyses moving forward, any relative differences of this metric between groups require a substantial effect to outweigh this error term. These findings are also

consistent with the relative size of these structures. As the endocast volume is the greatest it is therefore the least susceptible to volume differences resulting from small differences in segmentation.

Collection of three-dimensional landmark coordinate data represents the third source of data collection error prior to analysis. To address the precision of data collection associated with each of the landmarks described previously, the same subsample of ten individuals used to address error in modeling were landmarked on three separate occasions. Bilateral landmarks were collected only on the right side for assessment of error, and at least two weeks passed between each individual's consecutive landmarking session. Precision was calculated here as the mean absolute difference (MAD) between repeated measures on the same individual's scan data (i.e., MRI scan and associated 3D models), consistent with pervious morphometric analyses of precision and error (Aldridge et al., 2005a; Kohn et al., 1995; Weinberg et al., 2006). As the underlying coordinate system associated with each individual's scan data does not change between landmarking sessions, it is possible to directly compare landmark placement location in each coordinate axis. Table 2.3 provides the results of the precision analysis. A landmark was considered highly precise if MAD was less than 1mm in each of the three axes. Of the 59 landmarks assessed for placement precision, 50 meet this definition of highly precise in all three dimensions. An additional five landmarks have MAD scores >1.0mm but < 2.0mm in one of their three axes, and two landmarks' scores were > 1.0mm but < 2.0mm in two of the three assessed dimensions. The remaining three landmarks,

each related to assessing the extent of CSF in a particular MRI slice, had MAD scores of > 2.0mm in at least one dimension.

3.2 General cEAS Relationships

As the cEAS is bounded by the brain and endocranium, it is unsurprisingly tightly related in volume to these structures. Table 2.4 contains inter-element volume correlations of cEAS, brain, endocast and lateral ventricles. There is a positive relationship between total endocranial volume and each of its constituent components (brain, cEAS, and lateral ventricles). Controlling for total endocranial volume and assessing the fraction of cEAS within the endocranium revealed the persistence of strong positive correlation of with total endocrinal volume ($R = 0.42$; $p < 0.001$), and associated tradeoff though a reciprocally strong negative correlation with brain volume. With larger endocasts come relatively more space occupying cEAS overall.

Intra-cEAS correlations between measurements of thickness were observed in the sample (see Table 2.4). Thickness correlations with significance levels of $p < 0.1$ are presented in Table 2.5. Space thickness at the pre- and post-central gyri are unsurprisingly tightly positively correlated on both sides, but more strongly on the right (0.82, $p < 0.001$) than the left (0.66 $p < 0.001$). Additional positive correlations between several vault measurements and a separate pair of base measurements were also apparent. Only one pair of positively correlated thickness measures which the pairs came from the base and vault was identified, the anterior pons and frontal pole. Perhaps more interesting,

however, is the lack of correlations, and appearance of several areas of apparent trade off in the form of negative relationships. Most measures of cEAS thickness showed no significant correlation with other thickness measurements, indicating some level of independence of cEAS regional morphology. Some areas of interconnected thickness trade-off were identified. One of these trade-offs appears to be between the space anterior to the spinal cord (location 10) and the cEAS above the pre/postcentral gyri (locations 4 and 5). This space anterior to the spinal cord was also strongly negatively corelated with the cEAS length of CN VII (Location 8). Finally, Location 8 showed negative correlations with the vault cEAS thickness at temporal and occipital poles.

3.3 Asymmetry

Significant right-left asymmetry was identified in the volume of cEAS in this sample of normal healthy controls at each level of observation. In the majority of individuals, cEAS measures larger on the right than on the left side. On average, the right cEAS was approximately 5.5% or 6mL larger than the left. Assessing the constituents of cEAS reveals the asymmetry in this sample is likely driven by asymmetry in both the endocranial and brain volumes. Total endocranial volume differs significantly ($p < 0.001$) between right and left sides. This difference is a relatively small fraction of the total endocranial volume and accounts for an approximate 0.9% or a 9.5mL difference with the right side larger on average. As a fraction of endocranial volume, this pattern persists, with a greater relative volume of cEAS on the right (0.114 vs 0.109; $p < 0.001$). Though significant, this difference is small. Right and left hemispheres of the brains

examined here also differ significantly ($p < 0.001$) in volume, with the right hemisphere on average 4.1mL larger than the left. Asymmetry in the volume of cEAS was also found to be significant in both its superior and inferior components individually ($p < .001$). The quantity of asymmetry in cEAS volume did not correlate significantly with any other measurements of head or body size.

Asymmetry in the thickness of cEAS at the previously described locations was also detectable in some measurements. Of the 19 locations where thickness was measured, three locations differed significantly between right and left sides. The directionality of this thickness asymmetry was bidirectional. At the temporal pole and the post-central gyrus, cEAS was thicker on the left-side. However, the width of cEAS parallel to the path of cranial nerve VII was greater on the right side of individuals ($p < 0.01$).

3.2 Body Size and cEAS

Total and regional volumes of cEAS did not correlate significantly with height, weight, or BMI (Table 2.6). However, of all the subsampled regions (brain, endocast, cEAS, and ventricles) the volume of cEAS in its inferior component comes the closest to an appreciable level of statistical significance ($p = 0.17$). Brain volume did not correlate with height in this sample.

The amount of cEAS did in a few locations correlate with body size measures. The cEAS thickness was positively correlated to height and weight at location 8 (CN VII), but only on the left side. Thickness at the frontal pole (Location 1) was also strongly correlated with individual height ($r = 0.37$, $p = <$

0.05), but not weight and only on the right side. Interestingly, the only other significant relationship observed was a negative correlation between weight and thickness at location 2 (frontal vault) ($r = -0.28$, $p = 0.02$), only on the right side. This measure had no significant associated relationship to individual's height ($p = 0.4$) despite the strong height/weight relationship in the sample. Width of the cEAS at location 11 (posterior foramen magnum) was weakly positively correlated with height ($r = 0.2$, $p = 0.1$) and weight ($r = 0.2$, 0.08), but these final relationships do not meet criteria for statistical significance.

3.4 Sex Differences

The total volume and fraction of cranial extra-axial space (cEAS) in normal healthy controls was not found to differ significantly between males and females. Male cEAS was on average larger than female in this sample, but substantial variability exists within both sexes, far outweighing the small difference in their mean values. Subdivision of the cEAS into superior and inferior components also did not reveal any significant differences of means between the sexes. Of these two components, however, the inferior aspects of the cEAS reaches a higher level of significance when comparing males and females ($p = 0.051$). Further subdivision by side revealed the left inferior cEAS was significantly larger in males than in females ($p = 0.03$).

Healthy control individuals did differ significantly in both height and weight by sex with males significantly taller and heavier than females. The effects of body size on overall cEAS measurements are explored above (section 3.2). Only

one thickness measurement differed between males and females in this sample. The length of CN VII across the base of the cEAS (Location 8) was larger in males than in females, but again only on the left side ($p = 0.01$). Taking into account individual height reduces the significance of this mean difference substantially ($p = 0.17$). This is consistent with the overall volume findings presented earlier, and the EDMA results detailed below.

Males and females were found to differ in basal cEAS morphology. The left side was more dimorphic than the right, with only two landmark-pairs identified as significantly different between the sexes on the right side. Both of these landmark pairs (internal auditory meatus [O14] – medial clivus [O16] and the anterior pons [ML19] – facial nerve root [O12]) were also represented on the life side, as well as an additional ten landmark-pairs. Estimates and confidence intervals from the form-distance analysis of the basal cEAS on the left side are presented in Table 2.8 and illustrated in Figure 2.5. Differences are clustered around the placement of internal auditory meatus (IAM). In males, the IAM was more laterally located than in females. A few landmark pairs associated with the anterior placement of the lateral clivus were larger in females than in males. These differences were relatively small, however. In general, the landmark-pairs identified as larger in males were predominantly mediolaterally oriented, while those found to be larger in females were anterior-posterior and superior-inferior oriented.

Substantially less sexual dimorphism was identified through the EDM analyses of the vault cEAS landmarks (see Table 2.8 and Figure 2.6). The vault

landmark pairs identified by EDM analysis tend to span the entire sample area of cEAS, and are therefore more an expression of overall cranial vault size than cEAS specific morphology. This was true of both the left and right sides.

4.0 Discussion

The magnitude and driving forces behind the normal amount and distribution of cEAS was assessed from numerous morphological standpoints. The cEAS was found to vary consistently with demographic variables at several scales of observation. However, differences in regional distribution of cEAS was by no means consistent across its extent within the cranium. Overall size of the cEAS was surprisingly not found to vary significantly with any individualistic characteristics. This is in contrast to previously established relationships between both brain and endocast size with body size in significantly larger samples (Dekaban 1978, Ho et al. 1980). The result here may indicate that this random sample is not expansive enough to capture some smaller differences in brain/skull morphology and that overall differences in the size of cEAS may be detectable with a larger study. Despite this, several other aspects of the cEAS did still appear to vary meaningfully with overall size and other characteristics.

Asymmetry in the cEAS is consistent in magnitude and direction to that found in previous studies of the CSF (Leonard et al., 2008). Assessed as a fraction of total endocranial volume, the cEAS was detectably larger on the right side. The magnitude of this difference was, however, less than 0.5% of total endocranial volume and in turn may be within the error margins of volume

assessment. Even still, this very small relative difference in volume fraction might indicate an important level of conservation in cEAS morphology. The larger right hemisphere of the brain is encased in a larger endocast, but maintains essentially the same proportion of total space around it. The level of asymmetry is enough such that differences between the sexes, and changes associated with body size were more profound on the consistently less voluminous left side.

When subdivided into superior (vault) and inferior (basal) components, the two entities very clearly varied in distinctive ways. In general, thickness measurements of the cEAS did not correlate with one another. This indicates a certain level of independence across the cEAS's extent. However, correlations that were detected tended to be positive when between two measures of the same component, and negative when comparing between them. Specifically, within the vault cEAS, thickness measures were positively interconnected. Although a few trades off in thickness between basal and vault cEAS were apparent, the two areas appeared to be largely independent in thickness.

5.0 Conclusions

We hypothesized that: (1) the factors influencing cEAS morphology differ between its vault and basal components. The results here partially support this hypothesis. The magnitude of asymmetry, sexual dimorphism, and strength correlations between cEAS metrics and body size characteristics were not found to be homogenous or even similar across the extent of the cEAS. However, the cEAS is not uniformly affected by or correlated to any of the characteristics

examined here in regional volume, thickness, or shape. We hypothesized additionally that (2) basal cEAS morphology is driven by body size factors, while (3) vault cEAS is influenced by sex and asymmetry. The results here do not support these hypotheses, and contradicted them in some ways. Body size factors of height and weight actually correlated with more cEAS thickness metrics from the vault rather than the base. Sex differences and asymmetry in the cEAS were detectable in the basal cEAS to the same and greater extent than those observed in the vault. Surprisingly, these results are nearly the opposite of what was expected based on what is known about the functional properties and developmental history of these two semi distinct areas of cEAS. It is perhaps unsurprising however that the proposed model of a two-part cEAS delineated here by the brains widest point is an under simplification of the true regional complexity of the space. These results are compelling evidence for continued examination into the driving forces of cEAS morphology.

The attempt to model cEAS morphology here is undeniably limited by the morphological characteristics that were chosen for its measurement, and the resulting metrics produced. This model of the cEAS also reduces the morphology of cEAS to a single entity describable as brain and skull when in fact there are unconstrained fluid, and solid tissue components to it. Formally modeling of the dural sinus or cerebrospinal fluid component of the cEAS individual would increase cohesion between reality and the anatomic model proposed here. Additionally, further subdividing of the cEAS total volumes by brain lobes, and

zeroing in on areas of high variability with respect to thickness measurements will direct future investigations to this morphology.

Tables

Table 2. 1: HCP-YA healthy control sample demographic characteristics.

Male	32
Female	36
White	45
Black	15
Asian*	7
More Than One	1
Unknown	0
Total	**68**

Table 2. 2: Landmarks and abbreviated defintions.

LANDMARK	Definition
Foramen Cecum	Anterior wall of foramen cecum, midline
Crista Gali	Most superior point of the crista gali, midline
Planum Sphenoidale	Most posterior point of the horizontal sphenoid, midline
Chiasmatic Groove	Groove of the optic chiasm, midline
Pituitary Fossa	Most inferior point on the pituitary fossa, midline
Posterior Clinoid Shelf	Centre of the posterior clinoid shelf, midline
Basion	Anterior foramen magnum as opposite of nasion, midline
Anterior Spinal Cord	Anterior spinal cord at level of foramen magnum, midline
Posterior Spinal Cord	Posterior spinal cord at the level of foramen magnum, midline
Opisthion	Posterior foramen magnum, midline
Anterior Frontal	Most anterior projecting endocranial point, midline
Bregma	Anterior end of the endocranial sagittal suture, midline
Vertex	Most superior point of the endocast
Obelion	Sagittal suture at the location of parietal foramina, midline
Lambda	Posterior end of the endocranial sagittal suture, midline
Confluence	Confluences of dural venous sinuses, midline
Straight Sinus	Start of the straight sinus, midline
Superior Pons	Superior most point of the pons, midline
Anterior Pons	Anterior edge of the pons, midway down, midline
Inferior Poins	Inferior most point of the pons
Superior Ventricle	Superior most point of the lateral ventricle
Frontal Ventricle Endocast	Frontal endocast at the level of landmark O1
Frontal ventricle Brain	Brain at the level of the landmark O1, opposite of O2
Anterior Clinoid Process	Posterior most point of the anterior clinoid process
Endocranial Asterion	Intersection of occipital, temporal bones on endocranium
Trigeminal Root	Trigeminal nerve as it exits the pons
Facial Root	Facial nerve as it exits pontomedullary junction
Hypoglossal Canal	Middle of the hypoglossal canal at its internal surface
Internal Auditory Meatus	Most lateral aspect of the internal auditory meatus
Lateral Clivus at IAM	lateral aspect of the clivus at O14
Medial Clivus at IAM	Medial aspect of the clivus at same slice as O13 and 14
End of CSF at Temporal Pole	End of the CSF compartment laterally at the temporal pole
End of CSF at Trigeminal Root	End of the CSF compartment laterally at the coronal slice of CNV
Frontal End of CSF (Y)	Anterior end of CSF compartment at sagittal CNV
End of CSF Trigeminal Root	Posterior end of CSF compartment at sagittal CNV
Frontal Pole	Most anterior projection of frontal lobe
Superior Precentral Sulcus	Most superior point of the precentral gyrus
Superior Postcentral Sulcus	Most superior point of the postcentral gyrus
Inferior Precentral Sulcus	Most lateral point of the precentral gyrus
Inferior Postcentral Sulcus	Most lateral point of the postcentral gyrus

Brain Eurion	Most lateral aspect of the brain
Cerebellar Eurion	Most lateral aspect of the cerebellum
Occipital Pole	Most posterior aspect of the occipital lobe
Cerebellar Pole	Most posterior aspect of the cerebellum
Inferior Cerebellum	Most inferior point of the cerebellum, not the tonsil
Inferior Cerebellar Tonsil	Most inferior point of the cerebellar tonsil
Inferior Temporal Lobe	Most inferior point of the temporal lobe
Temporal Pole	Most anterior projection of temporal lobe
Frontal Pole	Most anterior projection of frontal endocast
Endocast Eurion	Most lateral point of the endocast
Occipital Pole	Most anterior projection of occipital endocast
Inferior Posterior Cranial Fossa	Most inferior point of the posterior cranial fossa
Inferior Middle Cranial Fossa	Most inferior point of the middle cranial fossa
Jugular Bulb	Inferior most point of the jugular bulb within the jugular foramen
Anterior Middle Cranial Fossa	Most anterior potin of the middle cranial fossa
Petrous Root	Intersection of the superior petrosal sinus with the transverse

Table 2. 3: Results of error assessment on 3D model creation. Endocast volumes were the least affected by measurement error, followed closely by 3D brain models. TEM: Technical error or measurement rTEM: Relative technical error of measurement (TEM scale for magnitude of measurement). R: Relative proportion of measurement FREE from error.

	TEM	rTEM	R
Endocast	42177	0.84	0.95
Brain	49877	1.12	0.94
Ventricles	1348	3.79	0.8

Table 2. 4: Landmark placement precision in each dimension. Name, group, sequence taken (Left and Right when paired) and x-y-z error in landmark placement precision. Highlight in yellow are dimensions with placement differences > 1.0mm, in red are dimensions > 3.0mm. (continued on next page)

LANDMARK	NUM.R	NUM.L	X	Y	Z
Foramen Cecum	1		0.00	0.53	0.80
Crista Gali	2		0.00	0.41	0.56
Planum Sphenoidale	3		0.00	1.04	0.62
Chiasmatic Groove	4		0.00	0.23	0.20
Pituitary Fossa	5		0.00	0.35	0.22
Posterior Cleinoid Shelf	6		0.00	0.36	0.54
Basion	7		0.00	0.26	0.38
Anterior Spinal Cord	8		0.00	0.17	0.37
Posterior Spinal Cord	9		0.00	0.15	0.34
Opisthion	10		0.00	0.21	0.34
Anterior Frontal	11		0.00	0.11	0.89
Bregma	12		0.02	0.73	0.31
Vertex	13		0.02	0.87	0.12
Obelion	14		0.02	1.89	1.57
Lambda	15		0.02	0.67	1.11
Confluence	16		0.02	0.32	0.36
Straight Sinus	17		0.02	0.52	0.53
Superior Pons	18		0.02	0.19	0.13
Anterior Pons	19		0.02	0.18	0.43
Inferior Poins	20		0.02	0.17	0.24
Superior Ventricle	1	21	1.26	1.24	0.12
Frontal Ventricle Endocast	2	22	0.64	0.19	0.12
Frontal ventricle Brain	3	23	0.57	0.26	0.12
Anterior Clinoid Process	9	29	0.19	0.22	0.21
Endocranial Asterion	10	30	0.46	0.91	0.88
Trigeminal Root	11	31	0.16	0.31	0.11
Facial Root	12	32	0.34	0.20	0.14
Hypoglossal Canal	13	33	0.17	0.34	0.24
Internal Auditory Meatus	14	34	0.42	0.17	0.16
Lateral Clivis at IAM	15	35	0.32	0.51	0.16
Medial Clivis at IAM	16	36	0.32	0.19	0.16
End of CSF at Temporal Pole	17	37	0.40	0.13	0.52
End of CSF at Trigeminal Root	18	38	1.95	0.21	2.25
Frontal End of CSF (Y)	19	39	0.14	3.60	3.61
End of CSF (Y) at Trigeminal Root	20	40	0.14	3.55	1.52
Frontal Pole	1	14	0.93	0.16	1.50
Superior Precentral Sulcus	2	15	0.37	0.40	0.07

Superior Postcentral Sulcus	3	16	0.34	0.43	0.09
Inferior Precentral Sulcus	4	17	0.47	0.57	1.23
Inferior Postcentral Sulcus	5	18	0.17	0.85	0.99
Brain Eurion	6	19	0.08	1.50	0.97
Cerebellar Eurion	7	20	0.22	0.66	0.80
Occipital Pole	8	21	0.38	0.04	0.99
Cerebellar Pole	9	22	0.30	0.21	0.61
Inferior Cerebellum	10	23	0.57	0.22	0.00
Inferior Cerebellar Tonsil	11	24	0.50	0.40	0.15
Inferior Temporal Lobe	12	25	0.31	0.58	0.02
Temporal Pole	13	26	0.24	0.02	0.35
Frontal Pole	1	9	0.34	0.06	0.50
Endocast Eurion	2	10	0.05	0.44	0.66
Occipital Pole	3	11	0.28	0.02	0.68
Inferior Posterior Cranial Fossa	4	12	0.97	0.56	0.34
Inferior Middle Cranial Fossa	5	13	0.35	0.28	0.05
Jugular Bulb	6	14	0.51	0.48	0.19
Anterior Middle Cranial Fossa	7	15	0.24	0.21	0.49
Petrous Root	8	16	0.56	0.70	0.74

Table 2. 5: Pearson correlation coefficients of total cEAS volume and its associated component volumes. (NS): p > 0.1, (*): 0.1 > p > 0.05, (**) : 0.05 > p > 0.01, (***): p < 0.01

	cEAS	Endocast	Brain	Ventricle	cEAS
cEAS	1				
Endocast	0.49 ***	1			
Brain	-0.71 ***	0.49 **	1		
Ventricle	0.36 ***	0.26 NS	-0.29 **	1	
% cEAS	~ 1.00 ***	0.42 ***	-0.76 ***	0.36 ***	1

Table 2. 6: Pearson correlation coefficients between various cEAS thickness measurements. Correlations for the right side are to the right on the diagonal, left sided thickness measurements to the left of the diagonal. Yellow indicates p < 0.1, Green indicates p < 0.05.

	1	2	3	4	5	6	7	8	9	10	11
1. Anterior FM	-					-0.2	0.3		-0.2		
2. Posterior FM		-									0.2
3. Pons			-	0.2							
4. Frontal Pole				-				0.3			
5. Temporal Pole					-						
6. Occipital Pole					0.2	-	0.4				
7. Eurion			-0.3	0.3			-				-0.2
8. Frontal Vault				0.3	0.2			-			
9. PreCentral G	-0.2								-	0.8	
10. PostCentral G	-0.2									-	
11 CNVII Path	-0.3		0.3		-0.2	-0.3					-

Table 2. 7: Correlation coefficients for cEAS volumes and body-size measure. I cEAS Vol: Inferior cEAS Volume, Post. FM: posterior foramen magnum (Location 11), CN VII: Cranial neve VII path (Location 8), F vault: Frontal vault (Location 2), F Pole: frontal pole (Location 1). Yellow indicates $p < 0.1$ and green indicates $p < 0.05$).

	I. cEAS Vol.	Post. FM	CN VII	F Vault	F Pole
Height	0.240	0.20	0.21	NS	0.37
Weight	NS	0.21	0.31	-0.28	NS

Table 2. 8: Landmarks selected for EDM analysis by basal and vault component. Landmark numbers are specific to their respective subsets, and reference numbers refer to the master list of landmarks provided in table 2.2.

Basal cEAS EDM Landmarks

LMK #	Ref. #	Landmark Name
L1	B3/B16	Postcentral Gyrus
L2	E1/E9	Frontal Pole
L3	E2/E10	Endoeurion
L4	E7/E15	Temporal Pole
L5	ML1	Foramen Cecum
L6	ML11	Anterior Frontal
L7	ML12	Bregma
L8	ML13	Vertex
L9	ML14	Obelion

Vault cEAS EDM Landmarks

L1	E8/E16	Petrous Root
L2	ML18	Superior Pons
L3	ML19	Anterior Pons
L4	ML20	Inferior Pons
L5	B11	Inferior Cerebellar Tonsil
L6	O11/O31	Trigeminal Root
L7	O12/O32	Facial Root
L8	O13/O33	Hypoglossal Canal
L9	O14/O34	Internal Meatus
L10	O15/O35	Lateral Clivus
L11	O16/O36	Medial Clivus
L12	O9/O29	Anterior Clinoid Process

Table 2. 9: Statistically significant results from EDM analysis of the basal cEAS comparing males and females. Est is estimated form-difference for given landmark pair with associated low and high confidence interval estimates for alpha = 0.01. Landmark pairs with estimates < 1.0 are relatively larger in males, those with estimates > 1.0 are relatively larger in females.

ILD Pair	Side	Est.	Low	High
L7-L9	L	0.92	0.88	0.96
L10-L11	L	0.93	0.88	0.98
L6-L9	L	0.94	0.90	0.98
L4-L8	L	0.96	0.94	0.99
L4-L9	L	0.98	0.96	0.99
L9-L11	L	0.98	0.96	0.99
L2-L9	L	0.98	0.96	0.99
L3-L9	L	0.98	0.97	0.99
L8-L9	L	0.98	0.96	0.99
L9-L11	R	0.98	0.95	0.99
L3-L7	R	1.02	1.00	1.03
L5-L10	L	1.026	1.010	1.044
L6-L10	L	1.052	1.004	1.100
L7-L10	L	1.057	1.027	1.093
L3-L7	L	1.021	1.007	1.038

Table 2. 10: Significant results from EDM analysis of the vault. Significant landmarks (L2): Frontal pole, (L3): Endoeurion, (L4): Temporal pole. Est. is estimated form-difference between females and males with confidence interval for alpha = 0.01.

ILD Pair	Side	Est.	Low	High
L3-L4	R	0.97	0.95	0.99
L2-L3	R	0.98	0.97	0.99
L3-L4	L	0.97	0.95	0.99
L2-L4	L	0.98	0.97	0.99
L2-L3	L	0.98	0.97	0.99

Figures

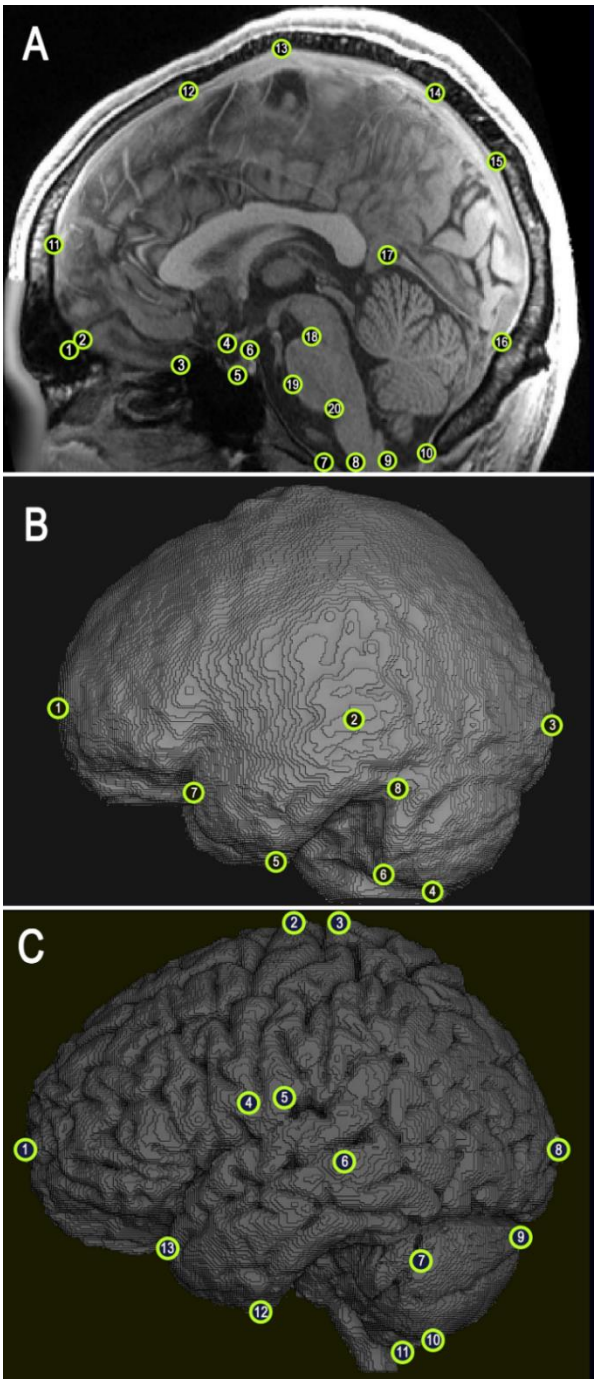

Figure 2. 1. Visualization of landmark locations taken from (A) MRI midsagittal slice, (B) endocast models, and (C) brain models. Numbers correspond to table 2.2 which contains landmark names and definitions divided by the groups seen here.

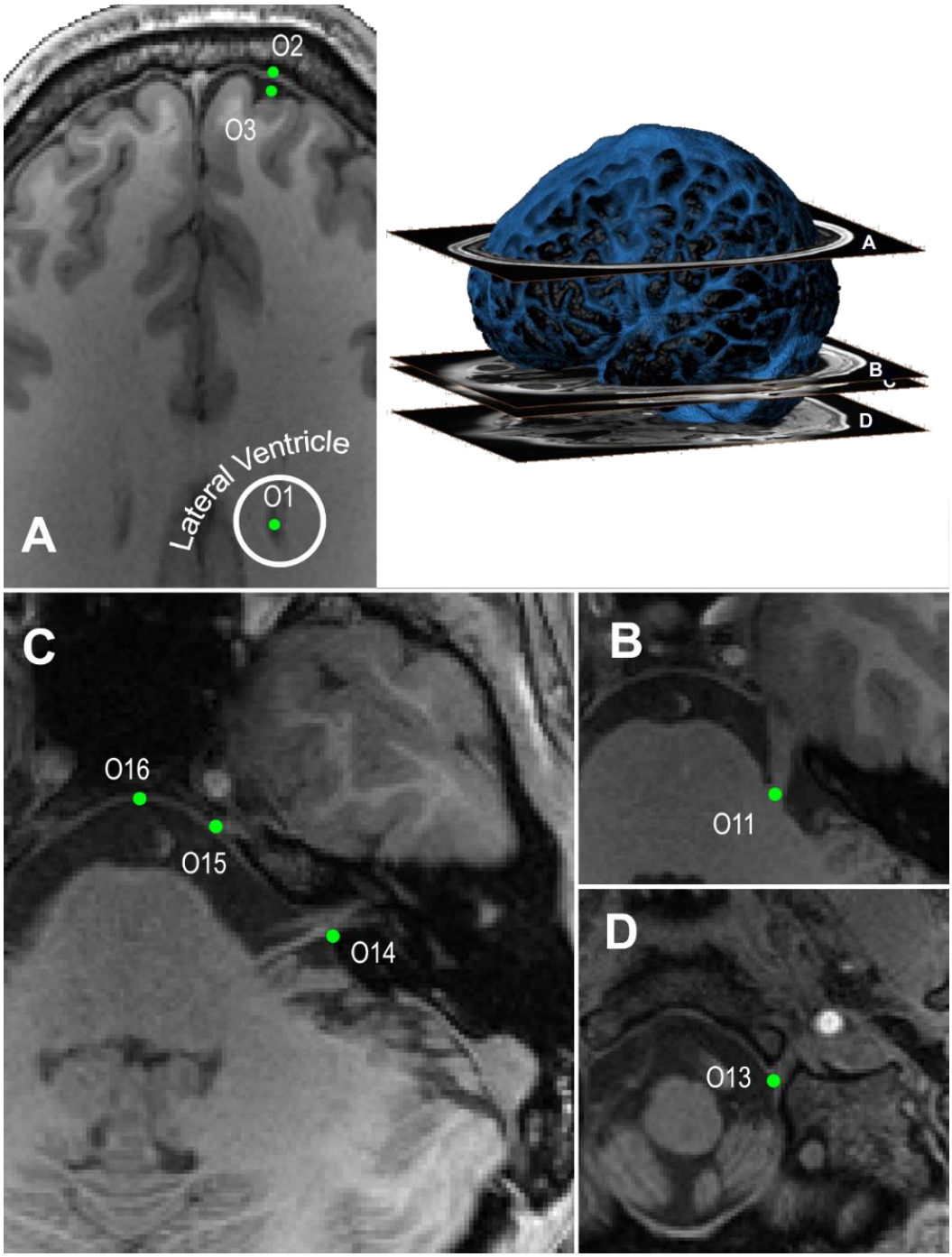

Figure 2. 2. Visual representation of orthogonal landmarks taken from MRI slice data. Relative positioning of transverse slices to 3D cEAS model in blue with actual slice data and landmark locations in panels A-D. (A) Superior-most lateral ventricle slice with landmarks O1-3. (B) Trigeminal root [O11]. (C) Lateral-most internal auditory meatus slice [O14], medial [O16] and lateral [O15] clivus landmarks. (D) Hypoglossal canal [O13] landmark slice.

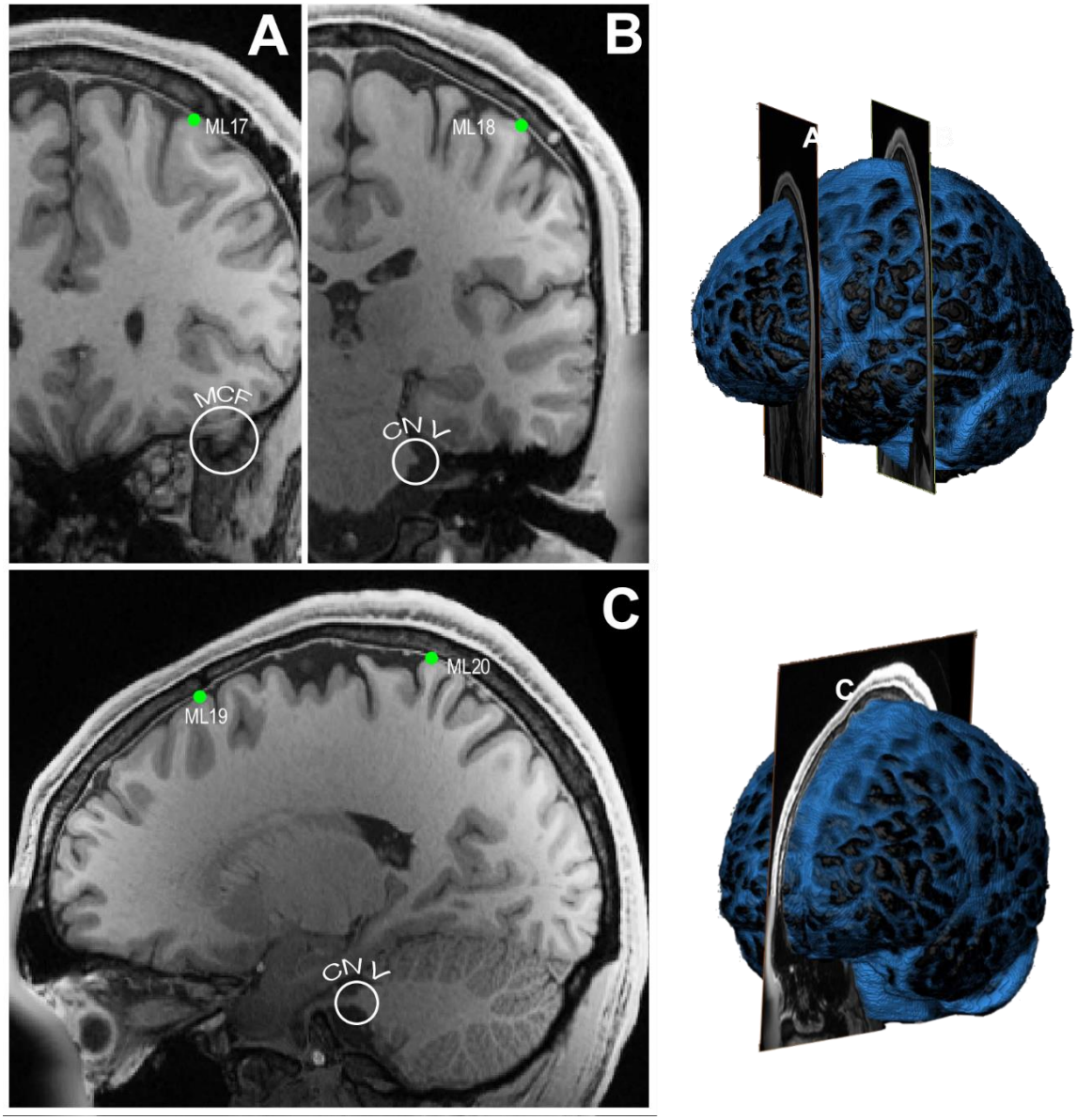

Figure 2. 3. Visual representation of the landmarks describing the end of CSF within the cranial vault cEAS. Blue 3D models of cEAS with locations of relevant planes defined by MRI slices are illustrated on the right with actual slices, the orienting landmark, and collected landmarks on the left. (A) Coronal slice at anterior-most middle cranial fossa. (B) Coronal slice at trigeminal nerve's exit from the pons. (C) Sagittal slice at the trigeminal nerve's exit from the pons.

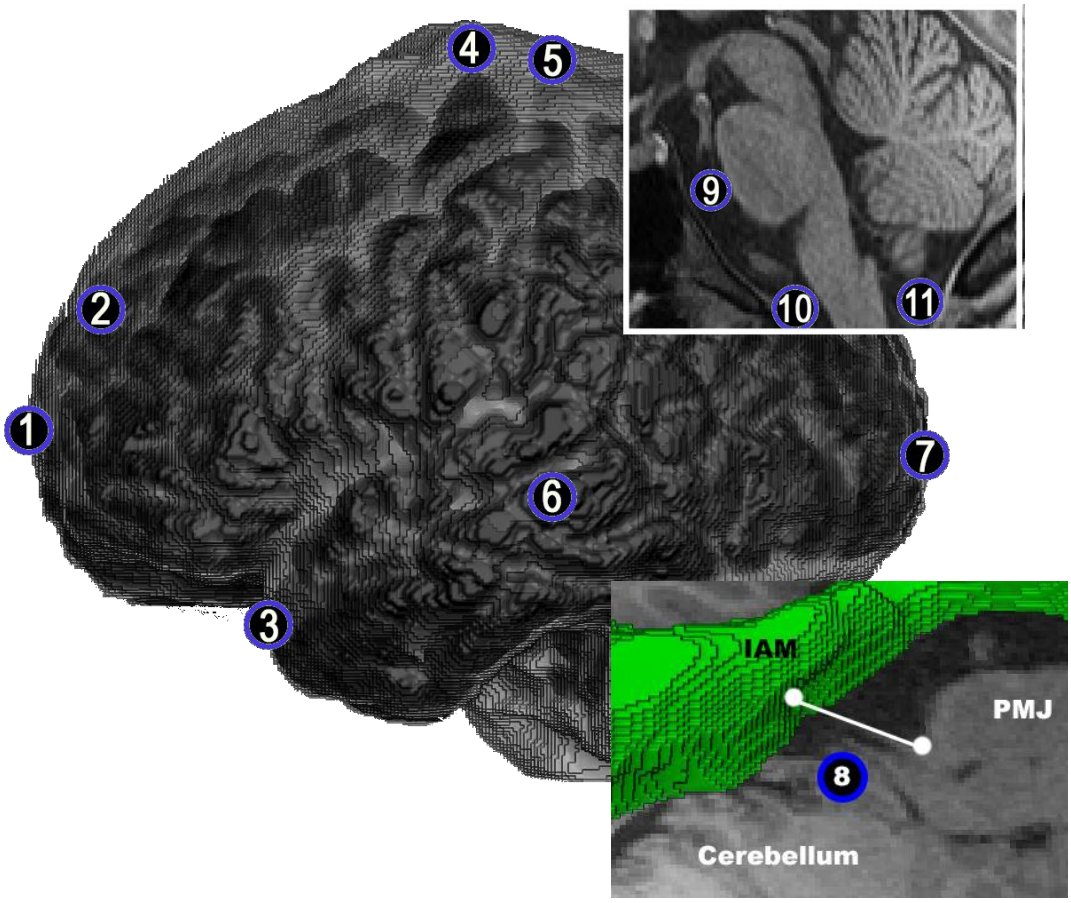

Figure 2. 4: Locations of cEAS thickness measurements 1-7 in blue circles on gray 3D model of cEAS and landmarks 9-10 on midsagittal MRI slice.

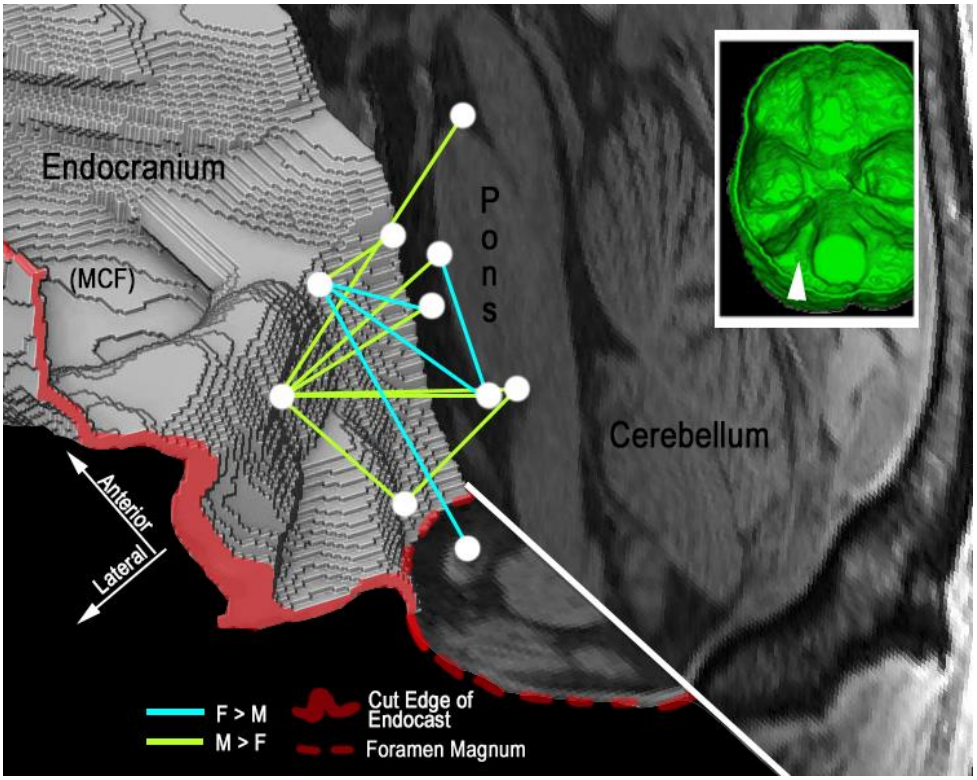

Figure 2. 5: Significant results from EDM analysis comparing male and female basal cEAS morphology. Autopsy view of the endocranium in green at inlay with white arrow showing the view from main figure. Landmark pairs relatively larger in males are in bright green, those relatively larger in females shown in light blue. (MCF) indicates the middle cranial fossa.

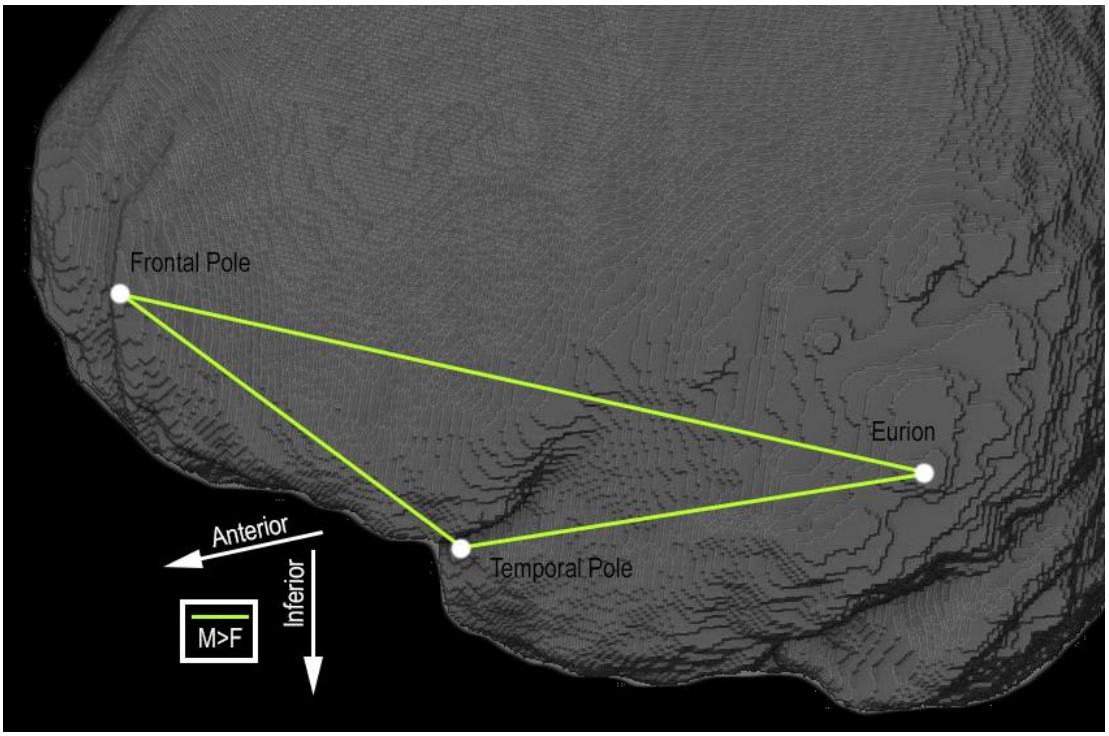

Figure 2. 6. Significant ILD results from EDM analysis comparing male and female vault cEAS morphology. Green lines indicate ILDs where males were relatively larger than females.

Chapter 3

Aging and Cranial Extra-Axial Space Morphology

Abstract

This section applies the direct measurement of cEAS morphology and variability to an aging sample. Aging is suspected to have the greatest influence on the size or shape of an individual's cEAS due in large part to the well-documented brain atrophy that comes with advancing age. Applying the same methods used to assess variation in normal young healthy individuals, that sample was here compared to an aging group of individuals with similar 'typical' health. As expected, cEAS increased in size with age, however, this was a result of both decreasing brain size and increased total endocranial volume. This increase in cEAS size was found to differ regionally, with some areas remaining relatively stable. In the clinic, the severity of brain atrophy is often measured using total intracranial volume as a stable proxy. However, this may be an incomplete picture of the evolving situational morphology of the cEAS.

1.0 Introduction

The cranial extra-axial space (cEAS) is one of, if not the most susceptible organs to the cruel process of aging. Cerebrospinal fluid (CSF) contained largely in the cEAS increases in volume as a direct response to cerebral atrophy. Described in more detail previously, the Monro-Kellie Doctrine again here applies

but now in reverse of its typical description (Mokri, 2001). Any decrease in the volume of one endocranial component (here the brain) necessitates an equal volume increase in another component (here the CSF) to maintain constant endocranial volume. Sometimes called hydrocephalus ‘ex vacuo,’ this tradeoff of brain for cEAS (CSF) volume has been observed and verified as a typical feature of aging numerous times and in several samples (Good et al., 2001b; Gur et al., 1991; Matsumae et al., 1996b). The details of this process have even more frequently been addressed in the framework of the brain’s anatomy, specifically.

Total brain volume reliably trends negatively with advancing age (Good et al., 2001b; Gur et al., 1991; Lemaître et al., 2005; Matsumae et al., 1996b; Mortamet et al., 2005; Raz et al., 2001). This negative slide begins as early as 20 years old and results in an approximate 10% loss in total brain volume by age 70 (Allen et al., 2002). Global brain volume loss increases in severity around the sixth decade of life, resulting in an additional 10% volume loss by age 80 (Scahill et al., 2003; Svennerholm et al., 1997). The apparent onset and rate of this additional decline is not homogeneous across the brain, varying regionally, and varies substantially between individuals (Allen et al., 2002).

Regions of the brain particularly susceptible to age-related reductions in the volume include the cerebral hemispheres, cerebellum, and subcortical nuclei (Golomb et al. 1993, Murphy et al 1996, Jernigan et al. 2001). Within the cerebrum, the frontal and temporal lobes have received significant attention, and appear to be the most affected by volume loss (Bartzokis et al. 2001). The temporal lobe overall, and specifically the hippocampus, also consistently

decrease in size with age (Allen et al., 2002). As a result of these local and widespread reductions in brain volume, the cEAS fills with CSF to occupy the space left by the atrophying brain. Due to its relatively thin distribution across the surface of the brain, these changes in cEAS can be relatively dramatic. This series of events relies on the assumption that endocranial skeletal morphology is mostly stable in adulthood.

Changes to the morphology and volume of the endocranium are most pronounced in development. During the first years of life, the brain increases in size dramatically and the cranial sutures remain patent and expandable. In the adult the endocranium is less anatomically dynamic, but some, albeit minor, fluctuations in its morphology have been documented. With advancing age, the endocranial sutures are more likely to become fused and visually obliterated (Junge and Hoffmeister, 1980; Meindl and Lovejoy, 1985; Ruengdit et al., 2020). In a similar trend, calcification or ossification and incorporation of periosteal dural elements into the bony endocranium is more common in advanced age (Kimball et al., 2015). Total endocranial volume, however, does not appear to vary significantly with age (Albert et al., 2007; Mortamet et al., 2005; Matsumae et al., 1996b). In instances where intracranial volume (ICV) does appear to vary with age, it has trended negatively and only slightly so as compared to the age-related changes observed in brain size (DeCarli et al., 2005; Irimia, 2020).

Given what has previously been reported about the structures of the cEAS, we hypothesize that (1) aging increases the overall volume of cEAS. The distribution of this volume increase is (2) non-homogenous across the cEAS's

extent and results in (3) increased variation of morphology with age in the cEAS. Lastly, the greater variation in cEAS morphology relative to its size makes it a (4) more sensitive morphological marker for changes in brain morphology or regional size changes than the brain is itself.

2.0 Methods

Similar to the sample assessed in chapter 2, individuals here were drawn from the Human Connectome Project (HCP). One of the offshoot projects of the HCP, the aging (A) sample was started to increase the age range of brain MRI data available for research. The HCP-A project is still collecting data, but at the time of this writing had released scans from 689 individuals of a planned total sample of 1200 of ages 36 to 100+ years. Individuals enrolled in this study were described as “typical” in their health condition for their age (Bookheimer et al., 2019; Harms et al., 2018). While participants are free of any pathological causes of cognitive decline (e.g. stroke, Alzheimer’s Disease), preclinical decline and prevalent conditions such as hypertension are represented in the cohort. Data were collected at four acquisition sites (University of Minnesota, Washington University St. Louis, Massachusetts General Hospital, and the University of California, Los Angeles) using a common digital and scanning protocol. The common protocol includes using the same model Siemens 3T Prisma scanner with 80mT/m gradients that are akin to the product grade version of the custom 100mT/m capable Connectome Scanner discussed in chapter 2. Scanning was also done on identical software versions using the same platform distributed

electronically. Structural (sMRI) data were acquired with a single T1 and T2 weighted scan resulting in 0.8mm isotropic voxels. These and additional specifics of scanning parameters used for the HCP-A sample can be found in Harms et al. (2018).

Structural scans from young individuals were the same as those described in detail in chapter two, from the Human Connectome Project – Young Adults (HCP-YA) sample. The HCP-YA individuals have higher quality MRI data than the HCP-A sample (0.7 vs 0.8mm). This is in part due to limitations on scanning time for older individuals. However, resolution of both data sets is higher than typical medical scan resolution (isotropic 1.0mm voxels), and these resolution differences are not likely to impart strong bias into the data.

2.1 Participants

Table 3.1 shows the breakdown of the two samples included here. A total of 113 individuals were modeled, landmarked, and assessed. This included the same 68 individuals between 22 and 36 years of age examined and detailed previously in chapter 2, referred to here as the HCP-YA sample. The remaining 45 individuals, include 24 males and 21 females aged 39 to 64 years, were drawn from the HCP-A sample described above and. The HCP-A sample self-described race was Asian (n = 6), Black or African American (n = 6), More than one (n = 2), and White (n = 28). Four individuals classified ethnicity as Hispanic or Latin (one Asian, one ‘more than one’, and two white). None of the additional demographic data available for the HCP-YA are currently available in the aging

sample. No additional exclusionary criteria were applied to the HCP-A sample before random selection of the 45 individuals for modeling.

2.2 Modeling and Data Collection Procedure

The same modeling methodology was applied to the HCP-A sample as was described in detail in chapter 2. Three-dimensional *in silico* endocast, brain, and lateral ventricle models were created in AVIZO 8.0. Models were segmented into superior/inferior and right/left sections, and voxel counts were collected for each. Due to the different voxel dimensions between the HCP-A and HCP-YA samples, slightly different conversion factors were applied to translate voxel counts to mL measurements of volume.

Three-dimensional landmark coordinate data were collected at the same 102 locations described in chapter two, in the same order, using the same strict definitions. Thickness metrics were calculated with the equations provided in Table S2.1 from the collected 3D coordinate data. Thickness metrics were scaled to their respective voxel dimensions in comparisons between the two samples. The subsamples of landmarks described in chapter two, representing the basal and vault cEAS were extracted for shape analysis.

In an attempt to minimize observer bias into the data, all modeling and landmark collection were performed blind to individuals' characteristics. All scans from the HCP-YA and HCP-A were pooled, assigned random accession numbers, and then modeled in ascending order.

2.3 Statistical Methods

Statistical analyses were performed using the software package R (R Core Team 2021). Volume data were assessed for assumptions of normalcy both visually with QQ-plots and quantitatively using Shapiro-Wilks tests. Group means were assessed using Students' t-tests (base R: t.test) for mean level differences in volume and thickness measurements. Statistical power assessments indicated that a sample of at least 30 individuals per group would be sufficient to detect differences in means of the magnitude expected here. Generalized linear modeling (glm) was used to examine cEAS morphology variable relationships with age. Models were ranked using Akaike's An Information Criterion (AIC) function to numerically compare them as necessary.

Principal components analyses (PCA) were also used to examine cEAS thickness measurements. Potentially highly interrelated measurements such as cEAS thickness can be summarized using PCA. PCA takes into account the interrelatedness of input variables by reorienting data into uncorrelated component axes that maximize multidimensional variance. The resulting principal components (PCs) describe a certain amount of variation in the given sample, taking into account the relative contributions of the different input measurements.

Analyses of morphology took place in winEDMA (Cole, 2002). Euclidean distance matrix (EDM) analyses are explained in detailed in section 2.3 of chapter 2.

3.0 Results

3.1 Volume of cEAS

Figure 3.1, and Tables 3.2 and 3.3 show endocranial volume relationships with age across the entire sample study (HCP-A + HCP-YA) and within the aging sample alone. Total cEAS ($r = 0.42$ $p < 0.001$), brain (-0.31 $p < 0.001$), and endocast or intracranial (IC) volume ($r = 0.30$ $p < 0.001$) volumes correlated significantly with age across the samples. Vault cEAS was found to differ significantly between young and aging samples, however no difference was observed in the basal cEAS. This was reflected in both the vault component of the brain as well as the total endocast. Superior or vault cEAS volume was strongly positively correlated with age in the aging group ($r = 0.33$, $p < 0.05$). Endocast volume however was not found to correlated with age inside of the aging sample, unlike both brain and cEAS. No correlation was found with the inferior component of any total feature. Superior/inferior components of the endocranium volume did not correlate with age either within the aging sample or across the combined sample.

No significant differences were found in total endocranial, brain, ventricular, or cEAS volume between males and females in individuals > 40 years of age. Volumes of cEAS subsections (superior/inferior and right/left) and quadrants also did not differ between males and females over the age of 40. Models of cEAS volume containing sex and sex-age interactions did not perform any better than those that only took into account individual age.

3.2 Distribution of cEAS

Results of cEAS thickness assessments are presented in tables 3.4 and 3.5. Comparing means, younger and older individuals differed significantly in cEAS thickness at 11 of 19 assessed locations. At locations around the vault, specifically in the vicinity of the frontal lobe, cEAS was significantly larger in older individuals. In contrast, the thickness of cEAS at cranial nerve VII (location 8) and the pons (location 10) were reduced in older individuals. Neither of these measurements showed a strong or statistically significant correlation with age across the combined sample or within the older individuals. The measurements most affected by age were those of the frontal pole, the frontal vault, and the precentral gyrus (locations 1, 2, and 4 respectively, see figure 2.5). No appreciable difference in the amount of cEAS were identified around the spinal cord, occipital pole, or most lateral extent (eurion).

The relationships among cEAS thicknesses also differed in the aging sample from those identified in healthy young individuals (see table 2.6 and 3.4). There are no apparent trade-off relationships in the HCP-A cEAS thickness results as were observed in HCP-YA described earlier. Only positive significant correlations between thickness measures were identified in the aging sample. The strongest of these relationships were all in the vicinity of the anterior frontal lobe (location 1, see figure 2.5).

Principal components analyses of cEAS thickness measures also indicate changes in cEAS interrelatedness with age. Graphic representation of PCA analysis is presented in Figure 3.2. Young adults assessed in chapter 2 showed

clear opposing groups of thickness measurements responsible for variation in PC1 and PC2 with a notably complex interplay between variances among measurements. This relation among cEAS thickness metrics is lost almost entirely with the addition of aging individuals. Interpretable as a measure of size, PC1 clusters the majority of cEAS thicknesses differentiating aging from young adults in one direction. The major exception to this is the pons, with other basal cEAS measures in this direction to a significantly lesser magnitude.

3.3 Shape of the cEAS

Euclidean distance matrix analyses also suggest the presence of shape differences in the cEAS of older vs younger individuals. Ratios and confidence intervals from winEDMA [FD] are provided in Table 3.7 for α=0.01. Statistically significantly different ILDs, those whose confidence intervals do not include 1, are illustrated in Figure 3.3. In the vault, significant shape differences present broadly as a relatively larger internal frontal chord (foramen cecum to bregma) in younger individuals and relatively wider and taller endocranial vaults in the older sample. Basal cEAS also differed between the older and younger samples (see Table 3.8). Older individuals examined here had increased cEAS in the cerebellar pontine cistern that approaches the prepontine cistern. Younger individuals, on the other hand, had relatively reduced cEAS in the most lateral and inferior cEAS, coupled with an increase in the height of the inferior pons and cerebellum.

4.0 Discussion

Older individuals had significantly greater cEAS volume than younger individuals. At the level of the mean, this difference is the result of not only smaller brains in older individuals but also larger endocasts. This is, however, an incomplete picture of the relationship between age and cEAS morphology. While older individuals had on average more endocranial capacity, this capacity was not found to correlate with age with the HCP-A sample. This is different from both brain and cEAS volumes which do correlate with age even within the aging sample alone.

Increased endocranial capacity in the HCP-A sample was an unexpected finding here. Endocranial capacity is allegedly a largely unchanging measurement in adulthood. The endocranial surface is not entirely stable over time, but the most notable feature in the literature seems to be additional ossification of periosteal dura mater, which would decrease intracranial volume as measured here. Further examination showed that the extra endocranial volume measure here is predominantly a feature of the superior or vault element. During this investigation, three individuals in the HCP-A sample were found to have especially voluminous vault cEAS due to the presence of deep fossae in the midline frontal and parietal bones (see Figure 3.4). Removal of these individuals from volume analyses did not eliminate the observed difference in endocranial volume, nor did it remove all older individuals with less extreme examples of these features. These large fossae present clear departures of the typically rounded endocranial morphology, and were observed in the younger sample as well, but not of the same magnitude (see Figure 3.4). These features

may play a role in this unexpected difference in endocranial volume with age, should it prove to be a finding repeated with another sample. However, for now, they represent an observational interest whatever the origin or potential significance.

Perhaps in contradiction to the hypothesis that this is an age-related feature, no positive relationship between age and total endocranial volume or vault endocranial volume was identified in either HCP-A or HCP-YA samples individually. If this volume increase is indeed a feature of age as it is with the cEAS, an appreciable correlation in at least one sample would be expected. The HCP-A sample was not as tightly controlled for potentially confounding health variables as was the HCP-YA. This was done to capture the effect of *aging* on cEAS morphology rather than age strictly. One overarching goal of these examinations was to assess the extent of normal variation in adult cEAS, and conditions such as elevated blood pressure or HbA1c measures are of such a high frequency in the aging population that exclusion of them entirely arguably creates a sample no longer representative of the normal aging population. Hidden in this weaker control and *not so great* science methods may be the variable responsible for the observed difference.

The two samples examined here did also differ slightly in the resolution of their sMRI data (isometric 0.7mm vs 0.8mm). It is possible this contributed to the directional difference in total ICV, however no apparent directional shift is visible in brain volumes collected from the same data. The creation of these two

anatomic models did differ slightly and the ease of their creation is by no means comparable; so it remains possible that this directional shit in endocranial volume observed here is the result of the 3D modeling process. It is of note, however, that both samples of sMRI data assessed here are of higher resolution than all structural assessments of brain aging discussed here and any mentioned in the review by Irimia 2020. The relative measurement error in 3D model endocast creation was also the lowest of the 3D models created for examination and centered in the basicranium, not the vault. These data cannot directly disprove that resolution differences may account for some of the observed differences observed here between HCP-A and HCP-YA individuals, however

As of writing, body size data were unavailable for the aging individuals. It is possible the HCP-A sample assessed here was randomly taller than the HCP-YA sample, accounting for the overall larger endocrania. This is unlikely as the basal features of cEAS appear more driven by height than those of the vault at least in younger individuals (see chapter 2), and these endocasts are larger specifically in the vault. In general, secular trends in population have been toward increasing height with birth year, the opposite of what this height explanation would require (Kim et al., 2018; Weisensee and Jantz, 2016). Other explanations for this mean difference may include broad unexpected secular population-level changes unassociated with body size, or simply that a casually biased sample was randomly selected. In any case, adding additional individuals from the HCP-A sample may shed additional light on the underlying cause of this unexpected finding. Single individual scans from the HCP-YA taken at a different resolution

may be available shortly for a precise assessment of voxel size on model creation at the scales discussed here.

The distribution of cEAS differed with age in multiple ways. Thickness measurements of the cEAS associated with the cerebrum were significantly positively related to an individual's age. As the cerebrum atrophies over time, the cEAS fills more space between the brain's surface and the relatively stable endocranial vault. Interestingly, the negative relationship between basal and vault cEAS measures observed in the HCP-YA sample was not observed in the aging sample. This appears to be due in part to the relative stability of the basal cEAS with age. The exception to this is the length of CN VII, which negatively correlates with age in the combined sample. Much like the increased endocranial volume, this difference is not apparent in either sample individually and is potentially related to body size. Reduced CN VII path length in the aging sample is more parsimonious with a hypothesized shorter sample, but until height data are made available this is speculative. Further complicating matters is the significant lateral component to this measurement, which is one of the dimensions in which the vault appears larger in the aging sample.

Shape differences elucidated through EDM analysis may help to clarify some of these patterns. Significant landmark pairs identified in the vault cEAS are collectively associated with overall endocast size and not cEAS morphology strictly. Aging individuals had relatively taller and wider vaults, while the younger individuals sampled were comparatively longer in the frontal chord (foramen cecum to bregma). Coupled with a positive correlation between vault but not

basal cEAS volume and age, these results support the extra endocranial volume origins in the vault. Some of this increased width's origin is reflected in the basal cEAS in an increased petrous length in the aging individuals. Basicranial width (biporionic width) is typically the most sexually dimorphic cranial measurement and is strongly associated with height (Weisensee and Jantz, 2016). This is a more direct indicator of the basicranial width of the measurements taken here than the cEAS thickness mentioned above. The increased endocranial width at this location is not enough to increase overall basal cEAS volume, however, and is partially counteracted by a reduction in the cerebellar pontine cistern's lateral extent in younger individuals.

5.0 Conclusions

Here we hypothesized that (1) aging increases the overall volume of cEAS. The data assessed here strongly supports this hypothesis. Overall and regional cEAS volumes increase with age, as does cEAS thickness at several locations. The distribution of this volume increase was hypothesized to be (2) non-homogenous across the cEAS's extent and result in (3) increased variation of morphology with age in the cEAS. The measurements taken here also support these hypotheses. cEAS thickness in the area of the frontal vault was positive correlated with age, but not in the lateral, posterior, or basal regions. Furthermore, the interrelatedness of cEAS measurements found in younger individuals (described in Chapter 2) was not observed in the older sample,

supporting the idea that cEAS morphological variation may be greater in the aging sample.

Tables

Table 3. 1: Sample breakdown. Details of sex and age distribution of HCP-A and comparison with HCP-YA samples. HCP-YA* is detailed extensively in chapter 2 section 2.1.

		HCP-YA*	HCP-A
Sex	**Male n**	32	22
Age	Mean	53.15	28.59
	Range	40-64	22-34
	SD	7.34	3.47
Sex	**Female n**	36	20
Age	Mean	51.05	29.31
	Range	39-64	22-34
	SD	7.56	3.52
Sex	**ALL n**	45	
Age	Mean	28.97	52.15
	Range	22-36	39-64
	SD	3.49	7.44

	S %	E_VS	E_VI	B_VS	B_VI	S_VI	S_VS	V_VOL	S_VOL	B_VOL	E_VOL	AGE
cEAS Fraction (S %)	-	0.020		0.000		0.000	0.000		0.000	0.000	0.000	0.030
E Superior (E_VS)	0.35	-	0.000	0.000	0.000		0.001		0.011		0.001	
E Inferior (E_VI)		-0.53	-	0.000	0.000	0.019					0.001	
B Superior (B_VS)	-0.52	0.55	-0.67	-	0.000	0.008	0.002		0.001	0.000		
B Inferior (B_VI)	-0.15	-0.56	0.88	-0.51	-					0.001	0.027	
S Superior (S_VI	0.73		0.35	-0.39		-	0.006		0.000	0.000	0.011	
S Inferior (S_VS)	0.91	0.50		-0.45		0.40	-		0.000	0.000	0.000	0.026
Ventricle (V_VOL)								-		0.013		
cEAS Total (S_VOL)	0.99	0.38		-0.50		0.72	0.92		-	0.000	0.000	0.047
B Total (B_VOL)	-0.70			0.52	0.46	-0.55	-0.53	-0.37	-0.62	-		0.006
E Total (E_VOL)	0.58	0.48	0.49		0.33	0.37	0.66		0.66		-	0.924
AGE	0.32						0.33		0.30	-0.41		-

	S %	E_VS	E_VI	B_VS	B_VI	S_VI	S_VS	V_VOL	S_VOL	B_VOL	E_VOL	AGE
cEAS Fraction (S %)	-	0.013	0.030	0.000	0.078	0.000	0.000	0.000	0.000	0.000	0.000	0.000
E Superior (E_VS)	0.24	-	0.000	0.000	0.000		0.000		0.005		0.000	
E Inferior (E_VI)	0.21	-0.65	-	0.000	0.000	0.000			0.013		0.000	
B Superior (B_VS)	-0.52	0.64	-0.7	-	0.000	0.000	0.000	0.003	0.000	0.000		0.006
B Inferior (B_VI)		-0.67	0.87	-0.55	-				0.163	0.000	0.030	
S Superior (S_VI	0.74		0.39	-0.39		-	0.000		0.000	0.000	0.000	
S Inferior (S_VS)	0.9	0.41		-0.44		0.4	-	0.000	0.000	0.000	0.000	0.000
Ventricle (V_VOL)	0.39			-0.28			0.4	-	0.000	0.000	0.060	0.000
cEAS Total (S_VOL)	1	0.27	0.24	-0.5		0.73	0.9	0.38	-	0.000	0.000	0.000
B Total (B_VOL)	-0.74			0.58	0.36	-0.56	-0.6	-0.38	-0.68	-	0.118	0.007
E Total (E_VOL)	0.55	0.44	0.38		0.21	0.38	0.59		0.62		-	0.001
AGE	0.42			-0.26			0.51	0.37	0.43	-0.26	0.32	-

Table 3. 2: Correlation matrix for volume relationships within the HCP-A (aging) sample. Pearson correlation (r) to the left and below diagonal, and significance values (p) for those where $p<0.05$ to the right and above the diagonal. Blank spaces left for non-significant correlations. (Previous Page)

Table 3. 3: Correlation matrix for volume relationships across all ages (HCP-A and HCP-YA) assessed collectively. Pearson correlation (r) to the left and below diagonal, and significance values (p) for those where $p<0.05$ to the right and above the diagonal. Blank spaces left for non-significant correlations. (Previous Page)

Table 3. 4: Correlation matrix for cEAS thickness relationships within the HCP-A (aging) sample. Pearson correlation (r) to the left and below diagonal, and significance values (p) for those where $p<0.05$ to the right and above the diagonal. Blank spaces left for non-significant correlations. (On Next Page)

Table 3. 5: Correlation matrix for cEAS thickness relationships across all ages (HCP-A and HCP-YA) assessed collectively. Pearson correlation (r) to the left and below diagonal, and significance values (p) for those where $p<0.05$ to the right and above the diagonal. Blank spaces left for non-significant correlations. (On Next Page)

Table 3.3	Fma	FMp	Pons	PoleF	PoleT	PoleO	Eurion	Maes	PreCG	PostCG	CN7	AGE
Ant. Foramen Magnum (FMa)	-						0.042			0.040	0.015	
Post. Foramen Magnum (FMp)		-										
Pons			-			0.009						
Frontal Pole (PoleF)				-				0.007				
Temporal Pole (PoleT)					-				0.009	0.005		
Occipital Pole (PoleO)			0.41			-						
Eurion	0.33						-		0.027	0.006		
Frontal Ventricle (Maes)				0.42				-		0.012		
Precentral Gyrus (preCG)					0.41		0.35		-	0.000		
Postcentral Gyrus (postCG)	0.33				0.44		0.44	0.40	0.72	-		
Cranial Nerve VII (cn7)	0.39										-	
Age												-

Table 3.4	Fma	FMp	Pons	PoleF	PoleT	PoleO	Eurion	Maes	PreCG	PostCG	CN7	AGE
Ant. Foramen Magnum (FMa)	-									0.031		
Post. Foramen Magnum (FMp)		-										
Pons			-								0.045	
Frontal Pole (PoleF)			-0.27	-				0.000		0.003		0.000
Temporal Pole (PoleT)					-	0.0159			0.027	0.001		
Occipital Pole (PoleO)					0.23	-						
Eurion						0.21	-		0.004	0.000		
Frontal Ventricle (Maes)				0.51				-		0.000		0.001
Precentral Gyrus (preCG)					0.21		0.28	0.29	-	0.000		
Postcentral Gyrus (postCG)	0.14			0.28	0.31		0.25	0.4	0.75	-		0.000
Cranial Nerve VII (cn7)			0.19								-	
Age				0.52				0.32		0.4		-

Table 3. 6: Form-difference matrix vault cEAS landmarks of HCP-A form matrix [F]/HCP-YA[F]. Confidence intervals are for 1000 resamples and alpha = 0.01. Landmark pairs with values that do not overlap with one are highlighted in green. Landmark numbers are found in the key presented in Table 2.8

HCP-A[F]/HCP-YA[F] LEFT					RIGHT Sided Vault ILDs				
Lmrks.		**Estimate**	**Low**	**High**	**Lmrks.**		**Estimate**	**Low**	**High**
L2	L4	0.94	0.83	1.04	L2	L4	0.94	0.84	1.05
L1	L2	0.94	0.88	1.00	L1	L2	0.94	0.88	1.01
L3	L9	0.97	0.87	1.06	L7	L8	0.98	0.93	1.01
L7	L8	0.98	0.92	1.02	L3	L7	0.98	0.95	1.01
L2	L6	0.98	0.96	1.00	L3	L5	0.98	0.97	1.00
L5	L6	0.99	0.96	1.01	L5	L9	0.98	0.95	1.01
L5	L9	0.99	0.95	1.02	L5	L6	0.99	0.97	1.01
L3	L5	0.99	0.97	1.01	L2	L6	0.99	0.97	1.00
L2	L5	0.99	0.98	1.00	L5	L8	0.99	0.98	1.00
L5	L7	0.99	0.98	1.00	L3	L6	0.99	0.98	1.00
L1	L5	0.99	0.98	1.01	L5	L7	0.99	0.98	1.00
L5	L8	0.99	0.98	1.01	L6	L9	0.99	0.97	1.01
L6	L9	0.99	0.97	1.01	L2	L5	0.99	0.98	1.00
L7	L9	1.00	0.95	1.04	L7	L9	0.99	0.95	1.04
L4	L5	1.00	0.99	1.01	L1	L5	1.00	0.98	1.01
L1	L9	1.00	0.98	1.02	L1	L9	1.00	0.98	1.02
L6	L8	1.00	0.99	1.01	L6	L8	1.00	0.99	1.01
L3	L6	1.00	0.99	1.01	L1	L3	1.00	0.99	1.01
L1	L6	1.00	0.97	1.03	L4	L5	1.00	0.99	1.01
L4	L9	1.00	0.98	1.03	L1	L4	1.00	0.94	1.06
L1	L8	1.00	0.99	1.01	L4	L9	1.00	0.98	1.03
L3	L7	1.00	0.97	1.03	L1	L8	1.00	0.99	1.02
L1	L3	1.00	0.99	1.01	L3	L4	1.00	0.99	1.02
L4	L8	1.01	0.99	1.02	L6	L7	1.01	0.99	1.02
L2	L9	1.01	0.98	1.03	L2	L9	1.01	0.98	1.03
L6	L7	1.01	0.99	1.02	L3	L8	1.01	0.91	1.10
L4	L6	1.01	0.99	1.03	L4	L8	1.01	1.00	1.02
L3	L4	1.01	1.00	1.02	L4	L6	1.01	0.99	1.03
L2	L8	1.02	1.00	1.03	L2	L3	1.01	1.00	1.02
L1	L7	1.02	0.99	1.04	L1	L6	1.02	0.98	1.04
L8	L9	1.02	0.94	1.09	L1	L7	1.02	0.99	1.04
L2	L3	1.02	1.01	1.03	L3	L9	1.02	0.91	1.11
L4	L7	1.02	1.00	1.04	L2	L8	1.02	1.00	1.03
L1	L4	1.03	0.97	1.10	L8	L9	1.02	0.95	1.08
L2	L7	1.05	1.02	1.07	L4	L7	1.03	1.01	1.05
L3	L8	1.05	0.97	1.14	L2	L7	1.05	1.02	1.07

Table 3. 7: Form-difference matrix of basicranial cEAS landmarks from the right sided. HCP-A[F]/HCP-YA[F]. Confidence intervals are for 1000 resamples and alpha = 0.01. Landmark pairs with values that do not overlap with one are highlighted in green. Landmark numbers are found in the key presented in Table 2.8 Right sided results.

Lmkrs		Estimate	Low	High
L3	L4	0.92	0.87	0.97
L4	L7	0.94	0.89	1.00
L7	L8	0.95	0.91	0.99
L10	L11	0.96	0.87	1.05
L4	L6	0.97	0.93	1.01
L3	L7	0.97	0.94	0.99
L1	L9	0.97	0.94	1.02
L2	L4	0.98	0.95	1.00
L3	L10	0.98	0.89	1.06
L10	L12	0.98	0.92	1.05
L3	L8	0.98	0.96	1.01
L1	L4	0.98	0.96	1.01
L3	L5	0.98	0.97	1.00
L1	L8	0.98	0.96	1.01
L5	L7	0.99	0.96	1.01
L5	L8	0.99	0.93	1.05
L1	L6	0.99	0.96	1.01
L1	L3	0.99	0.97	1.01
L1	L2	0.99	0.97	1.01
L6	L8	0.99	0.96	1.02
L3	L6	0.99	0.95	1.02
L1	L12	0.99	0.97	1.01
L1	L11	1.00	0.97	1.02
L4	L12	1.00	0.97	1.03
L3	L9	1.00	0.97	1.02
L8	L9	1.00	0.96	1.04
L4	L10	1.00	0.95	1.05
L1	L5	1.00	0.98	1.03
L4	L9	1.00	0.96	1.04
L11	L12	1.00	0.95	1.06
L2	L10	1.00	0.97	1.03
L6	L9	1.00	0.95	1.06
L5	L6	1.00	0.98	1.03

Lmkrs.		Estimate	Low	High
L1	L10	1.00	0.97	1.04
L1	L7	1.00	0.98	1.04
L5	L12	1.01	0.98	1.03
L4	L11	1.01	0.95	1.06
L2	L8	1.01	0.98	1.02
L8	L12	1.01	0.98	1.03
L2	L7	1.01	0.99	1.03
L2	L5	1.01	0.99	1.03
L2	L6	1.01	0.99	1.04
L5	L9	1.01	0.98	1.04
L7	L12	1.01	0.98	1.05
L2	L12	1.01	0.98	1.06
L5	L10	1.02	0.99	1.04
L8	L11	1.02	0.98	1.05
L2	L11	1.02	0.98	1.06
L9	L11	1.02	0.99	1.05
L4	L5	1.02	0.98	1.07
L8	L10	1.03	0.99	1.06
L6	L10	1.03	0.97	1.10
L4	L8	1.03	0.96	1.10
L7	L10	1.04	0.99	1.08
L3	L12	1.04	0.98	1.09
L6	L7	1.04	0.99	1.10
L9	L10	1.04	0.99	1.10
L2	L3	1.05	1.02	1.07
L3	L11	1.06	0.93	1.20
L7	L9	1.09	1.02	1.16

Figures

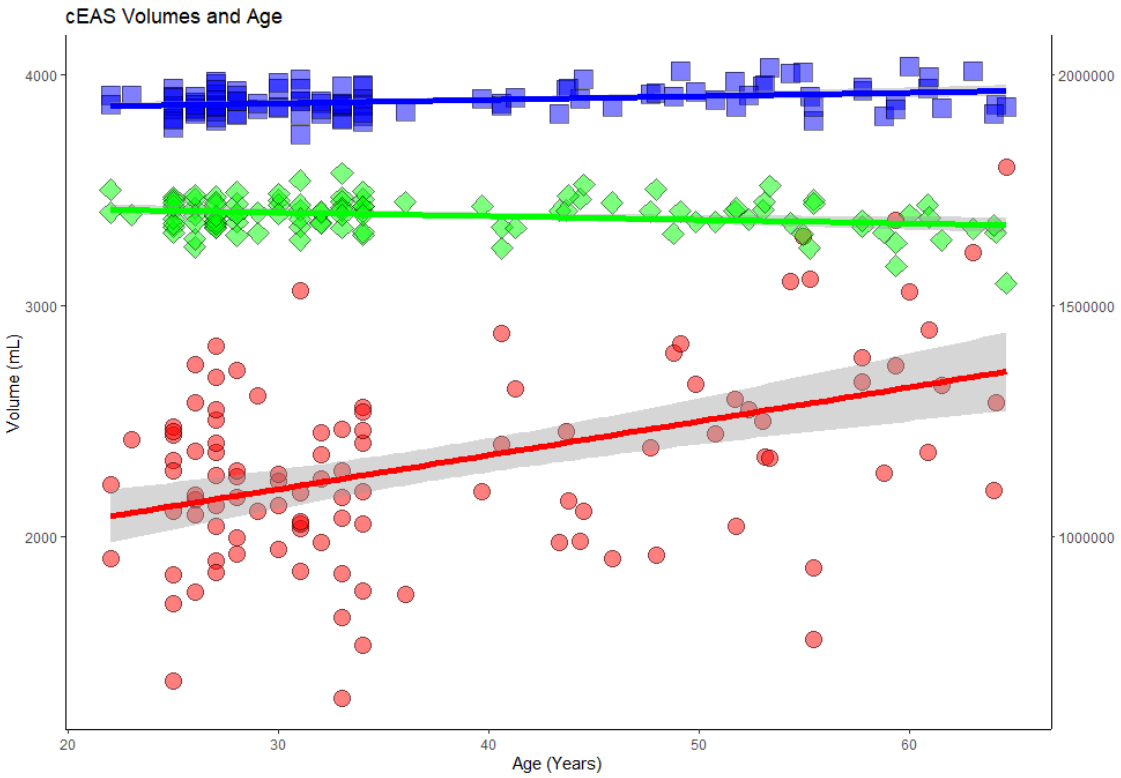

Figure 3. 1: Cranial extra-axial space volume and associated total intracranial (endocast) and brain volumes. The right axis is for unaltered brain and endocast volumes in mm^3. cEAS volumes on the left y-scale are in mL and scaled by a factor of 1/5 to better visually align the data. Red circles: cEAS Volume. Blue squares: total intracranial volume. Green diamonds: Total brain volume.

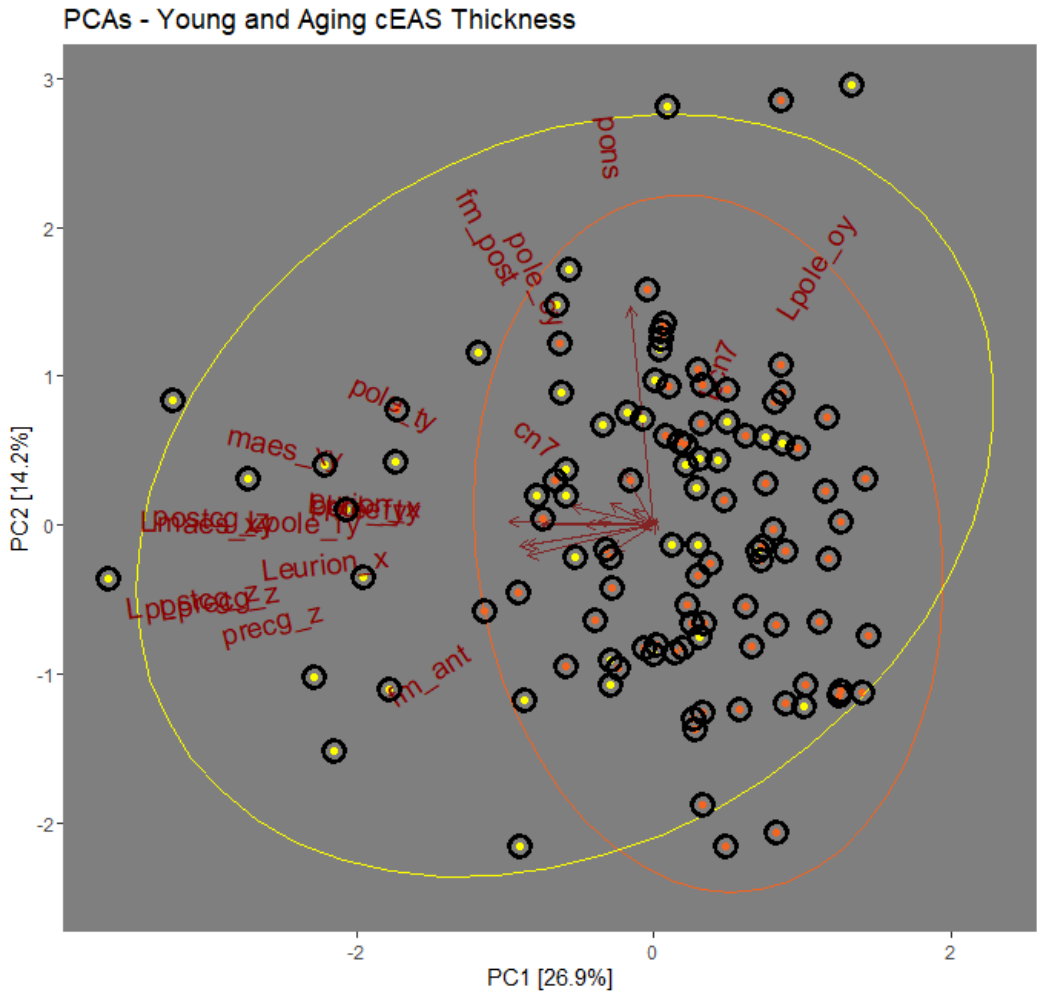

Figure 3. 2: PC1 and 2 from Principal components analysis of cEAS thickness measurements. Ellipses are for ggbiplot/ellipse.prob=0.95. Percentages are of variance explained by the given PC. Yellow are HCP-A individuals. Orange are HCP-YA individuals.

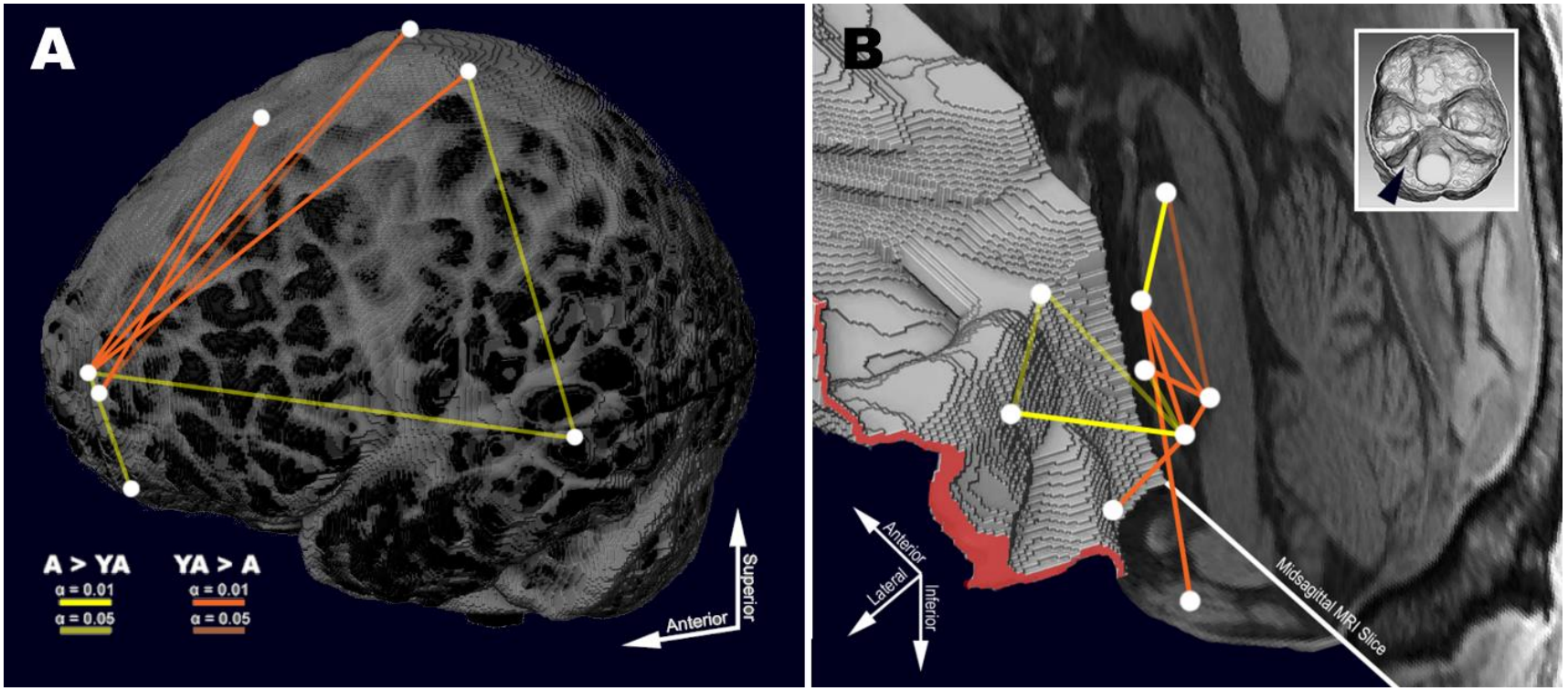

Figure 3. 3: Visual representation of significant results from EDM analysis of HCP-A and HCP-YA individuals. (A) Vault cEAS landmarks and (B) Basal cEAS landmarks and ILDs. Orange ILDs are those found to be relatively larger in young adults (HCP-YA), and in yellow are those larger in older or aging (HCP-A) individuals. Full opacity lines are for results of α=0.01 assessment, and 50% transparency are of results for α=0.05.

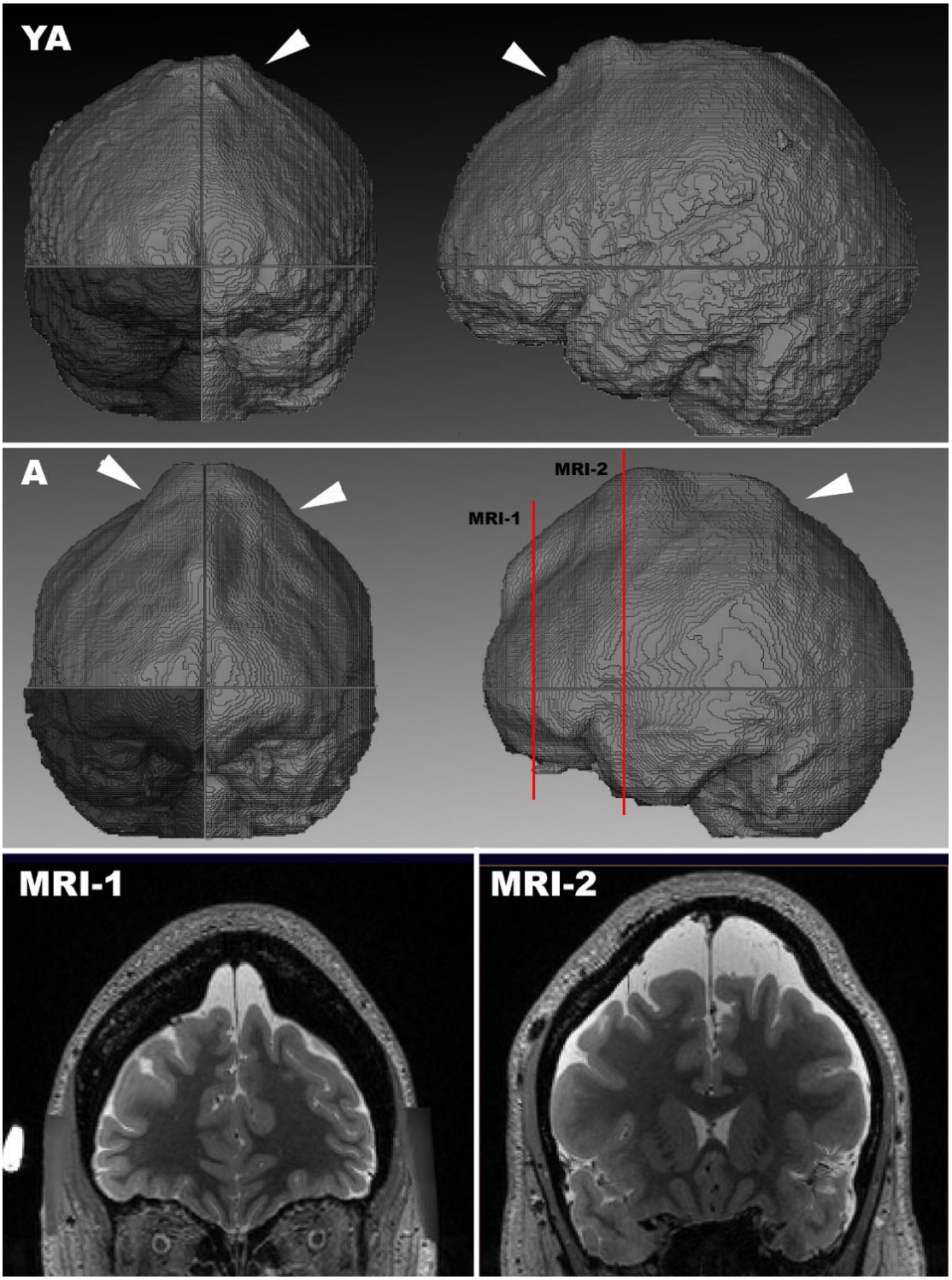

Figure 3. 4: Examples of midline fossa features. (YA) is from an HCP-YA individual (A) from aging HCP-A. Note sudden changes in endocranial roundness at white arrows. MRI slice locations in red for aging individual.

Chapter 4

Cranial Extra-Axial Space and Cannabis Use

Abstract

Public perceptions of cannabis over the last five decades have shifted dramatically and as a result, more individuals are readily consuming higher-potency cannabis products. Differentiating any anatomic consequences of long-term and high-strength cannabis use from pertinent clinical signs and the interactions of the two will be increasingly necessary as a result. Here we assessed the effect of cannabis use characteristics on cEAS morphology. In general, no significant changes were found to the morphology of the cEAS with any marijuana use characteristics. There is some indication of a slight difference in the basal cEAS of dependent individuals also related to the age of onset, which is consistent with findings in previous publications.

1.0 Introduction

Cannabis, or marijuana, is among the most widely used and abused drugs both globally and in the United States specifically. The 2020 US National Survey on Drug Use and Health reported 49.6 million users of marijuana in the last year, five times more users than the same year's second most used 'illicit' drug, [misused] prescription pain killers (SAMHSA, 2020). The Substance Abuse and Mental Health Services Administration (SAMHSA) also report the number of new cannabis users in that year as 2.8 million, outpaced only by alcohol. This is in

part due to the increasing legality and decriminalization of cannabis distribution across a significant portion of the United States.

As of late 2021, marijuana was entirely illegal in only four of the 50 states. Legalized cannabis for recreational purchase, on the other hand, is available in 18 states and prescribed medically in a further 19. With this increased cultural acceptance and widespread use, a better understanding of how cannabis affects the body broadly and the brain specifically is becoming progressively more important clinically.

1.1 A *Very* Brief History of Cannabis-Human Interaction

Cannabis sativa is a flowering plant native to Central Asia with a long and significant history of diverse exploitation by humans. In addition to being a source of workable fiber, archaeological evidence exists for use of seeds and leaves of the cannabis plant as a food source. Ingestion of the fruit (seeds), leaves, or the juice and oil byproducts of the plant likely led to the discovery of psychoactive and medicinal effects of the plant (Clarke and Merlin, 2013; McPartland et al., 2019). Genetic and phytochemical evidence suggests cultivation of *Cannabis sativa* specifically for these psychoactive and/or pharmaceutical purposes dates to at least 4000 years ago in Central Asia (Russo, 2007; Russo et al., 2008). Narcotic use of cannabis was widespread in the proverbial Old World and came to the Americas with some of its earliest colonizers (Small, 2015). Despite its recognized and appreciated effect on the brain, the primary psychoactive

molecule present in the cannabis plant, tetrahydrocannabinol (THC) would not be isolated for more than three millennia (Gaoni and Mechoulam, 1971).

1.2 Cannabis Use and Brain Morphology

As the chemical components of the cannabis plant were coming to light in a modern molecular scene, so too were the potential effects of its use on brain morphology. A year after the isolation of THC, Campbell reported on ‘atrophy’ in the brains of cannabis smokers in the Obstetrical and Gynecological Survey (1972). While Campbell’s papers are often the first cited in reviews of brain morphology and cannabis use, they bear little resemblance to studies of the structural morphology era that has evolved since. The majority of examinations in the following two decades took advantage of the ability to measure volume with the addition of a third dimension to medical imaging in the form of computed tomography (CT) scanning. Now able to examine the “whole brain”, teams working with CT quickly reported no differences in total brain volume (TBV) associated with any cannabis use parameters (Co, 1977; Kuehnle et al., 1977; Rubmaugh et al., 1980) Hannerz and Hindmarsh 1983, Wiesbeck and Taeschner 1991. Of these studies with negative findings, only Wiesbeck and Taeschner (1991) used any form of direct comparison with a control group, and in none was the sample of cannabis users greater than 19 individuals.

This timeframe would also see the first application of MRI to investigate cannabis’ effect on brain size and shape, as well as one of only two studies leading through 2021 to identify a TBV difference in adults associated with any

cannabis-use parameter. Aisley et al.'s (1993) examination of age of first marijuana use found that participants with age-of-onset before 17 years had lower total brain volumes, and were physically smaller in height and weight than non-using controls. The authors identified the effect in both males and females, but report a greater impact on males than on females (Aisly et al. 1993). Followed by an era largely devoid of published research into cannabis' effect on brain size, shape, or composition, Aisly et al.'s paper contained the largest sample of cannabis users up to then and until the twenty-first century, with 23 individuals (1993). One of the first papers to break this nearly decade-long stagnation appears to confirm some findings of its immediate predecessor and is the only other study to do so.

Wilson et al. (2000) compared 57 cannabis users by age of usage onset and verified that individuals who started smoking before age 17 had smaller total brain volumes than those that started after age 17. The authors also report that cannabis users who started before age 17 were physically smaller in height and weight, with the effect greater in males than in females (Wilson et al. 2000). No other study that reports on TBV has identified a statistically significant difference between cannabis using and non-using groups since then (DeLisi et al., 2006; Filbey et al., 2015; Gilman et al., 2014; Lopez-Larson et al., 2011; Solowij et al., 2013; Tzilos et al., 2005; Weiland et al., 2015; Yücel et al., 2008). It is of note that Tzilos et al. (2005) report an insignificant adjusted ($p = 0.33$) 45 mL difference between cannabis users and non-using controls. This is a greater

volume difference than the *significant* difference reported by Wilson et al. of 20mL in their male sample of early vs late cannabis users (2000).

All of these differences are small and represent approximately three percent differences in total brain volume where most studies are reporting an average brain volume of 1400-1600mm^3. Of those reporting on TBV, no other investigations detected differences related to cannabis use (Ashtari et al., 2011; Block et al., 2000; DeLisi et al., 2006; Gilman et al., 2014; McQueeny et al., 2011; Medina et al., 2007a; Schacht et al., 2012; Solowij et al., 2013; Weiland et al., 2015; Yücel et al., 2008). The sparce evidence for brain atrophy with cannabis use may be supported by investigations of cannabis abstinence.

The most marked difference reported between cannabis using and non-using individuals' total brain volume was observed in adolescents (< 20 years old). Ashtari et al.'s comparison between 14 non-users and 14 "treatment seeking" heavy-using individuals after six months of abstinence identified a 127mm^3 greater total brain volume in their cannabis-abstinent group (2011). Overall, the impact of cannabis on total brain volume appears to be only minimal, with the largest effects correlated to the age of the first usage. Considering the diverse physiology of the brain and well-known psychological effects of cannabis, it is unsurprising to suspect that cannabis may have stronger regional effects than global ones.

The cannabinoid receptors (CB1 and CB2) responsible for binding THC in the brain are found in variable concentrations across the brain. The highest receptor concentrations based on rat autoradiographic studies are within the

hippocampus, amygdala, orbitofrontal cortex, and cerebellum (Herkenham et al., 1991). This is consistent with many of the psychological effects of THC on the users, such as reduced short term memory, and altered sensation of time and contentiousness. To a lesser degree CB1 and CB2 receptors are present across the cerebrum, with the lowest concentrations in medulla (Mackie, 2008). Anatomic research has therefore focused on these regions of high receptor concentration and areas responsible for the altered mental status in THC-positive individuals.

The most widely examined of these regions, the hippocampus, consistently presents as *altered* in consistent cannabis users. The vast majority of studies examining the hippocampus report a volume decrease of between 6 and 10% in users compared to non-using controls (Ashtari et al., 2011; Battistella et al., 2014; Matochik et al., 2005; Medina et al., 2007b; Schacht et al., 2012; Yücel et al., 2016). Others have reported altered hippocampal morphology in cannabis users, but not a direct volume difference ((Solowij et al., 2013). The orbitofrontal cortex of the frontal lobe is the only other brain region to consistently show volume reduction in cannabis users across multiple available studies (Battistella et al., 2014; Filbey et al., 2014). These are the only regions to have consistent findings of the brain's morphologic response to cannabis use.

Investigations into numerous additional lobe-scale and subcortical regions have found contradictory results. A number of examinations have reported a volume reduction or shape alteration in the amygdala associated with cannabis use (Gilman et al., 2014; Lorenzetti et al., 2015; Schacht et al., 2012; Yücel et

al., 2008). However, another publication assessing 42 abstinent cannabis using teenagers found quite the opposite. 28-day abstinent female cannabis users had larger amygdalae than controls, while males were similar in size between groups (McQueeny et al., 2011). The most recent investigation of amygdala morphology found no detectable difference in either direction (Moreno-Alcázar et al., 2018). Complicating matters further, a study of the catechol-O-methyltransferase (COMT) gene and chronic cannabis use identified an influence of COMT polymorphism on amygdala volume in cannabis users and non-using controls. There is a correlation between number of allele copies and amygdala volume, but in opposing directions depending on the group (Batalla et al., 2013).

The cerebellum may be the brain region most volumetrically altered by cannabis use, with two studies reporting differences greater than 20% in regional cerebellar volumes (Cousijn et al., 2012; Solowij et al., 2011). Others, however, have found only slight volume reductions or no significant differences at all in cerebellar morphology associated with cannabis use characteristics (Block et al., 2000; Cohen et al., 2012; Medina et al., 2010). Across these regions, confounding results are at least in part due to differences in methodology, samples assessed, and comorbid tobacco and alcohol use. This is highlighted by the fact that the overall effect of cannabis on the cerebellum appears smallest when strong statistical control for confounding variables such as alcohol use is employed (Weiland et al., 2015).

Additional areas of the brain have received little to no attention, with several singular investigations into a structure's size, shape, or composition. So-

called altered gyrification has been observed in the different regions of the frontal and parietal lobes of cannabis-users (Gilman et al., 2014; Lopez-Larson et al., 2011; Mata et al., 2010). In general, these studies and those summarized above have relatively small samples, consisting of a handful of individuals. Broader extrapolation with many of these results is further complicated by the composition of these small samples, and the early evidence for sex-dependent or genetic trends.

Here we hypothesize that the previously reported potential regional effects of cannabis on the brain can be detected by assessing the cEAS. As the cEAS is a highly variable structure that directly changes morphology in response to any changes in the brain, an alteration of regional brain size or shape will be be reflected in the cEAS. (1) If marijuana use is associated with a volume reduction in any cerebral structures, then the relative vault cEAS should increase in volume and thickness. We also hypothesize that changes in the cEAS would be correlated with (2) marijuana use characteristics such as age of first use and total number of times used with heavier or dependent users showing more morphologic evidence of said use.

2.0 Methods

2.1 Participants

Individuals assessed here were drawn from the participants in the HCP-YA sample. For a detailed explanation of the HCP-YA sampling protocol, including exclusionary criteria and sMRI scanning protocol, see chapter 2. Table 4.1 contains the demographic information for the sample assessed here. The

marijuana-using (THC) group contained 47 individuals including 39 males and 8 females with a positive urine drug-screening for THC. Assessed individuals were between 22 and 36 years old, and right-handed. Self-reported race was recorded as white for 22, black or African American for 19, 1 Asian/Native Hawaiian/Pacific Islander, two 'more than one', and three unknown or not reported. Six individuals self-reported ethnicity as Hispanic/Latino, including the three categorized as race unknown. The healthy control (HC) or drugs-negative individuals used for comparison were drawn from the same sample assessed in chapter two. The HCs included 36 females and 32 males, with no self-reported history of any drug use other than marijuana, but with a negative urine screening. Additional detail on the HC sample can be found in table 2.1 of chapter 2.

In both samples, self-reporting through the Semi-Structured Assessment for the Genetics of Alcoholism (SSAGA) was used to further quantify marijuana use. Age at first use is portioned into four groups with specificity around the teenage years (1: < 14 years, 2: 15-17years, 3: 18-20years, 4: >21years). Total times used marijuana was grouped into five categories (0: never used, 1: 1-5x, 2: 6-10x, 3: 11-100x, 4: 101-1000, 5: >1000x). Table 4.2 contains the breakdown of the sample by these additional marijuana use characteristics. Twenty-two (22) of the THC-positive sample were SSAGA-classified as 'Marijuana dependent', all with use over 100x. The significant majority of THC-positive individuals assessed here were heavy users classified as a 4 or 5 on the SSAGA for total times used.

2.2 Three-Dimensional Modeling and Data Collection

The same exact modeling, subsampling, and landmarking procedures were used here as detailed in chapter 2 section 2.2. Three-dimensional endocast, brain, and ventricle models were created and subdivided into super/inferior quadrants. Three-dimensional landmark coordinate data were collected from 102 bilateral and midline landmarks detailed in chapter 2. Coordinate data were used to calculate thickness measurements of the cEAS at 19 locations detailed in chapter 2 figure 2.6. Landmarks were subdivided into basal and vault cEAS components listed in table 2.8 for EDM analyses.

2.3 Statistical Methods

Similar statistical methods were used here as are elaborated up on in the section 2.4 of chapter 2. Groups were compared for mean differences in the collected metrics, and linear models were fit to the marijuana use characteristics data. Principal components (PC) and Euclidean Distance Matrix (EDM) analyses were also used to assess cEAS thicknesses and landmark distributions. For detailed explanation of the purposes of these analyses, see section 2.4 of chapter 2.

3.0 Results

3.1 THC Positivity

No significant differences between the HC and THC were found in total, superior, or inferior volumes of cEAS after controlling for height. There is a statistically significant difference in height between the HC and THC positive

groups. This is partly due to the imbalanced sex ratio, and on average taller males as discussed in chapter 2. None of the individually calculated thickness measures assessed was found to differ between HC and THC positive groups either when height was taken into account, or when females were removed from analysis. This was true of both the right and left sides, as well as the magnitude of asymmetry at homologous locations.

The assessment of shape via EDM analyses were also affected by the sample sex imbalance. A significant number of ILDs identified as potentially different between the mixed-sex THC and HC samples were pervious identified as sex-differences in chapter 2, (Tables 2.9, 2.10, and Figure 4.1). Comparing only males from the HC and THC samples eliminates many of the mixed-sex identified ILD ratios. Figure 4.2 depicts the ILDs found to differ significantly between HC and THC-positive males. All right-side ILD ratios for the male only comparison can be found in Table 4.3. In the vault, significantly different ILDs were limited to large scale differences in the endocast rather than cEAS specific changes. Basal cEAS, on the other hand, appears to be broader in healthy controls males compared to THC-positive males. Only two ILDs were found to be statistically significantly different between the two groups at the higher level of statistical conservancy (alpha=0.01).

3.1 Characterized Marijuana Use

Each of the SSAGA marijuana use descriptors was strongly correlated with one another (Table 4.4). Dependent marijuana users were more likely to

have started younger, and used more times than non-dependent individuals. Differences in the cEAS associated with characteristics of marijuana use were detectable at only a marginal level of significance ($p < 0.10$). Total cEAS volume was positively correlated with marijuana abuse and dependance ($r = 0.21$, $p = 0.07$). This trend was also detectable in the volume of basal cEAS individually, but not in the vault component. Inferior cEAS volume was also weakly correlated to age at first use ($r = -0.23$, $p = 0.10$), but not total number of times used ($p = 0.81$).

Focal assessment of cEAS thickness did not identify any locations that individually account for the increased cEAS volume seen in marijuana dependent individuals (Table 4.5). The midline thickness of cEAS anterior and posterior to the spinal cord within the foramen magnum were both positively correlated to age at first use. Posterior to the spinal cord, the cEAS was found to decrease in size with increased total times marijuana used at a marginal level of statistical significance ($r = -0.21$, $p = 0.06$). No other relationships between marijuana use characteristics and cEAS thickness were identified. Principal components analysis of thickness measurements also did not identify any differences based on any use characteristics in the overall thickness measurement data (Figures 4.3 and 4.4) The first six principal components were assessed based on relative proportion of variance accounted for, which became less than that of the individual ILDs after PC6.

4.0 Discussion

Previous research into cannabis use and brain morphology has been largely inconclusive outside of hippocampal morphology, which is not without its disputes. Here we attempted to characterize brain atrophy related to cannabis use characteristics by measuring the cEAS. It was expected that if brain size is decreased and morphology is altered by THC-positivity, dependence, age of first use, or THC positivity then the cEAS should be measurably increased in size or altered in its respective morphology. THC-positivity itself was not found to directly affect cEAS morphology. However, some patterns of cEAS morphology do appear related to cannabis use characteristics.

Although no increase in total cEAS volume was associated with cannabis use, the inferior portion of cEAS volume was found to be larger in marijuana dependent individuals. This was directly associated with a decreased inferior brain volume in dependent individuals and no associated difference in endocast volume. This is consistent with the added finding of increased cEAS thickness around the spinal cord in younger cannabis using individuals. Unlike previous studies that found overall decreased body size with younger age of first use, here no difference in body size, endocast volume, or cEAS metrics previously associated with body size (see chapter 2 figure 2.6 and 2.7) was observed.

Most of the temporal lobe, importantly the pole, and cerebellum are included with the inferior models of brains and endocasts evaluated here. These areas were suspected to be the most affected by cannabis use and abuse and therefore reflect heavily in the cEAS. While basal cEAS volume was affected

positively, thickness measurements do not support the localized reductions specific to the temporal lobe or cerebellum as hypothesized. Thickness measurements, however, do indicate a change around the spinal cord and foramen magnum. Some studies, including those with negative overall findings, have mentioned increased CSF space around the temporal pole as an incidental observation of their cannabis using samples (DeLisi et al., 2006). No support was found for an increase in the distance between the temporal pole and the middle cranial fossa in the sample assessed here. It may be that the deep structures of the temporal lobe do not greatly impact the cortical surface morphology of the temporal lobe with respect to cannabis use, or that this effect is not measurable at the pole.

Overall changes to the cEAS indicative of generalized cerebral atrophy as explored in chapter 3 were also not detected. No vault cEAS measures increased with any cannabis use characteristics like in aging, and no changes in vault cEAS shape associated with MJ use characteristics were detectable.

5.0 Conclusions

In this section we hypothesized that: (1) cannabis (marijuana) use (THC positivity) would be associated with an increase in the total cEAS volume, or regional thickness measurements. The results of analyses preformed here do not support this hypothesis. No individual cEAS metrics were found to differ significantly between THC+ and HC groups. We also hypothesized that differences in the cEAS would be correlated with (2) marijuana use

characteristics with heavier or dependent users showing greater morphologic evidence of said use. Only very weak support for this hypothesis was found in the area around the foramen magnum/spinal cord. None of the expected increases to the temporal region cEAS or any vault thickness measurements were observed. The cEAS may however still be a valuable measure of the effect of THC on brain anatomy. The conclusions of this study may be limited by the relatively small sample assessed here for each of the individual cannabis use characteristics was relatively small for each category, and the measurements may not capture the full but perhaps mostly local complexity of the brains changes with marijuana use and abuse.

Additional examination of the cEAS morphology specific to the temporal lobe may be one such avenue of value with respect to these hypothesis specifically. The amount of cEAS around the temporal lobe was quantified in this study only as the anterior thickness from the temporal pole. This is undeniably an under simplification of the cEAS morphology in the area, and does not capture the full extent to with cEAS may vary in the region. Addition of more characteristics such as the temporal lobe's width, anterior curvature, or a focused regional volume of the cEAS may more adequately capture the morphology of this region and identify potential differences. Increasing the modeled sample would also increase the power to identify smaller differences than what was possible here. The limit to additional modeling being an overall lack of human will-power.

Tables

Table 4. 1: Sample demographics for healthy control/THC negative sample (HC) and THC positive (THC+) sample. (*) Includes individuals self-reporting native Hawaiian and native pacific islander.

	HC	THC +
Male	32	39
Female	36	8
White	45	22
Black	15	19
Asian*	7	1
Multiple	1	2
Unknown	0	3
Total	**68**	**47**

Table 4. 2: Marijuana-use quantification [A] Age at first use and [B] total times used. Healthy control (HC) individuals have a negative urine drug screening, (THC) individuals were positive for THC.

A	HC	THC	TOTAL
Never	42	2	44
1-5x	10	3	13
6-10x	5	4	9
11-100x	7	4	11
101-1000	2	9	11
>1000x	2	25	27

B	HC	THC	TOTAL
Never	42	2	44
< 14 Years	0	10	10
15-17 Years	10	21	31
18-20 Years	12	7	19
> 21 Years	4	7	11

Table 4. 3: Results of EDM analyses of THC+ and HC males. Landmark (LMK1 and LMK2) abbreviation numbers correspond to subsections elaborated upon in table 2.8. Confidence intervals are calculated for alpha level 0.10, only those not contained a ratio of 1 (sameness) are included.

Vault cEAS [F]THC+/[F]HC

LMK1	LMK2	LOW	EST	HIGH
L1	L6	0.98	0.97	0.99
L1	L4	1.02	1.01	1.04
L1	L2	1.03	1.01	1.05
L3	L8	1.15	1.07	1.22

Basal cEAS [F]THC+/[F]HC

LMK1	LMK2	LOW	EST	HIGH
L8	L9	0.95	0.93	0.98
L7	L9	0.96	0.95	0.99
L1	L2	0.97	0.95	0.99
L2	L9	0.97	0.96	0.99
L3	L9	0.98	0.96	0.99
L8	L10	1.05	1.01	1.08

Table 4. 4: Marijuana use characteristics correlation matrix. Pearson product moment correlation (r) values to the left and below the diagonal, significance (p) values to the right and above.

	D	1st	X
Dependence (D)	-	0.007	< 0.001
Age 1st Use (1st)	-0.36	-	< 0.001
Times Used (X)	0.64	-0.59	-

Table 4. 5: Marijuana use characteristics correlation to cEAS volume metrics. (*) indicate correlations with significance level 0.05 > p > 0.10. Other correlations not significant.

	D	1st	X
cEAS Volume	0.21*	-0.08	0.04
Superior cEAS Vol.	0.09	0.02	0.05
Inferior cEAS Vol.	0.20*	-0.23*	0.03

Table 4. 6: Marijuana use characteristics correlation to cEAS thickness metrics. (*) indicate correlations with significance level 0.05 > p > 0.10. (***bold**) indicates correlations with significance p < 0.05. Other correlations not significant. (D): Dependence (1st): Age first use (X): Times used.

	D	1st	X
Ant. Foramen Magnum (FMa)	0.04	0.24*	0.01
Post. Foramen Magnum (FMp)	-0.08	**0.27***	-0.21*
Pons	-0.06	0.03	0.03
Frontal Pole (PoleF)	0.15	0.05	0.00
Temporal Pole (PoleT)	0.06	-0.03	0.15
Occipital Pole (PoleO)	0.08	0.22	0.16
Eurion	0.15	-0.14	0.08
Frontal Ventricle (Maes)	-0.06	0.05	-0.01
Precentral Gyrus (preCG)	-0.10	0.03	-0.06
Postcentral Gyrus (postCG)	0.00	-0.09	0.05
Cranial Nerve VII (cn7)	0.03	0.02	0.17

Figures

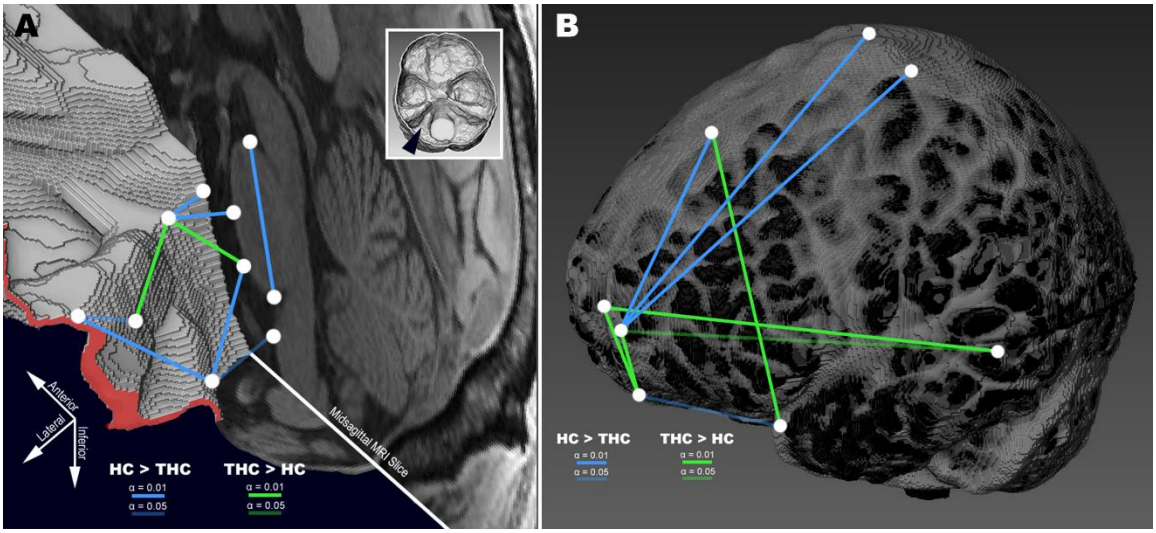

Figure 4. 1: Results of EDM analyses of (A) basicranial cEAS and (B) vault cEAS for combined male and female sample. Blue landmark pairs for HC>THC and green where THC>HC.

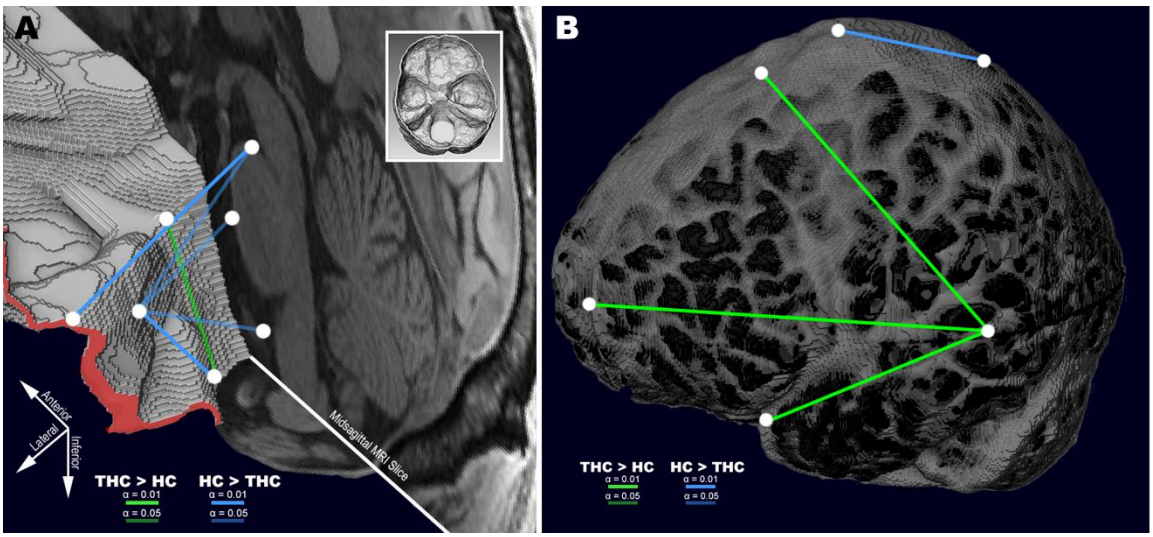

Figure 4. 2: Results of EDM analyses of (A) basicranial cEAS and (B) vault cEAS for male only sample. Blue landmark pairs for HC>THC and green where THC>HC. Full intensity lines are for alpha level 0.05, 50% transparency lines are for significant ILDs with alpha level 0.1.

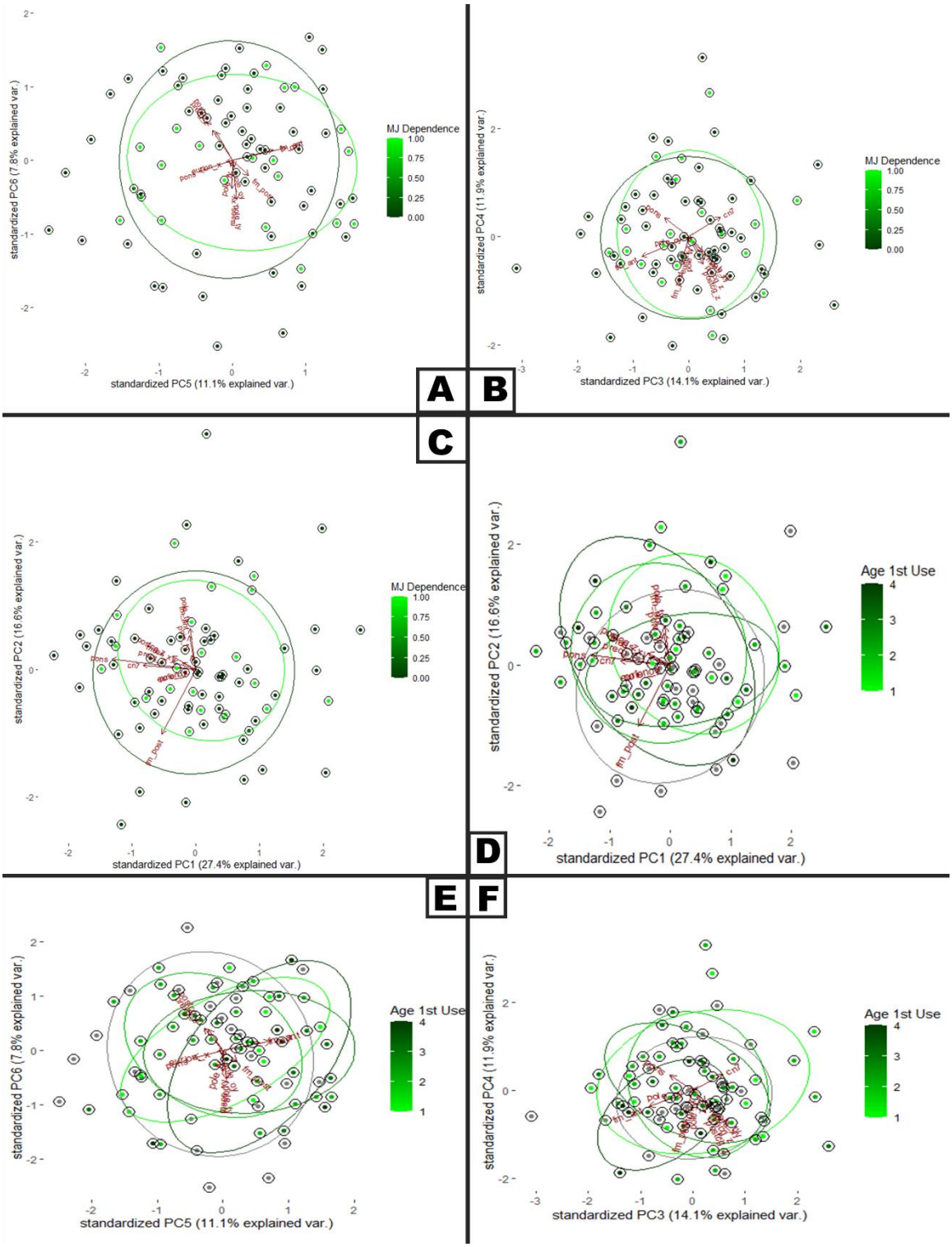

Figure 4. 3: Results of PCA for cEAS thickness measurements and marijuana use characteristics (A-C): Marijuana Dependence, (D-F): Age at 1st Use.

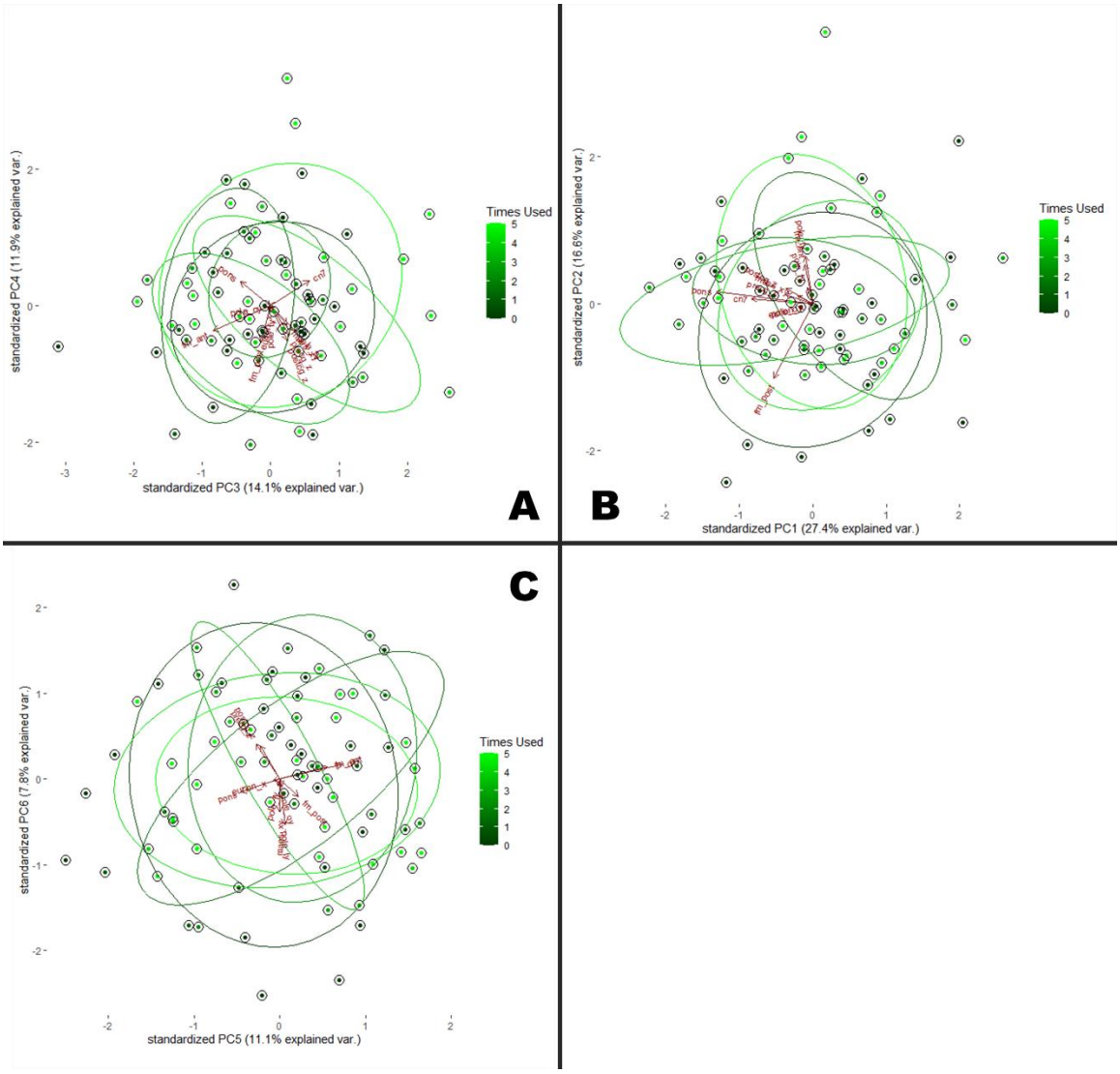

Figure 4. 4: Principal components of cEAS thickness measurements grouped by marijuana use characteristic (Times used).

Chapter 5

Conclusion

The brain is a convoluted organ with morphology that can be difficult to capture in isolation. Using the cEAS to assess the morphology of the brain relative to its container, the skull, may therefore allow for more precise assessments of the brain's morphology than attempts to assess it alone. The cranial extra-axial space (cEAS) is an exceptionally flexible organ morphologically considering its proximity and importance to its enclosed brain. Characteristics like the overall size, biological sex, and age were shown here to have a relatively strong influence over this variation, but a significant fraction remains unexplained in the context of normal or typical anatomic variation. There is still substantial room left for the identification of additional potential sources of this variation. The continued understanding of the driving forces of cEAS morphology may also then prove to make the cEAS a highly sensitive indicator of brain anatomy.

1.0 General Conclusions

Size, shape, and distribution of the cEAS were found to be highly variable in response to a number of individualistic characteristics in the present study. More absolute space was seen in taller, older, and male individuals than those that were shorter, younger, and/or female. Some patterns of this variation are consistent with previously identified patterns of morphology in the skull or brain as elaborated upon in earlier chapters. Males had more mediolaterally placed cEAS, and have previously been shown to be wider ectocranially than females

(Spradley and Jantz, 2011). Additionally, brains are consistently observed to shrink with age, and the cEAS appropriately was shown to increase in size concomitantly. However, the details surrounding these patterns are less straightforward upon deeper investigation. Not all regions of the cEAS appear equally tied to these characteristics, and differences in its morphology arise as a result of changes in both the brain and endocranium.

Characteristics of size (as described by height and weight), sex, and age appear to influence the frontal vault more than other regions of the cEAS, with some changes noted in the lateral aspects of the basal area. The reason for this may be partly due to short-term head positioning during MRI which exaggerates the frontal cEAS. Part of the standard head MRI is consistent supine positioning of each patient in the scanner. With the head in this position, the brain settles posteriorly toward the occipital bone, displacing the CSF anteriorly and into the frontal region. Over a longer time scale, the endocranium is generally assumed to be morphologically constant meaning that any change in cEAS would be ascribed to changes in brain tissue while the skeletal tissue remains invariable (Albert et al., 2007; Matsumae et al., 1996; Mortamet et al., 2005). The sample assessed here, however, seems to indicate total endocranial volume is not entirely stable with aging (see figure 5.1). Endocast volume increased with age in the sample, with the rate of increase appearing to be greater in females and within the vault component of the endocast. The effects of age, in general, are not the same in males and females. For example, females undergo menopause,

which is a much more sudden change in circulating hormone levels associated with a cessation of reproductive capability than changes in hormones of aging males. Additionally, osteoporosis is specifically an aging effect on bone that impacts females more significantly than males, in part due to hormonal differences. The changing hormonal landscape is also likely to affect the morphology of the cEAS, and is an additional aspect that may need to be taken into account when assessing morphology as a diagnostic tool. Do the differing effects of these hormonal changes on males vs females exaggerate the changes to cEAS morphology we suspect to see with dementia? Do they mimic or mask those changes? It may be that the more pronounced endocranial volume change in the females of this sample is related to menopause.

2.0 Areas of Additional Investigation

Human populations vary in a number of basic anatomic characteristics across geographic locations and with ancestry. The sample examined here was biased toward individuals self-described as race: ‘white’ and the inclusion of other groups undoubtedly added additional variation. There were however not sufficient numbers of individuals from the other self-described race groups to allow for meaningful comparisons among groups. Cursory assessment of the data in light of the self-described race categories do not indicate substantial differences in the typical morphology of the cEAS among groups (Figure 5.2). However, these cursory findings do not preclude the existence of differences with a more robust sample size. Males were observed consistently to have more

cEAS than females within each self-described race group. The correlation of cEAS volume to height was, however, strongly negative in black females (n = 16) in contrast to the positive correlation in all other modestly sampled groups (Figure 5.3). There are non-significant differences among groups in overall cEAS, with individuals self-described as Asian having the most and those self-described as ‘Black or African American’ having the least cEAS, on average. However, the range of presentations within the group most heavily represented in the study sample, self-described as ‘white,’ fully encapsulates that seen in both other groups. Principal components analysis of cEAS thicknesses found no appreciable clustering of individuals based on race in any of the first eight components, see figure 5.3.

Blood pressure (BP) was not well accounted for in this study between young and aging individuals in this sample. As one of the components taking up a fraction of the total endocranial volume, blood within the skull displaces CSF in the cEAS with every beat of the heart. It is possible then that BP influences the overall amount of cEAS. Systolic BP across the entire sample is only slightly positively correlated with total cEAS volume ($p = 0.2$). This correlation is possibly skewed due to the effects of continuous elevated blood pressure on the brain as opposed to a simple spontaneous measurement taken here, and the higher concentration of aging individuals with elevated BP in the overall sample. Assessment of the cEAS as a whole may not be sensitive to these changes either and increasing the complexity of this model to include a CSF-only component may shed

additional light on the relationship between blood and cEAS volumes. This would require further refinement of the current model, and is not data currently accessible without additional data collection.

3.0 Areas for Sample Expansion

Expansion upon the ‘normal’ sample examined here with respect to underrepresented categories currently (e.g., race, BP, tobacco and alcohol use, etc.) is clearly necessary. Additionally, higher yield investigation into the cEAS through other avenues may be warranted also. The two factors that may be of marked influence on cEAS are 1) cranial development and 2) head position relative to gravity during scanning. The significant variation seen in cEAS morphology after controlling for variables thought to play a substantial role in its size and shape may be partially accounted for by developmental and childhood differences. Extreme variation in cEAS during development was discussed earlier, and it seems likely that some of this variation continues to be visible into adulthood. Do infants that experience benign hydrocephalus have larger cEAS as they enter into adulthood? The cEAS may also be affected by pathology for a period, but experience a rebound or normalize before adulthood. This may be the case with cEAS changes associate with autism (Dhar et al., 2021; Shen et al., 2018). It begs the question then: why there is so much variation in the cEAS of young adults if not just as a holdover from development? The HCP-Development and Baby studies are ripe for addition to this examination. Between these two HCP projects, more than 1500 individuals between infancy and 21 years of age are being scanned using protocols consistent with the HCP as a whole. These

scans are therefore of similar quality and contain the necessary anatomy as those studied in this work but in the frame of development of the cEAS from birth.

It can be argued that the frontal vault cEAS, described in the preceding chapters as one of the more variable regions, exists only passively and intermittently. As animals who have a habitually upright posture, human heads are most often oriented with the orbits facing forward. In contrast, MR imaging typically, and in the HCP specifically, takes place with the participant supine and their orbits superiorly, upward and away from the pull of gravity. In a supine position the brain settles to the back of the skull, and CSF flows anteriorly into the frontal vault cEAS region, increasing its thickness in that area. The shape of the cEAS observed here is therefore not likely to be a precise representation of its morphology during much of normal functioning. It is quite likely that changes to the positioning of the head and settling of the brain within the cEAS represent the greatest source of intra-individual variation in its morphology over short periods of time. Modeling of the cEAS in various positions relative to the pull of gravity within even a single individual may shed greater light on the ‘true’ morphology of these structures inside the skull.

4.0 Potential Clinical Importance

The highly variable morphology of the cEAS may be exploitable as a diagnostic tool for numerous neurologic disorders. In the work presented here, a significant amount of variation not explainable by height, weight, sex, or age was

uncovered. Some of this variation may come from development as explored earlier, but other processes may be at play. Increased variability observed in the aging cEAS specifically may partly be the result of different preclinical processes taking place that could not be controlled for here. For example, dementia represents an especially common cluster of different diseases that result in loss of memory, language, problem-solving skills, and other brain functions (Geldmacher and Whitehouse, 1996). It is almost certain that some individuals included in this sample will go on to present with a clinical level of dementia. It may be that the anatomic processes at play in dementia are already at work, and are responsible for some of the variation observed here. The underlying causes such as Alzheimer's, vascular, frontotemporal, or Lewy body dementia may act on the brain subtly enough to be undetectable by brain shape alone, but differentiable through assessment of the responding cEAS, even at an early stage. It could be that by measuring cEAS thicknesses, small changes in the brain's configuration relative to the skull are detectable where changes in the brain alone would otherwise be overwhelmed by its overall significant variation. A sample of individuals with differing levels of and types of clinical dementia could shed further light on this. Some data of this type do exist in the HCP-Brain Aging and Dementia project, and may be easily exploitable and comparable to the data collected here with normal individuals. In the event the cEAS proves to be a highly specific indicator of dementia subtypes or another clinical pathologic process, earlier diagnosis means earlier and more precise treatment resulting in better patient outcomes.

Figures

Figure 5. 1: Height and total endocast volume with linear regression lines (r/ggplot: lm) and confidence intervals. Red is females. Blue is males. Numbers are randomly assigned catalog numbers specific to this project.

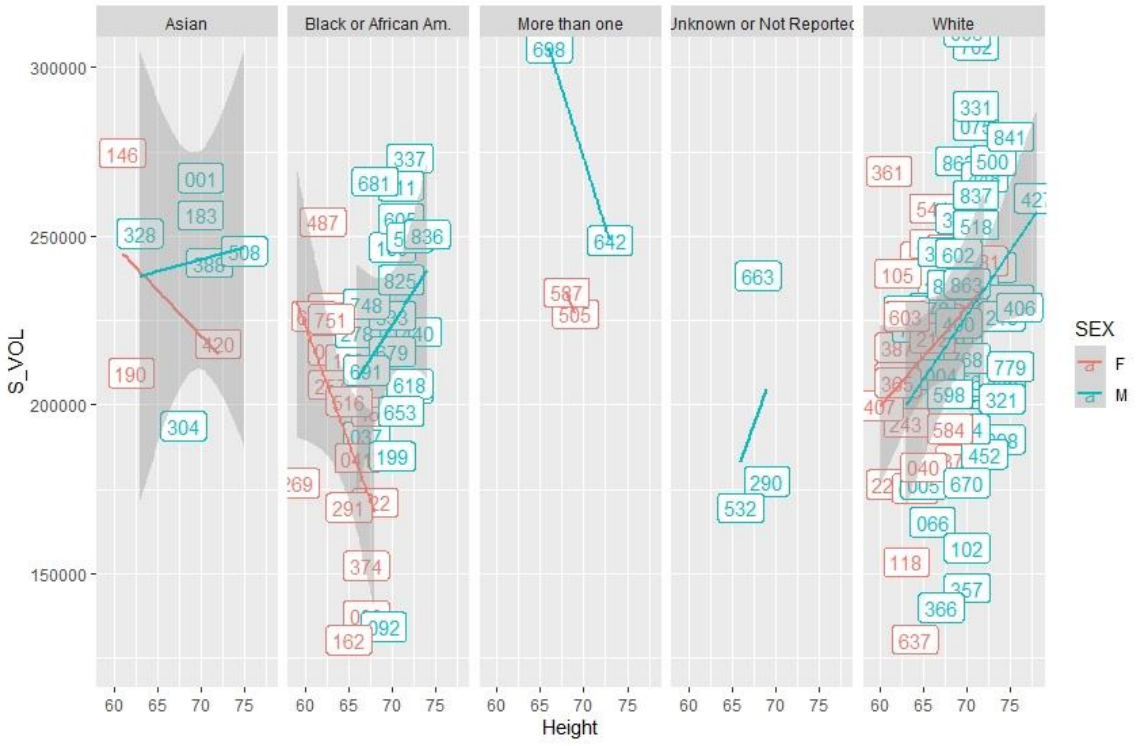

Figure 5. 2: Height and total cEAS volume with linear regression lines (r/ggplot: lm) and confidence intervals. Faceted by self-identified race categories. Blue is males, red is females. Numbers are randomly assigned catalog numbers specific to this project.

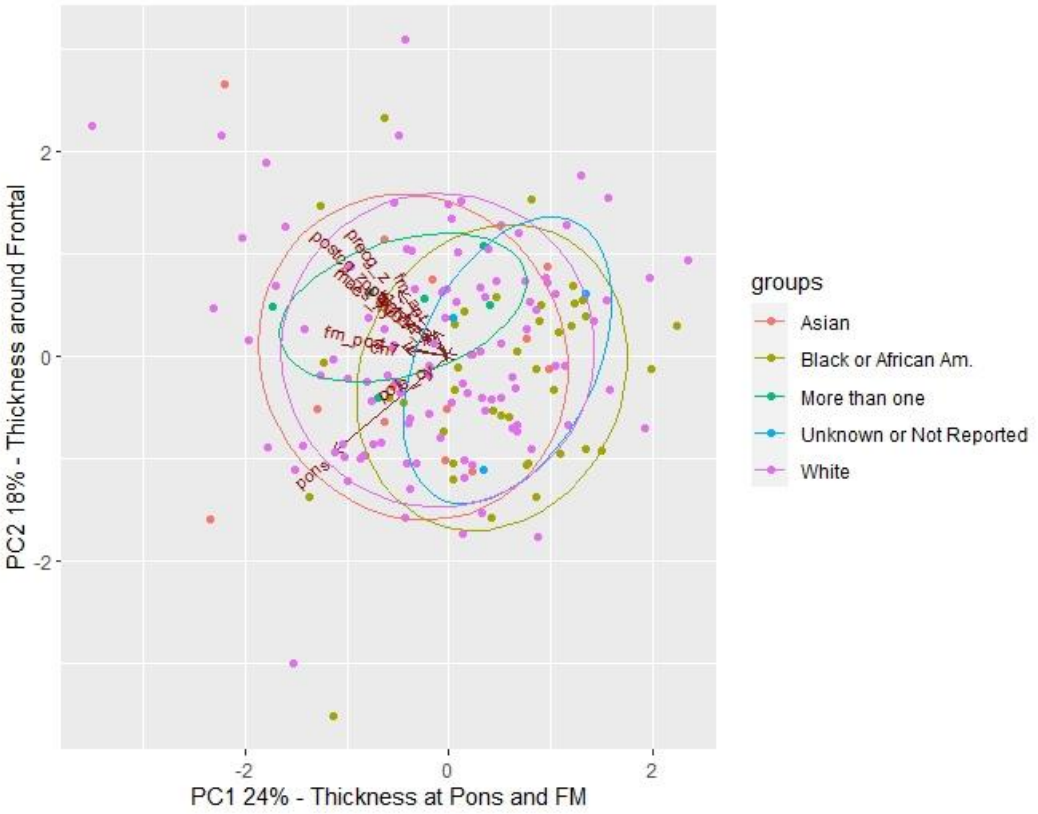

Figure 5. 3: Plot of PCA1 and 2 for cEAS thicknesses clusters by self-assigned race categories. Ellipses at 0.68 confidence.

Bibliography

Adeeb, N., Mortazavi, M.M., Deep, A., Griessenauer, C.J., Watanabe, K., Shoja, M.M., Loukas, M., Tubbs, R.S., 2013. The pia mater: a comprehensive review of literature. Childs Nerv. Syst. 29, 1803–1810. https://doi.org/10.1007/s00381-013-2044-5

Adeeb, N., Mortazavi, M.M., Tubbs, R.S., Cohen-Gadol, A.A., 2012. The cranial dura mater: a review of its history, embryology, and anatomy. Childs Nerv. Syst. 28, 827–837. https://doi.org/10.1007/s00381-012-1744-6

Albert, A.M., Ricanek, K., Patterson, E., 2007. A review of the literature on the aging adult skull and face: Implications for forensic science research and applications. Forensic Sci. Int. 172, 1–9. https://doi.org/10.1016/j.forsciint.2007.03.015

Aldridge, K., Boyadjiev, S.A., Capone, G.T., DeLeon, V.B., Richtsmeier, J.T., 2005a. Precision and error of three-dimensional phenotypic measures acquired from 3dMD photogrammetric images. Am. J. Med. Genet. A. 138A, 247–253. https://doi.org/10.1002/ajmg.a.30959

Aldridge, K., Kane, A.A., Marsh, J.L., Panchal, J., Boyadjiev, S.A., Yan, P., Govier, D., Ahmad, W., Richtsmeier, J.T., 2005b. Brain morphology in nonsyndromic unicoronal craniosynostosis. Anat. Rec. A. Discov. Mol. Cell. Evol. Biol. 285A, 690–698. https://doi.org/10.1002/ar.a.20201

Aldridge, K., Kane, A.A., Marsh, J.L., Yan, P., Govier, D., Richtsmeier, J.T., 2005c. Relationship BlackwellPublishing,Ltd. of brain and skull in pre- and postoperative sagittal synostosis 13.

Aldridge, K., Marsh, J.L., Govier, D., Richtsmeier, J.T., 2002. Central nervous system phenotypes in craniosynostosis. J. Anat. 201, 31–39. https://doi.org/10.1046/j.1469-7580.2002.00074.x

Allen, J.S., Damasio, H., Grabowski, T.J., 2002. Normal neuroanatomical variation in the human brain: An MRI-volumetric study. Am. J. Phys. Anthropol. 118, 341–358. https://doi.org/10.1002/ajpa.10092

Armstrong, D.L., 2002. Measurement of the subarachnoid space by ultrasound in preterm infants. Arch. Dis. Child. - Fetal Neonatal Ed. 86, 124F – 126. https://doi.org/10.1136/fn.86.2.F124

Ashtari, M., Avants, B., Cyckowski, L., Cervellione, K.L., Roofeh, D., Cook, P., Gee, J., Sevy, S., Kumra, S., 2011. Medial temporal structures and memory functions in adolescents with heavy cannabis use. J. Psychiatr. Res. 45, 1055–1066. https://doi.org/10.1016/j.jpsychires.2011.01.004

Batalla, A., Bhattacharyya, S., Yücel, M., Fusar-Poli, P., Crippa, J.A., Nogué, S., Torrens, M., Pujol, J., Farré, M., Martin-Santos, R., 2013. Structural and Functional Imaging Studies in Chronic Cannabis Users: A Systematic Review of Adolescent and Adult Findings. PLoS ONE 8, e55821. https://doi.org/10.1371/journal.pone.0055821

Battistella, G., Fornari, E., Annoni, J.-M., Chtioui, H., Dao, K., Fabritius, M., Favrat, B., Mall, J.-F., Maeder, P., Giroud, C., 2014. Long-Term Effects of Cannabis on Brain Structure. Neuropsychopharmacology 39, 2041–2048. https://doi.org/10.1038/npp.2014.67

Block, R.I., O'Leary, D.S., Ehrhardt, J.C., Augustinack, J.C., Ghoneim, M.M., Arndt, S., Hall, J.A., 2000. Effects of frequent marijuana use on brain tissue volume and composition: NeuroReport 11, 491–496. https://doi.org/10.1097/00001756-200002280-00013

Bookheimer, S.Y., Salat, D.H., Terpstra, M., Ances, B.M., Barch, D.M., Buckner, R.L., Burgess, G.C., Curtiss, S.W., Diaz-Santos, M., Elam, J.S., Fischl, B., Greve, D.N., Hagy, H.A., Harms, M.P., Hatch, O.M., Hedden, T., Hodge, C., Japardi, K.C., Kuhn, T.P., Ly, T.K., Smith, S.M., Somerville, L.H., Uğurbil, K., van der Kouwe, A., Van Essen, D., Woods, R.P., Yacoub, E., 2019. The Lifespan Human Connectome Project in Aging: An overview. NeuroImage 185, 335–348. https://doi.org/10.1016/j.neuroimage.2018.10.009

Breasted, J.H., 1930. The Edwin Smith Surgical Papyrus.

Brocklenhurst, G., 1979. The significance of the evolution of the cerebrospinal fluid. Ann. R. Coll. Surg. Engl. 61.

Bruner, E., Manzi, G., Arsuaga, J.L., 2003. Encephalization and allometric trajectories in the genus Homo: Evidence from the Neandertal and modern lineages. Proc. Natl. Acad. Sci. 100, 15335–15340. https://doi.org/10.1073/pnas.2536671100

Burgaleta, M., Head, K., Álvarez-Linera, J., Martínez, K., Escorial, S., Haier, R., Colom, R., 2012. Sex differences in brain volume are related to specific skills, not to general intelligence. Intelligence 40, 60–68. https://doi.org/10.1016/j.intell.2011.10.006

Chadduck, W., Chadduck, J., Boop, F., 1992. The Subarachnoid Spaces in Craniosynostosis. Neurosurgery 30, 867–71. https://doi.org/10.1097/00001665-199301000-00013

Clarke, R.C., Merlin, M.D., 2013. Cannabis: evolution and ethnobotany. University of California Press, Berkeley.

Co, B.T., 1977. Absence of cerebral atrophy in chronic cannabis users. Evaluation by computerized transaxial tomography. JAMA J. Am. Med. Assoc. 237, 1229–1230. https://doi.org/10.1001/jama.237.12.1229

Cohen, M., Rasser, P.E., Peck, G., Carr, V.J., Ward, P.B., Thompson, P.M., Johnston, P., Baker, A., Schall, U., 2012. Cerebellar grey-matter deficits, cannabis use and first-episode schizophrenia in adolescents and young adults. Int. J. Neuropsychopharmacol. 15, 297–307. https://doi.org/10.1017/S146114571100068X

Cole, T.M., 2002. WinEDMA. University of Missouri Kansas City.

Condon, B., Wyper, D., Grant, R., Patterson, J., Teasdale, G., 1986. Use of Magnetic Resonance Imaging to Meaure Intracranial Cerebrospinal Fluid Volume. Lancet Prelim. Commun. 327, 1355–1357.

Cousijn, J., Goudriaan, A.E., Ridderinkhof, K.R., van den Brink, W., Veltman, D.J., Wiers, R.W., 2012. Approach-Bias Predicts Development of Cannabis Problem Severity in Heavy Cannabis Users: Results from a Prospective FMRI Study. PLoS ONE 7, e42394. https://doi.org/10.1371/journal.pone.0042394

Curnes, J.T., 1987. MR imaging of peripheral intracranial neoplasms: extraaxial vs intraaxial masses. J. Comput. Assist. Tomogr. 11, 932–7.

Davis, P.J.M., Wright, E.A., 1977. A new method for measuring cranial cavity volume and its application to the assessment of cerebral atrophy at autopsy. Neuropathol. Appl. Neurobiol. 3, 341–358. https://doi.org/10.1111/j.1365-2990.1977.tb00595.x

DeCarli, C., Massaro, J., Harvey, D., Hald, J., Tullberg, M., Au, R., Beiser, A., D'Agostino, R., Wolf, P.A., 2005. Measures of brain morphology and infarction in the framingham heart study: establishing what is normal. Neurobiol. Aging 26, 491–510. https://doi.org/10.1016/j.neurobiolaging.2004.05.004

DeLisi, L.E., Bertisch, H.C., Szulc, K.U., Majcher, M., Brown, K., Bappal, A., Ardekani, B.A., 2006. [No title found]. Harm. Reduct. J. 3, 17. https://doi.org/10.1186/1477-7517-3-17

Dewan, M.C., Rattani, A., Mekary, R., Glancz, L.J., Yunusa, I., Baticulon, R.E., Fieggen, G., Wellons, J.C., Park, K.B., Warf, B.C., 2019. Global hydrocephalus epidemiology and incidence: systematic review and meta-analysis. J. Neurosurg. 130, 1065–1079. https://doi.org/10.3171/2017.10.JNS17439

Dhar, R., Hamzehloo, A., Kumar, A., Chen, Y., He, J., Heitsch, L., Slowik, A., Strbian, D., Lee, J.-M., 2021. Hemispheric CSF volume ratio quantifies progression and severity of cerebral edema after acute hemispheric stroke. J. Cereb. Blood Flow Metab. 41, 2907–2915. https://doi.org/10.1177/0271678X211018210

Filbey, F.M., Aslan, S., Calhoun, V.D., Spence, J.S., Damaraju, E., Caprihan, A., Segall, J., 2014. Long-term effects of marijuana use on the brain. Proc. Natl. Acad. Sci. 111, 16913–16918. https://doi.org/10.1073/pnas.1415297111

Filbey, F.M., McQueeny, T., Kadamangudi, S., Bice, C., Ketcherside, A., 2015. Combined effects of marijuana and nicotine on memory performance and hippocampal volume. Behav. Brain Res. 293, 46–53. https://doi.org/10.1016/j.bbr.2015.07.029

Frydrychowski, A.F., Szarmach, A., Czaplewski, B., Winklewski, P.J., 2012. Subarachnoid Space: New Tricks by an Old Dog. PLoS ONE 7, e37529. https://doi.org/10.1371/journal.pone.0037529

Frydrychowski, A.F., Wszedybyl-Winklewska, M., Bandurski, T., Winklewski, P.J., 2011. Flow-induced changes in pial artery compliance registered with a non-invasive method in rabbits. Microvasc. Res. 82, 156–162. https://doi.org/10.1016/j.mvr.2011.05.005

Gaoni, Y., Mechoulam, R., 1971. Isolation and structure of .DELTA.+-tetrahydrocannabinol and other neutral cannabinoids from hashish. J. Am. Chem. Soc. 93, 217–224. https://doi.org/10.1021/ja00730a036

Gilman, J.M., Kuster, J.K., Lee, S., Lee, M.J., Kim, B.W., Makris, N., van der Kouwe, A., Blood, A.J., Breiter, H.C., 2014. Cannabis Use Is Quantitatively Associated with Nucleus Accumbens and Amygdala Abnormalities in Young Adult Recreational Users. J. Neurosci. 34, 5529–5538. https://doi.org/10.1523/JNEUROSCI.4745-13.2014

Good, C.D., Johnsrude, I., Ashburner, J., Henson, R.N.A., Friston, K.J., Frackowiak, R.S.J., 2001a. Cerebral Asymmetry and the Effects of Sex and Handedness on Brain Structure: A Voxel-Based Morphometric Analysis of 465 Normal Adult Human Brains. NeuroImage 14, 685–700. https://doi.org/10.1006/nimg.2001.0857

Good, C.D., Johnsrude, I.S., Ashburner, J., Henson, R.N.A., Friston, K.J., Frackowiak, R.S.J., 2001b. A Voxel-Based Morphometric Study of Ageing in 465 Normal Adult Human Brains. NeuroImage 14, 21–36. https://doi.org/10.1006/nimg.2001.0786

Gur, R.C., Mozley, P.D., Resnick, S.M., Gottlieb, G.L., Kohn, M., Zimmerman, R., Herman, G., Atlas, S., Grossman, R., Berretta, D., 1991. Gender differences in age effect on brain atrophy measured by magnetic resonance imaging. Proc. Natl. Acad. Sci. 88, 2845–2849. https://doi.org/10.1073/pnas.88.7.2845

Hajdu, S.I., 2003. Discovery of the Cerebrospinal Fluid 3.

Harms, M.P., Somerville, L.H., Ances, B.M., Andersson, J., Barch, D.M., Bastiani, M., Bookheimer, S.Y., Brown, T.B., Buckner, R.L., Burgess, G.C., Coalson, T.S., Chappell, M.A., Dapretto, M., Douaud, G., Fischl, B., Glasser, M.F., Greve, D.N., Hodge, C., Jamison, K.W., Jbabdi, S., Kandala, S., Li, X., Mair, R.W., Mangia, S., Marcus, D., Mascali, D., Moeller, S., Nichols, T.E., Robinson, E.C., Salat, D.H., Smith, S.M., Sotiropoulos, S.N., Terpstra, M., Thomas, K.M., Tisdall, M.D., Ugurbil, K., van der Kouwe, A., Woods, R.P., Zöllei, L., Van Essen, D.C., Yacoub, E., 2018. Extending the Human Connectome Project across ages: Imaging protocols for the Lifespan Development and Aging projects. NeuroImage 183, 972–984. https://doi.org/10.1016/j.neuroimage.2018.09.060

Harper, C., Kril, J., 1985. Brain atrophy in chronic alcoholic patients: a quantitative pathological study. J. Neurol. Neurosurg. Psychiatry 48, 211–217. https://doi.org/10.1136/jnnp.48.3.211

Herkenham, M., Lynn, A., Johnson, M., Melvin, L., de Costa, B., Rice, K., 1991. Characterization and localization of cannabinoid receptors in rat brain: a quantitative in vitro autoradiographic study. J. Neurosci. 11, 563–583. https://doi.org/10.1523/JNEUROSCI.11-02-00563.1991

Hilton, H.B., 1962. Skeletal pigmentation due to tetracycline. J. Clin. Pathol. 15, 112–115. https://doi.org/10.1136/jcp.15.2.112

Iencean, S.M., Ciurea, A., Oblu, D.N., 2008. Intracranial hypertension: classification and patterns of evolution 1, 7.

Irimia, A., 2020. Cross-sectional volumes and trajectories of the human brain, gray matter, white matter and cerebrospinal fluid in 9,473 typically aging adults 54.

Isaza, J., Díaz, C.A., Bedoya, J.F., Monsalve, T., Botella, M.C., 2014. Assessment of sex from endocranial cavity using volume-rendered CT scans in a sample from Medellín,

Colombia. Forensic Sci. Int. 234, 186.e1-186.e10. https://doi.org/10.1016/j.forsciint.2013.10.023

James, A., 2005. The Art of Medicine in Ancient Egypt. Yale University Press, New York.

Jones, H.C., 1979. Comparative aspects of the cerebrospinal fluid systems in vertebrates. Sicenec Prog. 66, 171–190.

Junge, R., Hoffmeister, D.F., 1980. Age Determination in Raccoons from Cranial Suture Obliteration. J. Wildl. Manag. 44, 725. https://doi.org/10.2307/3808029

Kalmey, J.K., Rathbun, T.A., 1996. Sex Determination by Discriminant Function Analysis of the Petrous Portion of the Temporal Bone. J. Forensic Sci. 41, 14013J. https://doi.org/10.1520/JFS14013J

Kardong, K., 2008. Vertebrates Comparative Anatomy, Function, Evolution, 5th ed.

Kedarasetti, R.T., Drew, P.J., Costanzo, F., 2020. Arterial pulsations drive oscillatory flow of CSF but not directional pumping. Sci. Rep. 10, 10102. https://doi.org/10.1038/s41598-020-66887-w

Kim, Y.S., Park, I.S., Kim, H.J., Kim, D., Lee, N.J., Rhyu, I.J., 2018. Changes in intracranial volume and cranial shape in modern Koreans over four decades. Am. J. Phys. Anthropol. 166, 753–759. https://doi.org/10.1002/ajpa.23464

Kimball, D., Kimball, H., Matusz, P., Tubbs, R., Loukas, M., Cohen-Gadol, A., 2015. Ossification of the Posterior Petroclinoid Dural Fold: A Cadaveric Study with Neurosurgical Significance. J. Neurol. Surg. Part B Skull Base 76, 272–277. https://doi.org/10.1055/s-0034-1396598

Klasson, N., Olsson, E., Eckerström, C., Malmgren, H., Wallin, A., 2018. Estimated intracranial volume from FreeSurfer is biased by total brain volume. Eur. Radiol. Exp. 2, 24. https://doi.org/10.1186/s41747-018-0055-4

Kohn, L.A., Bhatia, G., Commean, P., Smith, K., Vannier, M., 1995. Anthropometric optical surface imaging system repeatability, prevision , and validation. Ann. Plast. Surg., Ann Plast Surg 34, 362–71.

Kuehnle, J., Mendelson, J.H., Davis, K.R., New, P.F.J., 1977. Computed Tomographic Examination of Heavy Marijuana Smokers. JAMA J. Am. Med. Assoc. 237, 1231–1232.

Lam, W.W.M., Ai, V.H.G., Wong, V., Leong, L.L.Y., 2001. Ultrasonographic measurement of subarachnoid space in normal infants and children. Pediatr. Neurol. 25, 380–384. https://doi.org/10.1016/S0887-8994(01)00349-6

Lele, S., 1993. Euclidean Distance Matrix Analysis (EDMA): Estimation of mean form and mean form difference. Math. Geol. 25, 573–602. https://doi.org/10.1007/BF00890247

Lele, S., Richtsmeier, J.T., 1991. Euclidean distance matrix analysis: A coordinate-free approach for comparing biological shapes using landmark data. Am. J. Phys. Anthropol. 86, 415–427. https://doi.org/10.1002/ajpa.1330860307

Lemaître, H., Crivello, F., Grassiot, B., Alpérovitch, A., Tzourio, C., Mazoyer, B., 2005. Age- and sex-related effects on the neuroanatomy of healthy elderly. NeuroImage 26, 900–911. https://doi.org/10.1016/j.neuroimage.2005.02.042

Leonard, C.M., Towler, S., Welcome, S., Halderman, L.K., Otto, R., Eckert, M.A., Chiarello, C., 2008. Size Matters: Cerebral Volume Influences Sex Differences in Neuroanatomy. Cereb. Cortex 18, 2920–2931. https://doi.org/10.1093/cercor/bhn052

Lewis, S., 1999. Quantifying measurement error. Curr. Res. Osteoarchaeol. 2, 4.

Lopez-Larson, M.P., Bogorodzki, P., Rogowska, J., McGlade, E., King, J.B., Terry, J., Yurgelun-Todd, D., 2011. Altered prefrontal and insular cortical thickness in adolescent marijuana users. Behav. Brain Res. 220, 164–172. https://doi.org/10.1016/j.bbr.2011.02.001

Lorenzetti, V., Solowij, N., Whittle, S., Fornito, A., Lubman, D.I., Pantelis, C., Yücel, M., 2015. Gross morphological brain changes with chronic, heavy cannabis use. Br. J. Psychiatry 206, 77–78. https://doi.org/10.1192/bjp.bp.114.151407

Mackie, K., 2008. Cannabinoid Receptors: Where They are and What They do. J. Neuroendocrinol. 20, 10–14. https://doi.org/10.1111/j.1365-2826.2008.01671.x

Maes, M., Vandoolaeghe, E., Degroote, J., Altamura, C., Roels, C., Hermans, P., 2000. Linear CT-scan measurements in alcohol-dependent patients with and without delirium tremens. Alcohol 20, 117–123.

Malinger, G., Lerman-Sagie, T., Achiron, R., Lipitz, S., 2000. The subarachnoid space: normal fetal development as demonstrated by transvaginal ultrasound. Prenat. Diagn. 20, 890–893. https://doi.org/10.1002/1097-0223(200011)20:11<890::AID-PD945>3.0.CO;2-Z

Marcus, D.S., Harms, M.P., Snyder, A.Z., Jenkinson, M., Wilson, J.A., Glasser, M.F., Barch, D.M., Archie, K.A., Burgess, G.C., Ramaratnam, M., Hodge, M., Horton, W., Herrick, R., Olsen, T., McKay, M., House, M., Hileman, M., Reid, E., Harwell, J., Coalson, T., Schindler, J., Elam, J.S., Curtiss, S.W., Van Essen, D.C., 2013. Human Connectome Project informatics: Quality control, database services, and data visualization. NeuroImage 80, 202–219. https://doi.org/10.1016/j.neuroimage.2013.05.077

Mata, I., Perez-Iglesias, R., Roiz-Santiañez, R., Tordesillas-Gutierrez, D., Pazos, A., Gutierrez, A., Vazquez-Barquero, J.L., Crespo-Facorro, B., 2010. Gyrification brain abnormalities associated with adolescence and early-adulthood cannabis use. Brain Res. 1317, 297–304. https://doi.org/10.1016/j.brainres.2009.12.069

Matochik, J.A., Eldreth, D.A., Cadet, J.-L., Bolla, K.I., 2005. Altered brain tissue composition in heavy marijuana users. Drug Alcohol Depend. 77, 23–30. https://doi.org/10.1016/j.drugalcdep.2004.06.011

Matsumae, M., Kikinis, R., Mórocz, I., Lorenzo, A.V., Albert, M.S., Black, P.McL., Jolesz, F.A., 1996a. Intracranial compartment volumes in patients with enlarged ventricles assessed by magnetic resonance—based image processing. J. Neurosurg. 84, 972–981. https://doi.org/10.3171/jns.1996.84.6.0972

Matsumae, M., Kikinis, R., Mórocz, I.A., Lorenzo, A.V., Sándor, T., Albert, M.S., Black, P.McL., Jolesz, F.A., 1996b. Age-related changes in intracranial compartment volumes in normal adults assessed by magnetic resonance imaging. J. Neurosurg. 84, 982–991. https://doi.org/10.3171/jns.1996.84.6.0982

McPartland, J.M., Hegman, W., Long, T., 2019. Cannabis in Asia: its center of origin and early cultivation, based on a synthesis of subfossil pollen and archaeobotanical studies. Veg. Hist. Archaeobotany 28, 691–702. https://doi.org/10.1007/s00334-019-00731-8

McQueeny, T., Padula, C.B., Price, J., Medina, K.L., Logan, P., Tapert, S.F., 2011. Gender effects on amygdala morphometry in adolescent marijuana users. Behav. Brain Res. 224, 128–134. https://doi.org/10.1016/j.bbr.2011.05.031

Medina, K.L., Nagel, B.J., Park, A., McQueeny, T., Tapert, S.F., 2007a. Depressive symptoms in adolescents: associations with white matter volume and marijuana use. J. Child Psychol. Psychiatry 48, 592–600. https://doi.org/10.1111/j.1469-7610.2007.01728.x

Medina, K.L., Nagel, B.J., Tapert, S.F., 2010. Abnormal cerebellar morphometry in abstinent adolescent marijuana users. Psychiatry Res. Neuroimaging 182, 152–159. https://doi.org/10.1016/j.pscychresns.2009.12.004

Medina, K.L., Schweinsburg, A.D., Cohen-Zion, M., Nagel, B.J., Tapert, S.F., 2007b. Effects of alcohol and combined marijuana and alcohol use during adolescence on hippocampal volume and asymmetry. Neurotoxicol. Teratol. 29, 141–152. https://doi.org/10.1016/j.ntt.2006.10.010

Meindl, R.S., Lovejoy, C.O., 1985. Ectocranial suture closure: A revised method for the determination of skeletal age at death based on the lateral-anterior sutures. Am. J. Phys. Anthropol. 68, 57–66. https://doi.org/10.1002/ajpa.1330680106

Ment, L.R., Duncan, C.C., Geehr, R., 1981. Benign enlargement of the subarachnoid spaces in the infant. J. Neurosurg. 54, 504–508. https://doi.org/10.3171/jns.1981.54.4.0504

Mokri, B., 2001. The Monro-Kellie hypothesis: Applications in CSF volume depletion. Neurology 56, 1746–1748. https://doi.org/10.1212/WNL.56.12.1746

Monro, A., 1783. Observations on the Structure and Functions of the Nervious Ststem. Lond. Med. J. 113–135.

Moreno-Alcázar, A., Gonzalvo, B., Canales-Rodríguez, E.J., Blanco, L., Bachiller, D., Romaguera, A., Monté-Rubio, G.C., Roncero, C., McKenna, P.J., Pomarol-Clotet, E., 2018. Larger Gray Matter Volume in the Basal Ganglia of Heavy Cannabis Users Detected by Voxel-Based Morphometry and Subcortical Volumetric Analysis. Front. Psychiatry 9, 175. https://doi.org/10.3389/fpsyt.2018.00175

Mortamet, B., Zeng, D., Gerig, G., Prastawa, M., Bullitt, E., 2005. Effects of Healthy Aging Measured By Intracranial Compartment Volumes Using a Designed MR Brain Database, in: Duncan, J.S., Gerig, G. (Eds.), Medical Image Computing and Computer-Assisted Intervention – MICCAI 2005, Lecture Notes in Computer Science. Springer Berlin Heidelberg, Berlin, Heidelberg, pp. 383–391. https://doi.org/10.1007/11566465_48

Mwachaka, P.M., Hassanali, J., Odula, P.O., 2009. Anatomic position of the asterion in Kenyans for posterolateral surgical approaches to cranial cavity. Clin. Anat. NA-NA. https://doi.org/10.1002/ca.20888

Ng Kee Kwong, K.C., Harbham, P.K., Selvaraj, B.T., Gregory, J.M., Pal, S., Hardingham, G.E., Chandran, S., Mehta, A.R., 2021. 40 Years of CSF Toxicity Studies in ALS: What Have We Learnt About ALS Pathophysiology? Front. Mol. Neurosci. 14, 647895. https://doi.org/10.3389/fnmol.2021.647895

Perini, T.A., de Oliveira, G.L., 2005. Technical error of measurement in anthropometry. Rev Bras Med Esporte 11, 5.

Peterson, M., Prigge, M.B.D., Bigler, E.D., Zielinski, B., King, J.B., Lange, N., Alexander, A., Lainhart, J.E., Nielsen, J.A., 2021. Evidence for normal extra-axial cerebrospinal fluid volume in autistic males from middle childhood to adulthood. NeuroImage 240, 118387. https://doi.org/10.1016/j.neuroimage.2021.118387

Rametti, G., Carrillo, B., Gómez-Gil, E., Junque, C., Zubiarre-Elorza, L., Segovia, S., Gomez, Á., Guillamon, A., 2011. The microstructure of white matter in male to female transsexuals before cross-sex hormonal treatment. A DTI study. J. Psychiatr. Res. 45, 949–954. https://doi.org/10.1016/j.jpsychires.2010.11.007

Raz, N., Gunning-Dixon, F., Head, D., Williamson, A., Acker, J.D., 2001. Age and Sex Differences in the Cerebellum and the Ventral Pons: A Prospective MR Study of Healthy Adults 7.

Reardon, W., 2000. Craniosynostosis. Diagnosis, evaluation and management. J. Med. Genet. 37, 727. https://doi.org/10.1136/jmg.37.9.727

Ribas, G., Yasuda, A., Rodrigues, A., Nishikuni, K., Ribas, E., 2006. Surgical Anatomy of Microneurosurgical Sulcal Key Points. Oper. Neurosurg. 59.

Rubmaugh, C., Fang, H., Wilson, G., Higgins, R., Mestek, M., 1980. Cerebral CT findings in drug abuse: Clinialc and Experimental Observations. J. Comput. Assist. Tomogr. 4, 330–334.

Ruengdit, S., Troy Case, D., Mahakkanukrauh, P., 2020. Cranial suture closure as an age indicator: A review. Forensic Sci. Int. 307, 110111. https://doi.org/10.1016/j.forsciint.2019.110111

Ruigrok, A.N.V., Salimi-Khorshidi, G., Lai, M.-C., Baron-Cohen, S., Lombardo, M.V., Tait, R.J., Suckling, J., 2014. A meta-analysis of sex differences in human brain structure. Neurosci. Biobehav. Rev. 39, 34–50. https://doi.org/10.1016/j.neubiorev.2013.12.004

Russo, E.B., 2007. History of Cannabis and Its Preparations in Saga, Science, and Sobriquet. Chem. Biodivers. 4, 1614–1648. https://doi.org/10.1002/cbdv.200790144

Russo, E.B., Jiang, H.-E., Li, X., Sutton, A., Carboni, A., del Bianco, F., Mandolino, G., Potter, D.J., Zhao, Y.-X., Bera, S., Zhang, Y.-B., Lü, E.-G., Ferguson, D.K., Hueber, F., Zhao, L.-C., Liu, C.-J., Wang, Y.-F., Li, C.-S., 2008. Phytochemical and genetic analyses

of ancient cannabis from Central Asia. J. Exp. Bot. 59, 4171–4182. https://doi.org/10.1093/jxb/ern260

Sakka, L., Coll, G., Chazal, J., 2011. Anatomy and physiology of cerebrospinal fluid. Eur. Ann. Otorhinolaryngol. Head Neck Dis. 128, 309–316. https://doi.org/10.1016/j.anorl.2011.03.002

Sarmento, S.A., Jácome, D.C., Andrade, E.M.F. de, Melo, A.V.A., Oliveira, O.R. de, Tedeschi, H., 2008. Relationship between the coronal suture and the central lobe: how important is it and how can we use it in surgical planning? Arq. Neuropsiquiatr. 66, 868–871. https://doi.org/10.1590/S0004-282X2008000600017

Scahill, R.I., Frost, C., Jenkins, R., Whitwell, J.L., Rossor, M.N., Fox, N.C., 2003. A Longitudinal Study of Brain Volume Changes in Normal Aging Using Serial Registered Magnetic Resonance Imaging. Arch. Neurol. 60, 989. https://doi.org/10.1001/archneur.60.7.989

Scelsi, C.L., Rahim, T.A., Morris, J.A., Kramer, G.J., Gilbert, B.C., Forseen, S.E., 2020. The Lateral Ventricles: A Detailed Review of Anatomy, Development, and Anatomic Variations. Am. J. Neuroradiol. 41, 566–572. https://doi.org/10.3174/ajnr.A6456

Schacht, J.P., Hutchison, K.E., Filbey, F.M., 2012. Associations between Cannabinoid Receptor-1 (CNR1) Variation and Hippocampus and Amygdala Volumes in Heavy Cannabis Users. Neuropsychopharmacology 37, 2368–2376. https://doi.org/10.1038/npp.2012.92

Schievink, W.I., 2003. Misdiagnosis of Spontaneous Intracranial Hypotension. Arch. Neurol. 60, 1713. https://doi.org/10.1001/archneur.60.12.1713

Shen, L., Saykin, A.J., Kim, S., Firpi, H.A., West, J.D., Risacher, S.L., McDonald, B.C., McHugh, T.L., Wishart, H.A., Flashman, L.A., 2010. Comparison of Manual and Automated Determination of Hippocampal Volumes in MCI and Early AD. Brain Imaging Behav. 4, 86–95. https://doi.org/10.1007/s11682-010-9088-x

Shen, M.D., Kim, S.H., McKinstry, R.C., Gu, Hongbin, Hazlett, Heather C., Nordahl, C.W., Emerson, R.W., Shaw, Dennis, Elison, J.T., Swanson, M.R., Fonov, V.S., Gerig, Guido, Dager, S.R., Botteron, K.N., Paterson, S., Schultz, R.T., Evans, Alan C., Estes, A.M., Zwaigenbaum, Lonnie, Styner, M.A., Amaral, D.G., Piven, Joseph, Piven, J., Hazlett, H.C., Chappell, C., Dager, S., Estes, A., Shaw, D., Botteron, K., McKinstry, R., Constantino, J., Pruett, J., Schultz, R., Zwaigenbaum, L., Elison, J., Evans, A.C., Collins, D.L., Pike, G.B., Fonov, V., Kostopoulos, P., Das, S., Gerig, G., Styner, M., Gu, H., 2017. Increased Extra-axial Cerebrospinal Fluid in High-Risk Infants Who Later Develop Autism. Biol. Psychiatry 82, 186–193. https://doi.org/10.1016/j.biopsych.2017.02.1095

Shen, M.D., Nordahl, C.W., Li, D.D., Lee, A., Angkustsiri, K., Emerson, R.W., Rogers, S.J., Ozonoff, S., Amaral, D.G., 2018. Extra-axial cerebrospinal fluid in high-risk and normal-risk children with autism aged 2–4 years: a case-control study. Lancet Psychiatry 5, 895–904. https://doi.org/10.1016/S2215-0366(18)30294-3

Small, E., 2015. Evolution and Classification of Cannabis sativa (Marijuana, Hemp) in Relation to Human Utilization 106.

Solowij, N., Jones, K.A., Rozman, M.E., Davis, S.M., Ciarrochi, J., Heaven, P.C.L., Lubman, D.I., Yücel, M., 2011. Verbal learning and memory in adolescent cannabis users, alcohol users and non-users. Psychopharmacology (Berl.) 216, 131–144. https://doi.org/10.1007/s00213-011-2203-x

Solowij, N., Walterfang, M., Lubman, D.I., Whittle, S., Lorenzetti, V., Styner, M., Velakoulis, D., Pantelis, C., Yücel, M., 2013. Alteration to hippocampal shape in cannabis users with and without schizophrenia. Schizophr. Res. 143, 179–184. https://doi.org/10.1016/j.schres.2012.10.040

Sowell, E.R., Peterson, B.S., Kan, E., Woods, R.P., Yoshii, J., Bansal, R., Xu, D., Zhu, H., Thompson, P.M., Toga, A.W., 2007. Sex Differences in Cortical Thickness Mapped in 176 Healthy Individuals between 7 and 87 Years of Age. Cereb. Cortex 17, 1550–1560. https://doi.org/10.1093/cercor/bhl066

Spector, R., Robert Snodgrass, S., Johanson, C.E., 2015. A balanced view of the cerebrospinal fluid composition and functions: Focus on adult humans. Exp. Neurol. 273, 57–68. https://doi.org/10.1016/j.expneurol.2015.07.027

Svennerholm, L., Boström, K., Jungbjer, B., 1997. Changes in weight and compositions of major membrane components of human brain during the span of adult human life of Swedes. Acta Neuropathol. (Berl.) 94, 345–352. https://doi.org/10.1007/s004010050717

Tzilos, G.K., Cintron, C.B., Wood, J.B.R., Simpson, N.S., Young, A.D., Pope, H.G., Yurgelun-Todd, D.A., 2005. Lack of Hippocampal Volume Change in Long-term Heavy Cannabis Users. Am. J. Addict. 14, 64–72. https://doi.org/10.1080/10550490590899862

Ucerler, H., Govsa, F., 2006. Asterion as a surgical landmark for lateral cranial base approaches. J. Craniomaxillofac. Surg. 34, 415–20.

van der Linden, D., Dunkel, C.S., Madison, G., 2017. Sex differences in brain size and general intelligence (g). Intelligence 63, 78–88. https://doi.org/10.1016/j.intell.2017.04.007

Van Essen, D.C., Smith, S.M., Barch, D.M., Behrens, T.E.J., Yacoub, E., Ugurbil, K., 2013. The WU-Minn Human Connectome Project: An overview. NeuroImage 80, 62–79. https://doi.org/10.1016/j.neuroimage.2013.05.041

Watanabe, Y., Abe, S., Takagi, K., Yamamoto, T., Kato, T., 2005. Evolution of subarachnoid space in normal fetuses using magnetic resonance imaging. Prenat. Diagn. 25, 1217–1222. https://doi.org/10.1002/pd.1315

Weiland, B.J., Thayer, R.E., Depue, B.E., Sabbineni, A., Bryan, A.D., Hutchison, K.E., 2015. Daily Marijuana Use Is Not Associated with Brain Morphometric Measures in Adolescents or Adults. J. Neurosci. 35, 1505–1512. https://doi.org/10.1523/JNEUROSCI.2946-14.2015

Weinberg, S.M., Naidoo, S., Govier, D.P., Martin, R.A., Kane, A.A., Marazita, M.L., 2006. Anthropometric Precision and Accuracy of Digital Three-Dimensional Photogrammetry: Comparing the Genex and 3dMD Imaging Systems with One Another and with Direct Anthropometry. J. Craniofac. Surg. 17, 477–483. https://doi.org/10.1097/00001665-200605000-00015

Weisensee, Jantz, 2016. An Examination of the Differential Effects of the Modern Epidemiological Transition on Cranial Morphology in the United States and Portugal. Hum. Biol. 88, 30. https://doi.org/10.13110/humanbiology.88.1.0030

Whitney, N., Sun, H., Pollock, J.M., Ross, D.A., 2013. The human foramen magnum—normal anatomy of the cisterna magna in adults. Neuroradiology 55, 1333–1339. https://doi.org/10.1007/s00234-013-1269-z

Wirakiat, W., Kaewborisutsakul, A., Kankuan-Kaewborisutsakul, W., 2021. Anatomic Position of the Asterion and Implication for Neurosurgical Procedure. Int. J. Morphol. 39, 1429–1435. https://doi.org/10.4067/S0717-95022021000501429

Yücel, M., Lorenzetti, V., Suo, C., Zalesky, A., Fornito, A., Takagi, M.J., Lubman, D.I., Solowij, N., 2016. Hippocampal harms, protection and recovery following regular cannabis use. Transl. Psychiatry 6, e710–e710. https://doi.org/10.1038/tp.2015.201

Yücel, M., Solowij, N., Respondek, C., Whittle, S., Fornito, A., Pantelis, C., Lubman, D.I., 2008. Regional Brain Abnormalities Associated With Long-term Heavy Cannabis Use. Arch. Gen. Psychiatry 65, 694. https://doi.org/10.1001/archpsyc.65.6.694

Zhu, Q., Dougherty, L., Margulies, S.S., 2003. IN VIVO MEASUREMENTS OF HUMAN BRAIN DISPLACEMENT 2.

Vita

I never planned on getting a Ph.D., or even attending any sort of graduate school. Despite being a good student and wildly interested in science, I hated school and had no interest in going to college even well into high school. At least until realizing that working for the National Transportation Safety Board (NTSB) would require some sort of education far exceeding than that being provided me by the public school system in the *great* state of Texas. Now, the NTBS doesn't exactly have a high demand for Doctors of Anatomy, so my overall lack of a plot for my life may not be taking me there, and yet everything leading up to this point almost feels like it has all been part of an elaborate plan for something even better. Perhaps scheme.

I grew up under the landing pattern of Houston's Intercontinental Airport, and my grandfather was mechanic for United Airlines (before they sucked), so I have been fond of commercial aviation for ages. Living near the Gulf Coast also meant unbearably hot and humid days spent indoors watching episodes of Air Crash Investigation. Mix this with the explosive popularity of o.g. CSI at the time, and I figured why not be a plane crash investigator. I applied to the University of Minnesota because my father had gone there for a bit, they had a stellar engineering program, and it was outside of Texas. I needed a change. I quickly realized physics, calculus, and engineering things in general were terminally boring to me, and this "Rise of Civilization" class in the *Anthropology* (a word I had never heard before) Department I was taking to fulfill a "liberal education"

requirement was actually intriguing to me. These anthropologists were excavating skeletons from thousands of years ago and telling fascinating stories about the lives and deaths of those people. I quickly transition majors, jumped into every skeletal analysis class I could, and started bothering professors for experience in their labs. The more I dove into osteology, and with the popularization of a new fictional crime show, *Bones* I saw how this skeletal analysis I had grown fond of was maybe still applicable to the forensic world I found so intriguing. This led me to the somewhat disappointing realization that graduate school would need to be a part of my life, and so I applied to a Masters of Forensic and Biological Anthropology at Mercyhurst University.

In my time there, I worked on forensic cases involving every kind of skeleton, and began my own osteological research concerning the cranium. My interest in reading bones led me to appreciate the skeleton as a reflection of other anatomy that reside in, on, and around it. My research had also raised more questions for me than answers, and I thought a broader appreciation of overall anatomy was my best avenue for understanding. Without abandoning my case work in forensics, I reached out to one of the few anthropologists investigating the cranium and its actual brain contents wholistically, Dr. Kristina Aldridge. Since coming to Mizzou to work with Dr. Aldridge I have come to embrace my lack of a plan that led me here, seemingly far away from engineering, and yet exactly in the realm of science and investigation that drew me out in the first place.